Circadian waves of transcriptional repression shape PIF-regulated photoperiod-responsive growth in Arabidopsis

Guiomar Martín[1], Arnau Rovira[1], Nil Veciana[1], Judit Soy[1], Gabriela Toledo-Ortiz[3,4], Charlotte M. M. Gommers[1], Marc Boix[1], Rossana Henriques[1], Eugenio G. Minguet[2], David Alabadí[2], Karen Halliday[4], Pablo Leivar[1,5], and Elena Monte[1,6,7,*]

[1]Center for Research in Agricultural Genomics (CRAG), CSIC-IRTA-UAB-UB, Campus UAB, Edifici CRAG, Bellaterra, 08193 Barcelona, Spain.

[2]Instituto de Biología Molecular y Celular de Plantas (IBMCP), CSIC-UPV, Ingeniero Fausto Elio s/n, 46022 Valencia, Spain

[3]Lancaster Environment Center, Lancaster University. Lancaster, LA1 4YQ, UK.

[4]The University of Edinburgh. CH Waddington Building, Max Born Crescent, Edinburgh, EH9 3BF, UK.

[5]Bioengineering Department, IQS School of Engineering. Via Augusta 390, 08017 Barcelona, Spain.

[6]Consejo Superior de Investigaciones Científicas (CSIC), 08028 Barcelona, Spain.

[7]Lead contact

[*]Corresponding author: elena.monte@cragenomica.es

Summary

Plants coordinate their growth and development with the environment through integration of circadian clock and photosensory pathways. In *Arabidopsis thaliana*, rhythmic hypocotyl elongation in short days (SD) is enhanced at dawn by the bHLH transcription factors PHYTOCHROME-INTERACTING FACTORS (PIFs) directly inducing expression of growth-related genes [1–6]. PIFs accumulate progressively during the night and are targeted for degradation by active phytochromes in the light, when growth is reduced. Although PIF proteins are also detected during the day hours [7–10], their growth-promoting activity is inhibited through unknown mechanisms. Recently, the core clock components and transcriptional repressors PSEUDO-RESPONSE REGULATORS PRR9/7/5 [11,12], negative regulators of hypocotyl elongation [13,14], were described to associate to G-boxes [15], the DNA motifs recognized by the PIFs [16,17], suggesting that PRR and PIF function might converge antagonistically to regulate growth. Here we report that PRR9/7/5 and PIFs physically interact and bind to the same promoter region of pre-dawn-phased, growth-related genes, and we identify the transcription factor CDF5 [18,19] as target of this interplay. In SD, *CDF5* expression is sequentially repressed from morning to dusk by PRRs and induced pre-dawn by PIFs. Consequently, *CDF5* accumulates specifically at dawn, when it induces cell elongation. Our findings provide a framework for recent TIMING OF CAB EXPRESSION 1 (TOC1/PRR1) data [5,20] and reveal that the long described circadian morning-to-midnight waves of the PRR transcriptional repressors (PRR9, PRR7, PRR5 and TOC1) [21] jointly gate PIF activity to dawn to prevent overgrowth through sequential regulation of common PIF-PRR target genes such as *CDF5*.

Results and Discussion

Genome-wide analysis of ChIP-sequencing (ChIP-seq) data for the PIF quartet (PIFq) (PIF1, 3, 4, 5)-associated [16] and PRR5-, PRR7-, and/or PRR9-associated [15] loci revealed an overlap of 1,460 genes between PIF-bound genes (57.5 % of all PIF-bound genes) and at least one of the three PRRs examined ("PIF-PRR genes") (Figure 1A left; Dataset 1). The overlap between PIF-bound and PRR5-, PRR7-, or PRR9-bound, when examined individually or in combination, is shown in Figure 1A middle (Dataset 1). Distance between PRR and PIF binding sites indicate that PRRs and PIFs associate to the same genomic regions (Figure 1A right), in accordance with results showing enrichment of G-box-containing motifs in PRR-bound regions [15,22]. We detected interaction of PIF3 and PIF4 with PRR5 (PIF4 in accordance to [20]), PRR7 and PRR9 by yeast two-hybrid assays (Figure S1A). We further confirmed PIF3-PRR interaction *in planta* by BiFc assays (Figure 1B). These data suggest that, similarly to recent findings for TOC1 and PIF3 and PIF4 [5,20], PIFs and PRRs may bind together at G-boxes to co-regulate the expression of shared PIF-PRR target genes. Based on the described activity of PRRs as transcriptional repressors [11,12,20], PIF-PRR interaction also agrees with the possibility that PRR5/7/9 might target PIFs to repress their ability to activate shared PIF-PRR target genes as shown recently for TOC1 and PIFs [5,20].

Functional classification indicated that "PIF-PRR" genes are enriched in growth-related categories (Figure S1B) and are overrepresented at the elongation phases 18-23 specifically under SD (Figure 1C, Figure S1C) (Dataset 1), suggesting that PIFs and PRRs jointly target genes involved in the induction of growth under SD conditions. We compared PRR- and PIF-bound genes with the recently defined PIF- and SD-induced (PIF/SD-induced) gene set of PIFq-regulated genes under SD containing dawn-phased and growth-related genes [4]. Strikingly, one gene (*CDF5*) was PIF/SD-induced and bound by all PRRs and PIFs (Figure 1D, Dataset 1). Previous ChIP experiments showed binding of PRR5/7/9 and possibly TOC1 to this G-box/PBE containing region [15,22,23] (Figure 1E, see legend for details). This region coincides with conserved noncoding sequences (CNS) among crucifer regulatory regions (Figure 1E) [24], suggesting that the binding sites on the *CDF5* promoter have been subjected to selective constraint, consistent with functionality relevance.

We verified binding of PRR7, TOC1, PIF3 and PIF4 to the *CDF5* promoter (*pCDF5*) region encompassing the G-boxes at different times under SD conditions by time-course analysis using ChIP-qPCR. Statistically significant and robust PRR7 binding to *pCDF5* was observed at ZT8 and ZT14, and was substantially decreased at ZT24, whereas maximum of TOC1 binding was at ZT14 (Figure 2A). For PIF3 and PIF4, tagged lines driven by the endogenous PIF3 promoter and 35S were used, respectively [25,26] (Figure S2A). Statistically significant binding of PIF3 to *pCDF5* was detected at ZT24, whereas significant PIF4 binding was detected in all three time points and incremented along the night (Figure 2A). These binding dynamics are consistent with the pattern of accumulation of each protein in SD [5,8,27]. Together, these data are consistent with binding of the PIFs, PRRs and TOC1 proteins in SD to the same region of the *CDF5* promoter located approximately 1000 bp upstream of the TSS, and with binding dictated by their protein abundance.

To examine how PIF and PRR7 interaction (Figures 1B and S1A) and binding to the *CDF5* promoter (Figure 2A) affect *CDF5* expression, we first tested *CDF5* expression in *pif* and *prr7* mutants under SD at ZT9 when PRR7 levels are maximum and PIFs start to accumulate [7,8,10,27,28]. *CDF5* levels were upregulated in *prr7* (Figure 2B), an effect strongly suppressed by the *pif* mutations in the *prr7pif* double mutants (Figure 2B), suggesting that PIFs and PRR7 regulate *CDF5* expression antagonistically as transcriptional activator and repressor, respectively. Interestingly, because PIF3 transcript and protein levels are not affected in *prr7* (Figures 2C and 2D), together these data suggest that, as described for TOC1 [5], PRR7 acts directly as transcriptional repressor of PIF3 activity in the regulation of *CDF5*. In agreement, the *prr7* long hypocotyl phenotype was also partially suppressed with genetic removal of PIF3 (Figure 2E). However, because the detected binding of PIF3 to the *CDF5* promoter at ZT9 or ZT14 was not statistically significant (Figure 2A), we cannot discard that the effect of PRRs on PIF3 might involve inhibition of PIF3 binding to *CDF5* promoter. Suppression of hypocotyl phenotype was also observed for *prr7pif4* and *prr7pif5* compared to *prr7* (Figures 2B and 2E), which suggests that PRR7 directly represses PIF4 transcriptional activity, as previously shown for TOC1 and PIF4 [20], and might also repress PIF5. This scenario might be potentially more complex given that *PIF4*/*5* transcription is regulated

by the clock under SD [2] and at least *PIF4* transcript levels are slightly higher in *prr7* (Figure 2C), in accordance with recent data showing *PIF4* de-repression in *prr* multiple mutants [29]. However, the observation that *CDF5* expression in overexpressing PIF4-HA lines at ZT8 was similar to *pif4* (Figure 2B), a time point where both PRR7 and PIF4 are co-bound to the *pCDF5* (Figure 2A), provides strong support that PRR7 directly suppresses PIF4 transcriptional activation activity towards *CDF5*.

We next examined the antagonistic PIF-PRR interaction in the direct regulation of *CDF5* across the diurnal cycle. Under SD, phytochrome imposes oscillation of PIF3 and probably PIF1 proteins to progressively accumulate during the night, and to degrade rapidly in the morning maintaining residual levels during the day [8,9]. For PIF4 and possibly PIF5, clock and light regulation result in PIF accumulation also during daytime (Figure 2C) [7,10]. In contrast, PRR accumulation is sequential (PRR9/7/5/TOC1) from morning to midnight (Figure 3A) [21,27]. We therefore expected *CDF5* to oscillate with a peak in the early morning and at the end of the night (where presence of the PIFs is maximum) and a trough from morning to midnight (when PRRs accumulate). Indeed, *CDF5* in the WT was detected during the first part of the day (ZT0-ZT3), then declined to almost undetectable levels through ZT15, and accumulated after ZT15 to peak at dawn (Figure 3B). Expression in *pifq* SD and in WT LL at dawn (a condition where PIFs do not accumulate) [28] was lower than WT SD (Figure 3B), supporting the notion that transcript induction leading to the oscillatory pattern of *CDF5* expression in SD depends on the presence of the PIFs (Figure 3B). Analysis of *CDF5* levels in single *pif* and multiple *pifq* (defective in PIF1/3/4/5) mutants at ZT24 showed that the PIF quartet (PIFq) collectively induces *CDF5* expression at dawn, with PIF1 having a lesser contribution (Figure 3C). *CDF5* transcript levels dropped in the WT after 1h of morning light (Figure 3B), concurrent with phy-induced PIF degradation. In contrast, at ZT9, when *CDF5* expression in the WT is almost non-detectable, *CDF5* expression was significantly higher in *prr5*, *prr7*, *prr79*, *prr59*, and *prr579,* with a major contribution for PRR7 (Figure S2B). Compared to WT, *CDF5* expression was higher in *prr7* from ZT3 through midnight (Figure 3D), whereas in *prr59* and *prr79* mutants *CDF5* expression was only slightly higher at dawn in *prr59* and higher from dusk to dawn in *prr79* (Figure 3D). In *toc1*, de-repression of *CDF5* was early compared to WT (Figure S2C), similar to

other PIF-TOC1 co-targets [5]. Because cross-regulation was described in the PRRs [30], with nuclear accumulation of TOC1 depending partly on PRR5, it is likely that TOC1 contributes to the phenotype of PRR5-deficient mutant backgrounds. We also characterized *PRR5* and *PRR7* expression in *prr79* and *prr59* double mutants, respectively. Levels of *PRR5* and *PRR7* were ~1.5-fold higher in *prr59* and *prr79* compared to WT, and *PRR5* phase was delayed in *prr79,* indicative of intricate cross-regulatory pathways (Figure S2D). Significantly, *CDF5* expression in the *prr579* mutant from ZT3-ZT21 was almost linear (Figure 3D), in accordance with the PRRs (with TOC1 possibly also contributing) being responsible for the repression of *CDF5* expression from morning to midnight.

To further examine the PIF-PRR antagonistic interplay, we artificially induced PIF accumulation at the beginning of the night period when PRR levels are high (Figure 3A) [27] by giving a far-red light pulse (FRp) at ZT8 [5,28]. As control we used *PIL1*, a direct PIF target and marker gene for PIF abundance and activity [8]. *PIL1* levels accumulated in the WT immediately after the FRp (Figure 3E), in agreement with the rapid accumulation of PIF proteins after a FRp [9,25,31], and to PRRs not interfering significantly with PIF activity in the regulation of *PIL1,* in accordance with *PIL1* not being a direct target of all PRRs [15]. In striking contrast, expression induction of the PIF-PRR target *CDF5* was repressed in the WT during the first part of the night (ZT8-ZT16) after a FRp, similarly to the control (-FRp) samples (Figure 3E). Interestingly, this repression was much lower in *prr5* and *prr7*, and not observed in *prr579*. In *toc1*, early *CDF5* expression compared to WT (Figures 3E and S2C) was more evident in (+FRp) samples.

Although part of the effect seen in *prr* mutants might come from elevated PIF4/5 levels due to their transcriptional derepression (Fig 2C), together these data support the conclusion that the PRR9/7/5 and TOC1 prevent the transcriptional activation of *CDF5* by PIFs. Given the sequential pattern of expression of *PRR9, 7, 5,* and *TOC1* (Figure 3A) [21], and the progressive accumulation of the PIFs along the night in SD conditions [8], our findings suggest that *CDF5* is sequentially targeted by *PRR9, 7, 5,* and *TOC1* to repress its expression from morning to midnight (when PRR and TOC1 levels are high), to gate PIF direct induction of *CDF5* to dawn when the levels of PRRs and TOC1 are low

and PIFs reach a peak in abundance. We propose that *CDF5* might be a novel target of this PRR and PIF interplay in the promotion of hypocotyl elongation.

Our findings suggest a model where the antagonistic regulation of *CDF5* gene expression by PRRs and PIFs described above might underlie rhythmic growth under SD. In agreement, we observed correlation between the magnitude of hypocotyl length under our SD conditions and *CDF5* levels in *prr* and *pifq* mutants (Figures S3A and S3B). To test this model genetically, we generated seedlings ectopically expressing *CDF5* in a *cdf5* mutant background *(CDF5OX)* (Figure S3C), and quantified the hypocotyl phenotype of WT, *CDF5OX*, and *cdf5* lines under SD. *cdf5* mutants were slightly shorter than WT SD-grown seedlings, whereas *CDF5OX* lines suppressed the *cdf5* phenotype and showed a range from subtle to robustly elongated hypocotyls compared to WT (Figures 4A). We analyzed the elongation rate of *cdf5* and *CDF5OX* lines under SD compared to WT (Figure 4B). As described, the growth rate of WT seedlings is highest during the second half of the night [2]. Elongation rate of *cdf5* seedlings was similar to WT during the day and first part of the night, but it was reduced during the last part of the night, when *CDF5* expression in the WT is maximum, consistent with their short phenotype. Interestingly, elongation rate of *CDF5OX* seedlings was constantly high during the day and most part of the night (Figure 4B). Together, our data suggest that transcriptional control of *CDF5* expression by the PIFs and PRRs is a key regulatory mechanism in growth control.

Next, to genetically test the interplay between CDF5, PIFs and PRRs, we generated *prr7cdf5*, *pifqcdf5* and *pifqCDF5OX* and mutants (Figure S3C) to study their hypocotyl phenotypes. We observed that in SD the quintuple *pifqcdf5* mutant displayed a phenotype similar to *pifq*, indicating that the *cdf5* mutation did not have an additive effect on *pifq* mutation (Figure 4A). This result agrees with PIFq and CDF5 acting in the same signaling pathway. Overexpression of *CDF5* in the *pifq* background partially restored the *pifq* phenotype (Figures 4A), providing additional evidence that CDF5 contributes to growth downstream of the PIFs. Finally, comparison of *prr7* with *prr7cdf5* mutants showed that the long phenotype of *prr7* under SD is reduced when CDF5 is removed in *prr7cdf5* (Figures 4A), suggesting that exaggerated growth in *prr7* is partially a consequence of having elevated levels of CDF5. Together, our results confirm our model

where PRRs and PIFs directly and antagonistically regulate *CDF5* expression to precisely gate CDF5 growth-promoting activity to the end of the night.

We hypothesized that CDF5 might control the expression of growth-related genes at dawn downstream of PIFq. We selected a few PIF-regulated [4], growth-related cell wall [32] and SD growth-marker genes [6,8] to test for their expression in *cdf5* and *CDF5OX* lines. As shown in Figure 4C, *PIL1* and *XTR7* were not significantly affected in *cdf5* or *CDF5OX*, and *IAA19*, *YUCCA8* and three selected cell wall related genes (*AGP4*, *PME*, and *FLA9*) show either significant down-regulation in *cdf5* (*IAA19*), up-regulation in *CDF5OX* (*PME, AGP4*), or both (*YUC8* and *FLA9*), compared to the WT. Interestingly, *AGP4* and *PME* are not PIF-bound genes. These results suggest branching downstream of PIFq, with CDF5 regulating a subset of the PIFq-regulated growth-related genes, in accordance to the partial suppression of the *pifq* phenotype by *CDF5OX* shown above (Figure 4A). Examination of the hypocotyl cell size in SD-grown WT, *cdf5* and *CDF5OX* seedlings by confocal microscopy imaging clearly showed elongated cells in *CDF5OX* hypocotyls compared to WT, whereas cells in *cdf5* appeared shorter (Figure 4D left), which was confirmed by quantification of the hypocotyl cell length (Figure 4D right). Next, we tested *prr7*, which exhibited a longer cell phenotype partially suppressed by genetic removal of *CDF5* in *prr7cdf5* (Figure 4D). In contrast, cell length in *pifq* was shorter than WT, a phenotype that was partially recovered by *CDF5OX* (Figure 4C right). Together, these results support a role for CDF5 in the promotion of cell elongation under the inductive growth condition of SDs downstream of PRRs and PIFs.

Conclusions

Here we found that members of the PRR family of transcriptional repressors (PRR5, 7, and 9), with a key role in the regulation of the central circadian oscillator and clock output processes in plants [12], target growth-related genes that are directly induced by the growth-promoting PIF transcription factors. Given the coincident DNA-binding specificity of PRRs and PIFs (Figure 1A) [15,33], the PIF-PRR physical interaction in the nucleus (Figures 1B and S1A), and their accumulation dynamics during short-day photoperiods (Figure 3A) [2,7,8,11,21], we propose a model in which successive binding of the PRR9, PRR7, and PRR5 to the G-box elements of shared PIF and PRR target genes (like the growth-promoting *CDF5*) acts to sequentially repress transcription of the

PIF-induced transcriptional network starting in the morning (Figure 4E, Figure S4). Given that PRR9/7/5 have not been shown to bind DNA directly, our results agree with the possibility that PIFs might bridge the binding of PRRs to DNA, although competition by direct binding of PRR to G-boxes, or through a PRR- and G-box- binding factor different than PIFq, cannot be completely discarded based on our results. These findings define an expanded framework for previous results showing PRR1/TOC1 repression of PIF transcriptional activity at midnight [5]. At dawn, PRRs and TOC1 are not present, PIF protein accumulation reaches a maximum, and elongation is promoted by PIF-induced expression of growth-promoting genes like *CDF5* (Figure 4E). Collectively, our data reveal that gating of growth occurs not only at the post-dusk hours of the night as previously described for TOC1 [5], but instead starts in the morning and covers all the day period until midnight through the sequential action of the PRR family of transcriptional repressors. The molecular mechanism described here could explain why growth rate under short-day photoperiods is low [2] from morning to midnight in the presence of low PIF3 and PIF1 [9,34] and considerable high amounts of PIF4 (and likely PIF5) [7,10], a regulation critical for fitness by preventing overgrowth (Figure 4A). Our results reveal that gating of growth has evolved in plants to encompass the orchestrated sequential action of members of the PRR family (PRR9/7/5/1) of transcriptional repressors that peak in waves from morning to midnight. This function highlights the dual role of the PRR family of clock oscillator components, as regulators of central clock components and cycling outputs [11,21,35], and as repressors of the physiological output of growth in combined regulation with light pathways that control accumulation of PIFs.

Acknowledgements

We thank D. Somers, S.Prat, G. Coupland, and R. McClung for sharing seed and plasmid resources. We thank G. Steele for generating double and triple *prr* mutants, and the *prrpif* mutant combinations. The work in this manuscript was supported by grants from the Spanish "Ministerio de Economía y Competitividad" (MINECO) BIO2012-31672 and BIO2015-68460-P, and from the Generalitat de Catalunya 2014-SGR-1406 to E.M.; by Marie Curie IRG PIRG06-GA-2009-256420 grant to P.L.; by the European Commission (PCIG2012-GA-2012-334052) and by MINECO (BIO2015-70812-ERC; RYC-2011-

09220) to R.H.; by Royal Society Grant RG2016R1 to G. T-O; by MINECO BIO2013-43184-P to D.A; by MINECO AGL2014-57200-JIN to E.G.M. We acknowledge financial support by the CERCA programme/Generalitat de Catalunya and from MINECO through the "Severo Ochoa Programme for Centers of Excellence in R&D" 2016-2019 (SEV-2015-0533)".

Author contributions

G.M., P.L., and E.M. conceived and designed the study, G.M., A.R., N.V., J.S., G.T-O., C.M.M.G., M.B., R.H., E.G.M., D.A., K.H., P.L., and E.M. acquired, analyzed and interpreted data. G.M., P.L., and E.M. wrote the manuscript.

Declaration of Interests

The authors declare no competing interests.

References

1. Niwa, Y., Yamashino, T., and Mizuno, T. (2009). The Circadian Clock Regulates the Photoperiodic Response of Hypocotyl Elongation through a Coincidence Mechanism in Arabidopsis thaliana. Plant Cell Physiol. *50*, 838–854.

2. Nozue, K., Covington, M.F., Duek, P.D., Lorrain, S., Fankhauser, C., Harmer, S.L., and Maloof, J.N. (2007). Rhythmic growth explained by coincidence between internal and external cues. Nature *448*, 358–361.

3. Nomoto, Y., Kubozono, S., Yamashino, T., Nakamichi, N., and Mizuno, T. (2012). Circadian Clock- and PIF4-Controlled Plant Growth: A Coincidence Mechanism Directly Integrates a Hormone Signaling Network into the Photoperiodic Control of Plant Architectures in Arabidopsis thaliana. Plant Cell Physiol. *53*, 1950–1964.

4. Martín, G., Soy, J., and Monte, E. (2016). Genomic Analysis Reveals Contrasting PIFq Contribution to Diurnal Rhythmic Gene Expression in PIF-Induced and -Repressed Genes. Front. Plant Sci. *7*, 962.

5. Soy, J., Leivar, P., González-Schain, N., Martín, G., Diaz, C., Sentandreu, M., Al-Sady, B., Quail, P.H., and Monte, E. (2016). Molecular convergence of clock and photosensory pathways through PIF3–TOC1 interaction and co-occupancy of target promoters. Proc. Natl. Acad. Sci. U. S. A. *113*, 4870–4875.

6. Nozue, K., Harmer, S.L., and Maloof, J.N. (2011). Genomic Analysis of Circadian Clock-, Light-, and Growth-Correlated Genes Reveals PHYTOCHROME-INTERACTING FACTOR5 as a Modulator of Auxin Signaling in Arabidopsis.

Plant Physiol. *156*, 357–372.

7. Bernardo-García, S., de Lucas, M., Martínez, C., Espinosa-Ruiz, A., Davière, J.-M., and Prat, S. (2014). BR-dependent phosphorylation modulates PIF4 transcriptional activity and shapes diurnal hypocotyl growth. Genes Dev. *28*, 1681–1694.

8. Soy, J., Leivar, P., González-Schain, N., Sentandreu, M., Prat, S., Quail, P.H., and Monte, E. (2012). Phytochrome-imposed oscillations in PIF3 protein abundance regulate hypocotyl growth under diurnal light/dark conditions in Arabidopsis. Plant J. *71*, 390–401.

9. Monte, E., Tepperman, J.M., Al-Sady, B., Kaczorowski, K.A., Alonso, J.M., Ecker, J.R., Li, X., Zhang, Y., and Quail, P.H. (2004). The phytochrome-interacting transcription factor, PIF3, acts early, selectively, and positively in light-induced chloroplast development. Proc. Natl. Acad. Sci. U. S. A. *101*, 16091–16098.

10. Yamashino, T., Nomoto, Y., Lorrain, S., Miyachi, M., Ito, S., Nakamichi, N., Fankhauser, C., and Mizuno, T. (2013). Verification at the protein level of the PIF4-mediated external coincidence model for the temperature-adaptive photoperiodic control of plant growth in Arabidopsis thaliana. Plant Signal. Behav. *8*, e23390.

11. Nakamichi, N., Kiba, T., Henriques, R., Mizuno, T., Chua, N.-H., and Sakakibara, H. (2010). PSEUDO-RESPONSE REGULATORS 9, 7, and 5 Are Transcriptional Repressors in the Arabidopsis Circadian Clock. Plant Cell *22*, 594–605.

12. Farré, E.M., and Liu, T. (2013). The PRR family of transcriptional regulators reflects the complexity and evolution of plant circadian clocks. Curr. Opin. Plant Biol. *16*, 621–629.

13. Nakamichi, N., Kita, M., Ito, S., Yamashino, T., and Mizuno, T. (2005). PSEUDO-RESPONSE REGULATORS, PRR9, PRR7 and PRR5, Together Play Essential Roles Close to the Circadian Clock of Arabidopsis thaliana. Plant Cell Physiol. *46*, 686–698.

14. Kaczorowski, K.A., and Quail, P.H. (2003). Arabidopsis PSEUDO-RESPONSE REGULATOR7 Is a Signaling Intermediate in Phytochrome-Regulated Seedling Deetiolation and Phasing of the Circadian Clock. Plant Cell *15*, 2654–2665.

15. Liu, T.L., Newton, L., Liu, M.-J., Shiu, S.-H., and Farré, E.M. (2016). A G-Box-Like Motif Is Necessary for Transcriptional Regulation by Circadian Pseudo-Response Regulators in Arabidopsis. Plant Physiol. *170*, 528–539.

16. Pfeiffer, A., Shi, H., Tepperman, J.M., Zhang, Y., and Quail, P.H. (2014). Combinatorial Complexity in a Transcriptionally Centered Signaling Hub in Arabidopsis . Mol. Plant *7*, 1598–1618.

17. Martínez-García, J.F., Huq, E., and Quail, P.H. (2000). Direct Targeting of Light Signals to a Promoter Element-Bound Transcription Factor. Science *288*, 859–863.

18. Fornara, F., de Montaigu, A., Sánchez- Villarreal, A., Takahashi, Y., Ver Loren van Themaat, E., Huettel, B., Davis, S.J., and Coupland, G. (2015). The GI–CDF module of Arabidopsis affects freezing tolerance and growth as well as flowering. Plant J. *81*, 695–706.

19. Fornara, F., Panigrahi, K.C.S., Gissot, L., Sauerbrunn, N., Rühl, M., Jarillo, J.A., and Coupland, G. (2009). Arabidopsis DOF Transcription Factors Act Redundantly to Reduce CONSTANS Expression and Are Essential for a Photoperiodic Flowering Response. Dev. Cell *17*, 75–86.

20. Zhu, J.-Y., Oh, E., Wang, T., and Wang, Z.-Y. (2016). TOC1–PIF4 interaction mediates the circadian gating of thermoresponsive growth in Arabidopsis. Nat. Commun. *7*, 13692.

21. Matsushika, A., Makino, S., Kojima, M., and Mizuno, T. (2000). Circadian Waves of Expression of the APRR1/TOC1 Family of Pseudo-Response Regulators in Arabidopsis thaliana: Insight into the Plant Circadian Clock. Plant Cell Physiol. *41*, 1002–1012.

22. Nakamichi, N., Kiba, T., Kamioka, M., Suzuki, T., Yamashino, T., Higashiyama, T., Sakakibara, H., and Mizuno, T. (2012). Transcriptional repressor PRR5 directly regulates clock-output pathways. Proc. Natl. Acad. Sci. U. S. A. *109*, 17123–17128.

23. Huang, W., Pérez-García, P., Pokhilko, A., Millar, A.J., Antoshechkin, I., Riechmann, J.L., and Mas, P. (2012). Mapping the Core of the Arabidopsis Circadian Clock Defines the Network Structure of the Oscillator. Science *336*, 75–79.

24. Haudry, A., Platts, A.E., Vello, E., Hoen, D.R., Leclercq, M., Williamson, R.J., Forczek, E., Joly-Lopez, Z., Steffen, J.G., Hazzouri, K.M., *et al*. (2013). An atlas of over 90,000 conserved noncoding sequences provides insight into crucifer regulatory regions. Nat Genet *45*, 891–898.

25. Lorrain, S., Allen, T., Duek, P.D., Whitelam, G.C., and Fankhauser, C. (2008). Phytochrome-mediated inhibition of shade avoidance involves degradation of growth-promoting bHLH transcription factors. Plant J. *53*, 312–323.

26. Al-Sady, B., Ni, W., Kircher, S., Schäfer, E., and Quail, P.H. (2006). Photoactivated Phytochrome Induces Rapid PIF3 Phosphorylation Prior to Proteasome-Mediated Degradation. Mol. Cell *23*, 439–446.

27. Fujiwara, S., Wang, L., Han, L., Suh, S.-S., Salomé, P.A., McClung, C.R., and Somers, D.E. (2008). Post-translational Regulation of the Arabidopsis Circadian Clock through Selective Proteolysis and Phosphorylation of Pseudo-response

366 Regulator Proteins. J. Biol. Chem. *283*, 23073–23083.

367 28. Soy, J., Leivar, P., and Monte, E. (2014). PIF1 promotes phytochrome-regulated
368 growth under photoperiodic conditions in Arabidopsis together with PIF3, PIF4,
369 and PIF5. J. Exp. Bot. *65*, 2925–2936.

370 29. Hayama, R., Sarid- Krebs, L., Richter, R., Fernández, V., Jang, S., and Coupland,
371 G. (2017). PSEUDO RESPONSE REGULATORs stabilize CONSTANS protein
372 to promote flowering in response to day length. EMBO J. *36*, 904–918.

373 30. Wang, L., Fujiwara, S., and Somers, D.E. (2010). PRR5 regulates phosphorylation,
374 nuclear import and subnuclear localization of TOC1 in the Arabidopsis circadian
375 clock. EMBO J. *29*, 1903–1915.

376 31. Shen, H., Moon, J., and Huq, E. (2005). PIF1 is regulated by light-mediated
377 degradation through the ubiquitin-26S proteasome pathway to optimize
378 photomorphogenesis of seedlings in Arabidopsis. Plant J. *44*, 1023–1035.

379 32. Pelletier, S., Van Orden, J., Wolf, S., Vissenberg, K., Delacourt, J., Ndong, Y.A.,
380 Pelloux, J., Bischoff, V., Urbain, A., Mouille, G., *et al*. (2010). A role for pectin
381 de-methylesterification in a developmentally regulated growth acceleration in
382 dark-grown Arabidopsis hypocotyls. New Phytol. *188*, 726–739.

383 33. Heyndrickx, K.S., de Velde, J. Van, Wang, C., Weigel, D., and Vandepoele, K.
384 (2014). A Functional and Evolutionary Perspective on Transcription Factor
385 Binding in Arabidopsis thaliana. Plant Cell *26*, 3894-3910.

386 34. Huq, E., Al-Sady, B., Hudson, M., Kim, C., Apel, K., and Quail, P.H. (2004).
387 PHYTOCHROME-INTERACTING FACTOR 1 Is a Critical bHLH Regulator of
388 Chlorophyll Biosynthesis. Science *305*, 1937–1941.

389 35. Kamioka, M., Takao, S., Suzuki, T., Taki, K., Higashiyama, T., Kinoshita, T., and
390 Nakamichi, N. (2016). Direct Repression of Evening Genes by CIRCADIAN
391 CLOCK-ASSOCIATED1 in the Arabidopsis Circadian Clock. Plant Cell *28*, 696–
392 711.

393 36. Kikis, E.A., Khanna, R., and Quail, P.H. (2005). ELF4 is a phytochrome-regulated
394 component of a negative-feedback loop involving the central oscillator
395 components CCA1 and LHY. Plant J. *44*, 300–313.

396 37. Leivar, P., Monte, E., Oka, Y., Liu, T., Carle, C., Castillon, A., Huq, E., and Quail,
397 P.H. (2008). Multiple Phytochrome-Interacting bHLH Transcription Factors
398 Repress Premature Seedling Photomorphogenesis in Darkness. Curr. Biol. *18*,
399 1815–1823.

400 38. Khanna, R., Shen, Y., Marion, C.M., Tsuchisaka, A., Theologis, A., Schäfer, E.,
401 and Quail, P.H. (2008). The Basic Helix-Loop-Helix Transcription Factor PIF5
402 Acts on Ethylene Biosynthesis and Phytochrome Signaling by Distinct

Mechanisms. Plant Cell *19*, 3915-3929.

39. Michael, T.P., Salomé, P.A., Yu, H.J., Spencer, T.R., Sharp, E.L., McPeek, M.A., Alonso, J.M., Ecker, J.R., and McClung, C.R. (2003). Enhanced Fitness Conferred by Naturally Occurring Variation in the Circadian Clock. Science *302*, 1049–1053.

40. Fujimori, T., Yamashino, T., Kato, T., and Mizuno, T. (2004). Circadian-Controlled Basic/Helix-Loop-Helix Factor, PIL6, Implicated in Light-Signal Transduction in Arabidopsis thaliana. Plant Cell Physiol. *45*, 1078–1086.

41. Más, P., Alabadí, D., Yanovsky, M.J., Oyama, T., and Kay, S.A. (2003). Dual Role of TOC1 in the Control of Circadian and Photomorphogenic Responses in Arabidopsis. Plant Cell *15*, 223–236.

42. Liu, T., Carlsson, J., Takeuchi, T., Newton, L., and Farré, E.M. (2013). Direct regulation of abiotic responses by the Arabidopsis circadian clock component PRR7. Plant J. *76*, 101–114.

43. Nicol, J.W., Helt, G.A., Blanchard Steven G., J., Raja, A., and Loraine, A.E. (2009). The Integrated Genome Browser: free software for distribution and exploration of genome-scale datasets. Bioinformatics *25*, 2730–2731.

44. Huang, D.W., Sherman, B.T., Tan, Q., Collins, J.R., Alvord, W.G., Roayaei, J., Stephens, R., Baseler, M.W., Lane, H.C., and Lempicki, R.A. (2007). The DAVID Gene Functional Classification Tool: a novel biological module-centric algorithm to functionally analyze large gene lists. Genome Biol. *8*, R183.

45. Toledo-Ortiz, G., Johansson, H., Lee, K.P., Bou-Torrent, J., Stewart, K., Steel, G., Rodríguez-Concepción, M., and Halliday, K.J. (2014). The HY5-PIF Regulatory Module Coordinates Light and Temperature Control of Photosynthetic Gene Transcription. PLoS Genet. *10*, e1004416.

46. Ni, M., Tepperman, J.M., and Quail, P.H. (1998). PIF3, a Phytochrome-Interacting Factor Necessary for Normal Photoinduced Signal Transduction, Is a Novel Basic Helix-Loop-Helix Protein. Cell *95*, 657–667.

47. Wang, L., Kim, J., and Somers, D.E. (2013). Transcriptional corepressor TOPLESS complexes with pseudoresponse regulator proteins and histone deacetylases to regulate circadian transcription. Proc. Natl. Acad. Sci. U. S. A. *110*, 761–766.

48. Tanaka, Y., Kimura, T., Hikino, K., Goto, S., Nishimura, M., Mano, S., and Nakagawa, T. (2012). Gateway Vectors for Plant Genetic Engineering: Overview of Plant Vectors, Application for Bimolecular Fluorescence Complementation (BiFC) and Multigene Construction. InTech.

49. Martín, G., Leivar, P., Ludevid, D., Tepperman, J.M., Quail, P.H., and Monte, E. (2016). Phytochrome and retrograde signalling pathways converge to

antagonistically regulate a light-induced transcriptional network. Nat. Commun. *7*, 11431.

Figure Legends

Figure 1. Analysis of coincident co-binding of PRRs and PIFs to dawn-phased genes under SD identifies *CDF5* as a PIF- and PRR5/7/9-bound gene. (A) (Left) Comparison of PIF-bound [16] and PRR5-, 7- and/or PRR9-bound genes [15] (gene lists provided in Dataset 1) defines three groups of genes: "PIF only" (1,384 genes), "PRR only" (3,013 genes), and "PIF-PRR" (1,460 genes). (Middle) Percentage of PIF-bound genes in genes bound by single or a combination of PRRs. (Right) Frequency of pairwise distance in base pairs (bp) between the PIF- and PRR- binding sites in each of the "PIF-PRR" co-bound genes. **(B)** BiFC assay of the PRRs and PIF3 fusions to N- and C-terminal fragments of YFP, respectively, in transfected onion cells. The combinations of PIF3-cYFP and TOC1-nYFP or pGW-nYFP were used as positive and negative control, respectively. (Left) YFP fluorescence image. (Center) Bright-field image. (Right) Merge of YFP fluorescence and bright-field image. **(C)** Expression phases in SD of gene sets defined in (A): "PIF–PRR" (purple), "PRR only" (pink), and "PIF only" (yellow). Phases are indicated on the circumference, and fold-change phase enrichment of genes (count/expected) on the radius. Day is shown in yellow; night in gray. See also Figure S1 and Dataset 1. **(D)** Comparison of PIF- [16], PRR5-, 7-, and PRR9-bound genes [15], and "PIF/SD-induced" genes [4] (see Dataset 1 for details) **(E)** Visualization of ChIP-seq and ChIP-qPCR data in the genomic region encompassing the *CDF5* locus co-bound by PIFs, PRRs and TOC1. For PIF (orange), ChIP-seq tracks show the pile-up of all the reads obtained from MACS analyses (model based for ChIP-seq) of the dataset from each experiment [16]. Each corresponding WT-ChIP/input control is overlaid in dark gray. For PRR (purple), filled rectangles indicate the PRR9, PRR7 and PRR5 peaks defined by ChIP-seq in [15]. Empty rectangles indicate peaks only described by ChIP-qPCR, in [22] for PRR9 and in Figure 2A for TOC1. Conserved non-coding sequences (CNS) (blue) are defined in [24]. G- and PBE-box: vertical lines indicate motif positions. See also Figure S1 and Dataset 1.

Figure 2. PRR7 represses PIF3 ability to induce *CDF5* expression in SD. (A) PRR7, TOC1, PIF3, and PIF4 binding to the G-box containing region of the *CDF5* promoter at ZT8, ZT14, and ZT24 under SD. For ChIP-qPCR analysis, samples of SD-grown *pPRR7::PRR7-GFP* (PRR7-GFP), *pTOC1::TOC1:YFP* (TMG), *pPIF3::YFP:PIF3*

(YFP-PIF3), and *35S::PIF4-HA* (PIF4-HA), were harvested at the indicated times during the third day and were immunoprecipitated using anti-GFP or anti-HA antibodies. Data are from three independent ChIP experiments, and error bars indicate SE. Statistically significant differences between mean values by Student's *t*-test relative to WT are shown (*P<0.05; **P<0.01 and ***P<0.001). n.s., not significant. WT controls were Col-0 for YFP-PIF3, PIF4-HA, and PRR7-GFP, and C24 for TMG seedlings. Ab: samples immunoprecipitated with antibody. No Ab: control samples immunoprecipitated without antibody. **(B)** *CDF5* expression levels in WT, *pif3*, *pif4*, *pif5*, *prr7*, *prr7pif3*, *prr7pif4*, *prr7pif5, and* PIF4-HA. Samples were harvested at ZT9 during the third day of growth (ZT8 for PIF4-HA), analyzed by qRT-PCR and normalized to *PP2A*. Data are from three independent biological replicates relative to WT set at one. Different letters denote statistically significant differences among means by Tukey-b test (P<0.05). Error bars indicate SE. **(C)** WT and *prr7* seedlings grown for 2 d in SD conditions were harvested during the third day at the indicated times. Expression levels of *PIF3* and *PIF4* were analyzed by qRT-PCR, and values were normalized to *PP2A*. Data plotted are mean ± SE relative to *PIF4* WT at ZT3 set at one, n = 2 independent biological experiments, each assayed in triplicate. **(D)** PIF3 protein levels in 3-day old SD-grown WT and *prr7* seedlings at ZT24. C-blue, coomassie blue; NS, non-specific bands. **(E)** Hypocotyl length in seedlings as in (B) (except for PIF4-HA) grown for 3 days in SD. Different letters denote statistically significant differences among means by Tukey-b test (P<0.05). Data are means ± SE of at least 50 seedlings. See also Figure S2.

Figure 3. PRRs and PIFs antagonistically regulate *CDF5* to dawn-phase its expression under diurnal SD conditions. **(A)** Transcriptional waves of *PRR9/7/5* and *TOC1* expression during the third day in SD at the indicated times. Each gene is expressed relative to its maximum expression value set at one. **(B-D)** *CDF5* expression in WT, *pif*, and *prr* analyzed by qRT-PCR **(B)** Expression in 2-day-old SD-grown seedlings harvested during the third day at the indicated times in seedlings kept under SD or moved to continuous light (LL). Data are relative to WT SD ZT3. **(C)** Expression in 3-day-old seedlings at ZT24 grown as in (B). Data are from two independent biological replicates and are relative to WT samples set at one. Percentage is the contribution of each PIF to *CDF5* expression in SD considering *pifq* and WT values as 0% and 100%,

respectively. Error bars indicate SE. **(D)** Expression in WT, *prr5*, *prr7*, *prr9*, *prr59*, *prr79*, and *prr579* seedlings grown for 2 d in SD conditions during the third day at the indicated times. Expression is relative to *CDF5* WT at ZT3. **(E)** *PIL1* and *CDF5* expression in WT, *prr* and *toc1* analyzed by qRT-PCR. Two-day-old SD-grown seedlings were treated with a 15-min far-red pulse (FRp) at ZT8 on the third day ((+) FRp samples, in red), and harvested during the night at ZT9, ZT12, ZT16 and ZT20. (-) FRp control samples (in black) did not receive a FRp. Data are relative to ZT8 set at one for each genotype. (A-E) All samples were normalized to *PP2A*. (A-B, D-E) Data plotted are mean ± SE, n=2 independent biological experiments, each assayed in triplicate. See also Figures S2 and S3.

Figure 4. PRR- and PIF-mediated regulation of cell elongation requires CDF5. (A) Hypocotyl length of WT, *cdf5*, *CDF5OX*, *pifq*, *pifqCDF5OX*, *prr7*, and *prr7cdf5* grown for 3 and 4 days in SD (left). Data are means ± SE of at least 35 seedlings. Different letters denote statistically significant differences among means by Tukey-b test ($P<0.05$). Visible phenotypes of 3-day-old seedlings are shown in the right. Scale bar = 5 mm. **(B)** Hypocotyl elongation rate for WT, *cdf5* and *CDF5OX 5.7* under SD conditions. Seedling growth was monitored every 2 hours during the third day. Average of 12 seedlings is shown, and SE is indicated by the shaded area. **(C)** Expression of PIF-regulated growth marker genes (top) and cell wall genes (bottom) in 3-day-old SD-grown WT, *cdf5* and *CDF5OX 5.7* seedlings at ZT24, analyzed by qRT-PCR and normalized to *PP2A*. Data are from three independent biological replicates normalized to WT set at one. Error bars indicate SE. Statistically significant differences between mean values by Student's *t*-test relative to WT are shown (*$P<0.05$; **$P<0.01$ and ***$P<0.001$). n.s., not significant. **(D)** (Left) Visual phenotypes of cell area in 3d-old SD-grown WT, *cdf5* and *CDF5OX 5.7* seedling hypocotyls. Scale bar = 200μm. (Right) Quantification of cell length in WT, *cdf5*, *CDF5OX 5.7*, *pifq*, *pifqCDF5OX* (*pifqOX* in the figure), *prr7*, and *prr7cdf5*. Seedlings were grown for 3 days in SD. Data are means ± SE of at least 100 cells from 3-4 independent seedlings. Different letters or an asterisk denote statistically significant differences among means by Tukey-b test ($P<0.05$) or by t-test ($P<0.05$), respectively. **(E)** Model of the proposed role of PRRs as repressors of PIF activity to regulate cell elongation through CDF5. PIFs bind to the *CDF5* promoter and induce *CDF5*

transcription in the absence of PRRs. If PRRs are present, PRRs repress PIF transcriptional activity though direct PIF-PRR interaction. Based on current data, PRRs and PIFs could bind to the same or different nearby G-boxes, or alternatively, PRRs could bind indirectly to G-boxes through DNA-bound PIFs or other G-box and PRR-binding factors. Sequential PRR9/7/5 and PRR1/TOC1 accumulation from morning to midnight gate PIF-induction of *CDF5* to dawn, when it induces hypocotyl cell elongation by upregulating growth-related genes like *YUC8*, or *FLA9*. See also Figures S3 and S4.

STAR Methods

Contact for Reagent and Resource Sharing

Further information and requests for resources and reagents should be directed to and will be fulfilled by the Lead Contact, Elena Monte (elena.monte@cragenomica.es).

Experimental Model

The *Arabidopsis thaliana* (L.) accession Columbia (Col-0), C24, and mutants used here were obtained from the mentioned references or generated in this work (See Key Resources Table).

Method Details

Seedling Growth and Hypocotyl and Cell Measurements

Arabidopsis thaliana seeds used in this manuscript include the previously described *cdf5-1* [19], *toc1-101* [36], *pPRR7::PRR7-GFP* (PRR7-GFP) [27], *pPIF3::YFP:PIF3* (YFP-PIF3) [26], *p35S::PIF4-HA* [25], *pif1-1* [34], *pif3-3* [9], *pif4-2* [37], *pif5-3* [38], *pifq* [37], *prr5-1*, *prr7-3*, and *prr9-1* [39], *pif3-1* [9], *pif4-101* [25], *pil6-1* (*pif5* mutant) [40], and the newly generated *prr7-3pif3-1* (*prr7pif3*), *prr7-3pif4-101* (*prr7pif4*), *prr7-3pil6-1* (*prr7pif5*), *prr7-3prr9-1* (*prr79*), *prr5-1prr9-1* (*prr59*), *prr5-1prr7-3prr9-1* (*prr579*), and *prr7-3cdf5-1* (*prr7cdf5*) in Col-0 ecotype, and *pTOC1::TOC1:YFP* (TMG) [41] in C24 ecotype. *CDF5OX* lines were generated by cloning the *CDF5* ORF under the regulation of the 35S promoter in the pH7FWG2 vector. The resulting 35S::CDF5-GFP construct was transformed into *cdf5* to generate *CDF5OX* lines, and into *pifq* to generate *pifqCDF5OX* lines.

565 Seeds were sterilized and plated on Murashige and Skoog medium without sucrose.
566 Seedlings were stratified for 4d at 4C in darkness, and seedling growth was done in short
567 days (8h light + 16h dark) or continuous white light (85μmol·m-2·s-1) for the time
568 indicated in each experiment. Hypocotyl measurements in Figures 2E, 4A and S3B were
569 done using Image J (National Institutes of Health). Saturating FR pulses were 30μmol·m-
570 2·s-1 for 15min. Samples at ZT0 and ZT24 were collected in the dark, whereas at ZT8
571 were in the light. For hypocotyl growth rate measurements (Figure 4B), image acquisition
572 was done using the ActiveWebCam software (www.pysoft.com) under infrared light
573 background using modified webcams (Microsoft Life Cam Studio). Twelve seedlings
574 were measured individually every 2 hours throughout the diurnal cycle, the difference in
575 hypocotyl length between the two time points was calculated, and the elongation rate was
576 expressed as mm/h. The mean and SE for the 12 seedlings are represented. Cell size was
577 visualized in seedlings stained with propidium iodine (10μg/ml) (Calbiochem) using a
578 confocal laser microscope Leica SP5 (570 nm-666 nm). Cell length was measured in
579 pictures taken with an optic microscope (AixoPhot DP70) (Figure 4D).

580 ChIP-seq Data Analysis and Visualization

581 Comparison of ChIP-seq data shown in Figure 1A was performed using PIF- [16] and
582 PRR9/7/5-associated peaks from [15], which contained novel PRR9 and re-analyzed
583 ChIP-seq data for PRR5 [22] and PRR7 [42], considering only the PRR binding sites
584 located upstream of the transcriptional start site TSS as in [16]. The same comparison
585 was performed in Figure 1D adding the PIF/SD-induced gene set from [4]. Distance
586 between PIF and PRR peaks was calculated separately for all the different pair-wise
587 combinations associated to a given gene. To jointly visualize the Chip-Seq data for PRR
588 [15] and PIFs [16],and the conserved noncoding sequences (CNS) regions [24] (Figure
589 1E), the Integrated Genome Browser (IGB) [43] was used. Data was obtained from
590 http://mustang.biol.mcgill.ca (CNS), GSE71397 (PRRs) and GSE43286 (PIFs).
591 Expression phases shown in Figures 1C and S1C were analyzed using the PHASER tool
592 (http://phaser.mocklerlab.org) for SD (Col-0_SD), LD (longday), and LL (LL23_LDHH).
593 The PHASER tool generated over-representation p-values for each phase (Dataset 1).
594 DAVID system [44] was used to identify enriched GO biological terms (Figure S1B).

595 Chromatin Immunoprecipitation (ChIP) Assays

Chromatin immunoprecipitation (ChIP) and ChIP-qPCR assays (Figure 2A) were performed as in [5,45]. For PIF3-YFP, all process was performed in the dark under green safelight. Seedlings (3g) were vacuum-infiltrated with 1% formaldehyde and cross-linking was quenched by vacuum infiltration with 0.125 M glycine for 5 min. Tissue was ground, and nuclei-containing cross-linked protein and DNA were purified by sequential extraction on Extraction Buffer 1 (0.4M Sucrose, 10 mM Tris-HCL pH8, 10mM $MgCl_2$, 5mM ß-mercaptoethanol, 0.1mM PMSF, 50 µM MG132, proteinase inhibitor cocktail), Buffer 2 (0.25M Sucrose, 10mM Tris-HCL pH8, 10mM $MgCl_2$, 1% Triton X-100, 5mM ß-mercaptoethanol, 0.1mM PMSF, 50 µM MG132, proteinase inhibitor cocktail), and Buffer 3 (1.7M Sucrose, 10 mM Tris-HCL pH8, 0.15% Triton X-100, 2mM $MgCl_2$, 5mM ß-mercaptoethanol, 0.1mM PMSF, 50 µM MG132, proteinase inhibitor cocktail). Nuclei were resuspended in nuclei lysis buffer (50 mM Tris-HCL pH8, 10 mM EDTA, 1 % SDS, 50 µM MG132, proteinase inhibitor cocktail), sonicated for 10X 30sec, and diluted 10X in Dilution Buffer (0.01% SDS, 1% Triton X-100, 1.2 mM EDTA, 16.7 mM Tris-HCL pH8, 167 mM NaCl). Overnight incubation was performed with the corresponding antibody (or with no antibody as control) at 4C overnight, and immunoprecipitation was performed using dynabeads. Washes were done sequentially in Low Salt Buffer (0.1% SDS, 1% Triton X-100, 2 mM EDTA, 20 mM Tris-HCL pH8, 150 mM NaCl), High Salt Buffer (0.1% SDS, 1% Triton X-100, 2 mM EDTA, 20 mM Tris-HCL pH8, 500 mM NaCl), LiCl Buffer (0.25M LiCl, 1% NP40, 1% deoxycholic acid sodium, 1 mM EDTA, 10 mM Tris-HCL pH8), and TE X1. Immunocomplexes were eluated in Elution Buffer (1%SDS, 0.1M $NaHCO_3$), de-crosslinked overnight at 65C in 10 mM NaCl, and then treated with proteinase K. DNA was purified using Qiagen columns, eluted in 100 uL of Qiagen elution buffer, and 2 uL were used for qPCR (ChIP-qPCR) using *CDF5* promoter-specific primers (Table S1) spanning the region containing the predicted binding sites for the PIFs [16]. Three biological replicates were performed for all the "Antibody" samples (two for WT TMG at ZT8), and one for the "No Antibody". Calculations of percent input were done following the protocol available at www.thermofisher.com.

Yeast Two-Hybrid Assays

For yeast two-hybrid assays shown in Figure S1A, we used PIF3 (pGAD424) and PIF4 (pGADT7) described previously [7,46]. PRR fragments were PCR-amplified from PRR templates [47] with primers containing restriction sites (XmaI/BamHI for PRR5 and PRR9, EcoRI/XmaI for PRR7) (Table S1), cloned into pTOPO vector (NZYTech), sequenced and cloned into pGBKT7 (Clontech). To assess interactions, constructs were co-transformed into yeast AH109 cells (Clontech). Yeast transformants were selected on synthetic dropout medium (SD) deficient in leucine and tryptophan (-LT), and interaction was assayed quantitatively by a ß-Galactosidase assay performed using ortho-nitrophenyl- ß-D-galacpyranoside as a substrate following manufacturer´s instructions.

Bimolecular Fluorescence Complementation (BiFC) Assays

For bimolecular fluorescence complementation (BiFC) shown in Figure 1B, the coding regions of PIF3 and TOC1 [5] were cloned into pGWcY and pGWnY vectors [48], respectively. PRR5-, PRR7- and PRR9-nYFP are from [47]. Preparation of samples and bombardment of onion cells were done as in [5]. Briefly, the inner layers of spring onions were cut in 2 x 2 cm squares and used for particle bombardment. Each sample was transfected with 1 μg of each plasmid coupled to tungsten particles using a Biolistic Particle Delivery System PDS-1000 (Bio-Rad). After bombardment, onions were exposed to a saturating 15 min FR pulse and incubated overnight in dark conditions. The upper epidermal layer was removed, placed in a microscope slide and visualized using a confocal laser scanning microscope Olympus FV1000 (Objective Lens UPLSAPO 20X, Laser Wavelength: 514 nm, Emission window: 525-600 nm).

Protein Extraction and Immunoblot

Total protein extracts to detect endogenous PIF3 were prepared from 3 day-old SD-grown seedlings harvested at ZT24 in the dark (Figure 2D). Total protein extracts to detect endogenous PIF3 were prepared from 3 day-old SD-grown seedlings harvested at ZT24 in the dark (Figure 2D). Extraction buffer and protein quantification were done essentially as described [49]: Samples were collected and frozen in liquid nitrogen, and manually ground under frozen conditions before resuspension in boiling extraction buffer (100 mM MOPS (pH 7.6), 2% SDS, 10% glycerol, 4mM EDTA, 50mM Sodium metabisulfite ($Na_2S_2O_5$), $2gl^{-1}$ aprotinin, $3gl^{-1}$ leupeptin, $1gl^{-1}$ pepstatin and 2 mM

PMSF). Total protein was quantified using a Protein DC kit (Bio-Rad), and ß-mercaptoethanol was added just before loading. Aliquots of 100 ug for each sample were treated for 5min at 95C and subjected to 12.5% SDS- PAGE gels. Proteins were then transferred to Immobilon-P membrane (Millipore), and immunodetection of endogenous PIF3 was performed using a anti-PIF3 antibody [26] (1:10,000 dilution) incubated with Hikari solution (Nacalai Tesque). Peroxidase-linked anti rabbit secondary antibody (1:5,000 dilution) and a SuperSignal West Femto chemiluminescence kit (Pierce) were used for detection of luminescence using LAS-4000 Image imaging system (Fujifilm). The membrane was stained with Coomassie blue as a loading control.

Gene Expression Analysis

Quantitative RT-PCR, RNA extraction, cDNA synthesis and qRT-PCR were done as described [49]. Briefly, 1 mg of total RNA extracted using the RNeasy Plant Mini Kit (Qiagen) were treated with DNase I (Ambion) according to the manufacturer's instructions. First-strand cDNA synthesis was performed using the SuperScript III reverse transcriptase (Invitrogen) and oligo dT as a primer (dT30). cDNA was then treated with RNase Out (Invitrogen) before 1:20 dilution with water, and 2 ul was used for real-time PCR (Light Cycler 480; Roche) using SYBR Premix Ex Taq (Takara) and primers at a 300 nM concentration. Gene expression in time-course analyses (Figures 2C, 3A, 3B, 3D, 3E, S2C and S2D) was measured in two independent biological replicates, with three technical replicates for each biological sample, and the mean of the biological replicates ± SE is shown. For specific time points in Figures 2B, 4C, S2A, S2B, and S3C, gene expression was measured in three independent biological replicates, and in Figure 3C, corresponds to two biological replicates, with three technical replicates for each biological sample. *PP2A* (*AT1G13320*) was used for normalization.

Quantification and Statistical Analysis

Differences between means were statistically analyzed by one-way analysis of variance using Tukey-b post hoc multiple comparison test (IBM SPSS Statistics Software) or homoscedastic Student's t-test (Excel Microsoft), as indicated in the figure legends. Statistically significant differences were defined as those with a P value < 0.05. Significance level is indicated as * $P < 0.05$, ** $P < 0.01$ and *** $P < 0.001$.

Supplemental Tables

Dataset 1: Comparison of genome-wide loci associated to PIFs and PRR9, 7 and 5. Related to Figure 1.

Table S1: List of Oligonucleotides. Related to STAR Methods.

CellPress

TABLE FOR AUTHOR TO COMPLETE

Please upload the completed table as a separate document. ***Please do not add subheadings to the Key Resources Table.*** *If you wish to make an entry that does not fall into one of the subheadings below, please contact your handling editor. (****NOTE:*** *For authors publishing in Current Biology, please note that references within the KRT should be in numbered style, rather than Harvard.)*

KEY RESOURCES TABLE

REAGENT or RESOURCE	SOURCE	IDENTIFIER
Antibodies		
Anti-GFP	Invitrogen	Cat# A11122
Peroxidase-linked anti rabbit secondary antibody	Sigma	Cat# NA934
Anti-PIF3	[26]	N/A
Anti-HA	Abcam	Cat# 9110
Bacterial and Virus Strains		
AH109	Clontech	N/A
E. coli DH5α	N/A	N/A
A. tumefaciens GV3031	N/A	N/A
Chemicals, Peptides, and Recombinant Proteins		
Formaldehyde	ThermoFisher Scientific	Cat# 28908
Glycine	GE Healthcare Life Sciences	Cat# 17-1323-01
EDTA	Thermo Scientific	Cat# 17892
Tris-HCL	Sigma	Cat# C4706-2G
Proteinase K	ThermoFisher Scientific	Cat# EO0491
Sucrose	Applichem	Cat# A1125.1000
MgCl2	Calbiochem	Cat# 442611
PMSF	Applichem	Cat# A0999,0025
MG132	Merck	Cat# 474790
Proteinase Inhibitor Cocktail	Roche	Cat# 4693116001
Triton X-100	Applichem	Cat# A1388.10000
NaCl	Scharlau	Cat# SO02271000
LiCl	Merck	Cat# 1,056,790,250
NP40	Sigma	Cat# 74385
Deoxycholic acid sodium	Sigma	Cat# D6750
$NaHCO_3$	Merck	Cat# 6329
Dropout medium (-AHLT)	Clontech	Cat# 630428
Yeast Nitrogen Base w/o aa & ammonium sulfate	Conda	Cat# 1553.00
Ammonium Sulfate	Sigma	Cat# A4418
D-Glucose	Applichem	Cat# 3O000431
European bacteriological Agar	Conda	Cat# 1800.00
His	Sigma	Cat# H8125
Trp	Sigma	Cat# T0254
Leu	Sigma	Cat# L8912
Ade	Sigma	Cat# A9126

Propidium iodine	Calbiochem	Cat# 537059-
Ortho-nitrophenyl- ß-D-galacpyranoside	ThermoFisher Scientific	Cat# 34055
DNase I	Ambion	Cat# AM2224
RNase Out	Invitrogen	Cat# 10777019
SYBR Premix Ex Taq	Roche	Cat# 04707516001
MOPS (pH 7.6)	Sigma	Cat# M1254
SDS	Amresco	Cat# 0227
Glycerol	Applichem	Cat# A2926
EDTA	Thermo Scientific	Cat# 17892
Aprotinin	Applichem	Cat# A2132
Leupeptin	Applichem	Cat# A2183
Pepsatin	Applichem	Cat# A2205
PMSF	Applichem	Cat# A0999
ß-mercaptoethanol	Fluka	Cat# 03700
GFP Agarose Beads	MBL	Cat# D153-8
rProtein A-Sepharose	Bionova	Cat# 1-888-752-2568
Hikari solution	Nacalai Tesque	Cat# 02270-81
Sodium metabisulfite	Sigma	Cat# 255556
XmaI	Roche	Cat# ER0171
BamHI	Roche	Cat# 10 220 612 001
EcoRI	Roche	Cat# 10 703 737 001
T4 DNA Ligase	NZYtech	Cat# MB00703
BP Clonase II	Gateway	Cat# 11789-020
LR Clonase II	Gateway	Cat# 11791-020
Critical Commercial Assays		
RNeasy Plant Mini	Qiagen	Cat# 74904
SuperScript III reverse transcriptase	Invitrogen	Cat# 18080044
Protein DC	Bio-Rad	Cat# 5000121
SuperSignal West Femto chemiluminescence	Thermo Scientific	Cat# 34095
QIAquick gel extraction kit	Qiagen	Cat# QIA28704
Dynabeads	Invitrogen	Cat# 10004D
Immobilon-P membrane	Millipore	Cat# IPVH00010
Experimental Models: Organisms/Strains		
Col-0	N/A	N/A
C24	N/A	N/A
cdf5-1	[19]	N/A
toc1-101	[36]	N/A
pPRR7::PRR7-GFP (PRR7-GFP)	[27]	N/A
pPIF3::YFP:PIF3 (YFP-PIF3)	[26]	N/A
p35S::PIF4-HA (PIF4-HA)	[25]	N/A
pTOC1::TOC1:YFP (TMG)	[41]	N/A
pif1-1	[34]	N/A
pif3-3	[9]	N/A
pif4-2	[37]	N/A

pif5-3	[38]	N/A
pifq	[37]	N/A
prr5-1	[39]	N/A
prr7-3	[39]	N/A
prr9-1	[39]	N/A
pif3-1	[9]	N/A
pif4-101	[25]	N/A
pil6-1 (pif5)	[40]	N/A
prr7-3pif3-1 (*prr7pif3*)	This paper	N/A
prr7-3pif4-101 (*prr7pif4*)	This paper	N/A
prr7-3pil6-1 (*prr7pif5*)	This paper	N/A
prr7-3prr9-1 (*prr79*)	This paper	N/A
prr5-1prr9-1 (*prr59*)	This paper	N/A
prr5-1prr7-3prr9-1 (*prr579*)	This paper	N/A
prr7-3cdf5-1 (*prr7cdf5*)	This paper	N/A
35S::CDF5-GFP (*CDF5OX*)	This paper	N/A
pifqCDF5OX	This paper	N/A
pifqcdf5	This paper	N/A
Oligonucleotides		
See Table S2	N/A	N/A
Recombinant DNA		
pH7FWG2	Gateway	N/A
PIF3 in pGAD424	[46]	N/A
PIF4 in pGADT7	[7]	N/A
NZY-A PCR cloning kit	NZYTech	Cat# MB05302
pGBKT7	Clontech	Cat# PT3248-5
pGWcY	[48]	N/A
pGWnY	[48]	N/A
Software and Algorithms		
ActiveWebCam software (www.pysoft.com)	N/A	N/A
Integrated Genome Browser (IGB)	[43]	N/A
PHASER (http://phaser.mocklerlab.org)	N/A	N/A
DAVID system	[44]	N/A
IBM SPSS Statistics Software	N/A	N/A
Excel	N/A	N/A

Figure 1

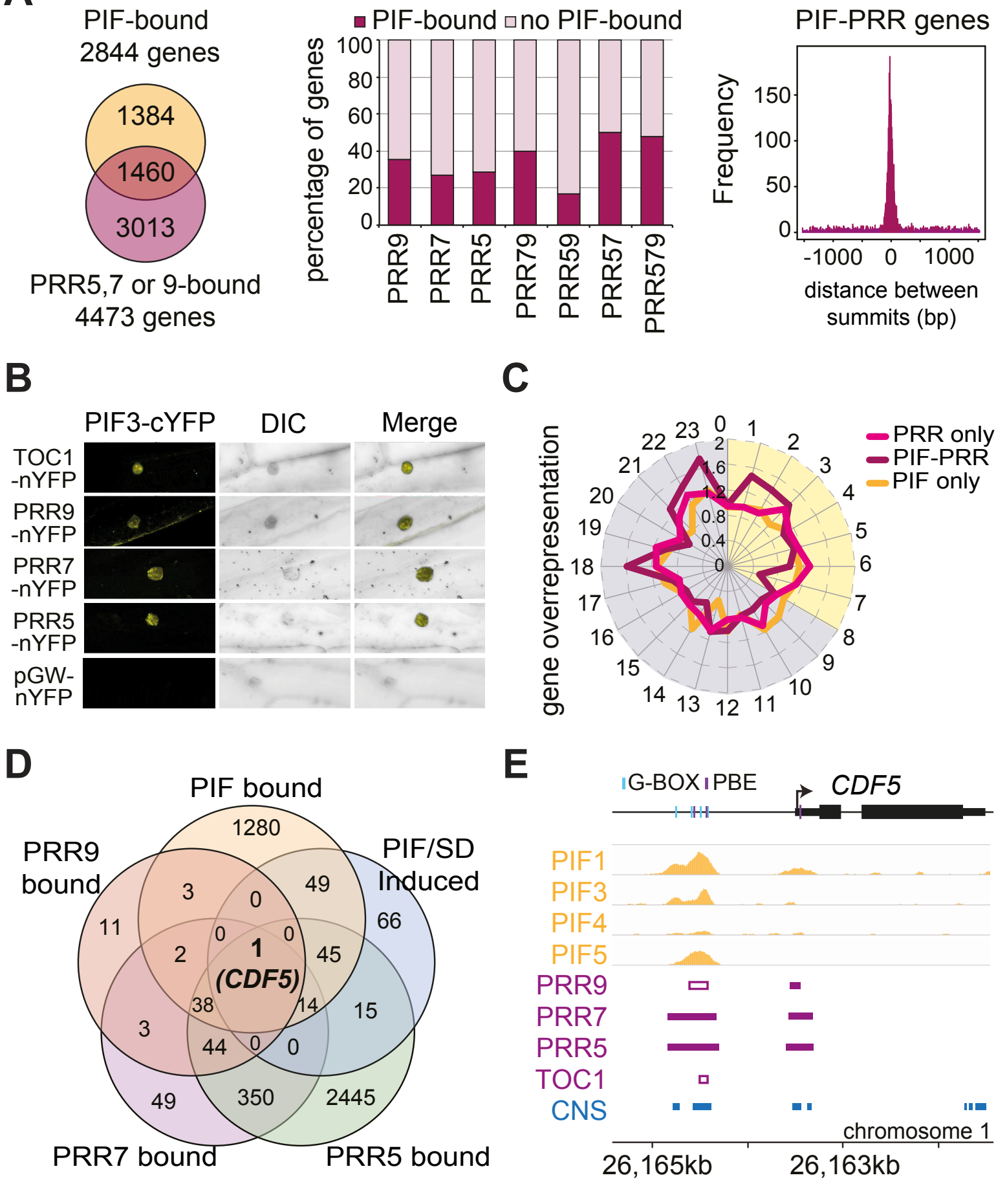
A
PIF-bound
2844 genes
1384
1460
3013
PRR5,7 or 9-bound
4473 genes
PIF-bound
no PIF-bound
percentage of genes
100
80
60
40
20
0
PRR9
PRR7
PRR5
PRR79
PRR59
PRR57
PRR579
PIF-PRR genes
Frequency
150
100
50
0
-1000
0
1000
distance between
summits (bp)
B
PIF3-cYFP
DIC
Merge
TOC1
-nYFP
PRR9
-nYFP
PRR7
-nYFP
PRR5
-nYFP
pGW-
nYFP
C
gene overrepresentation
PRR only
PIF-PRR
PIF only
D
PIF bound
PRR9
bound
PIF/SD
Induced
PRR7 bound
PRR5 bound
1280
3
0
49
11
66
0
0
2
1
(CDF5)
45
38
14
15
3
44
0
0
49
350
2445
E
G-BOX
PBE
CDF5
PIF1
PIF3
PIF4
PIF5
PRR9
PRR7
PRR5
TOC1
CNS
chromosome 1
26,165kb
26,163kb

Figure 2

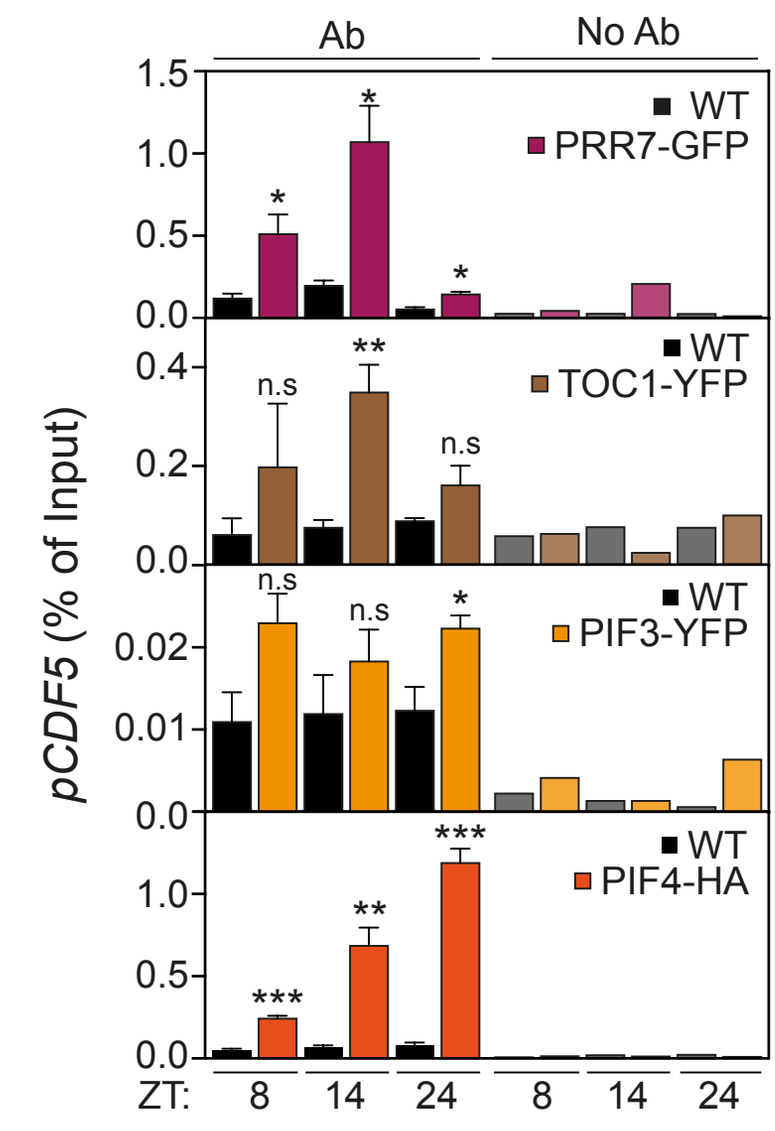
A
Ab
No Ab
WT
PRR7-GFP
TOC1-YFP
PIF3-YFP
PIF4-HA
pCDF5 (% of Input)
n.s
ZT:
8
14
24

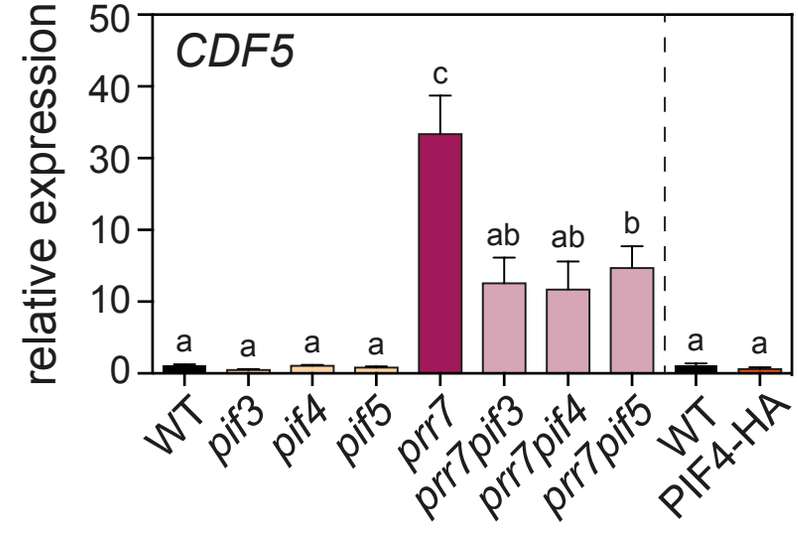
B
CDF5
relative expression
WT
pif3
pif4
pif5
prr7
prr7pif3
prr7pif4
prr7pif5
PIF4-HA

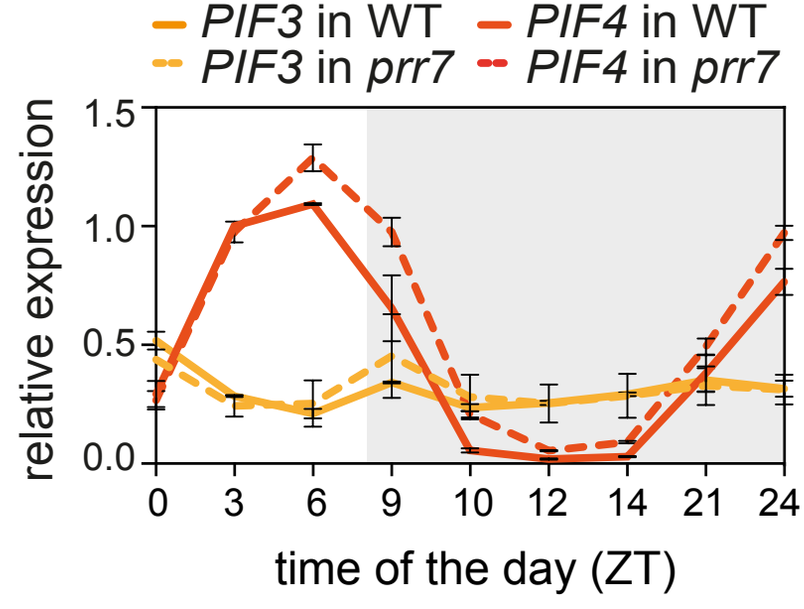
C
PIF3 in WT
PIF4 in WT
PIF3 in prr7
PIF4 in prr7
relative expression
time of the day (ZT)

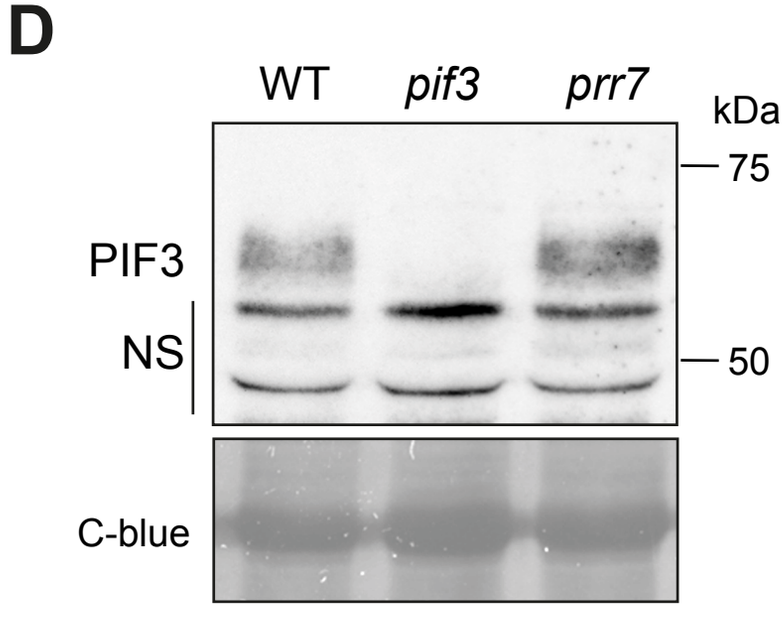
D
WT
pif3
prr7
kDa
75
50
PIF3
NS
C-blue

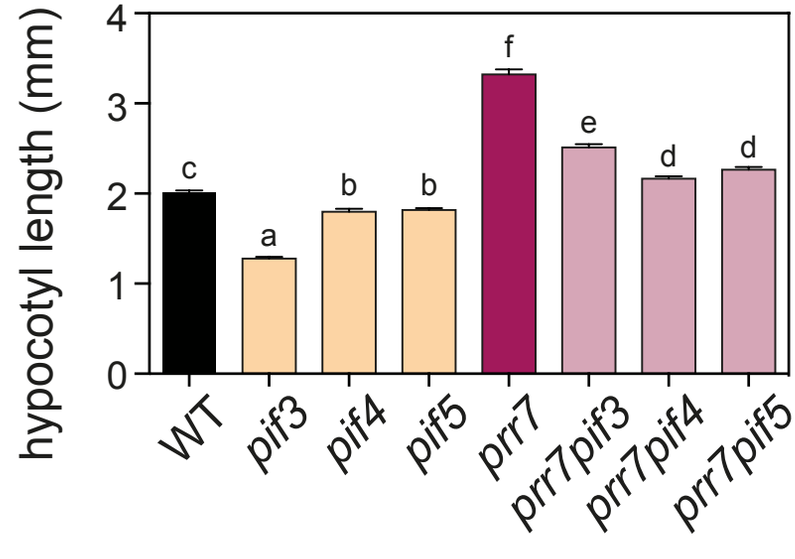
E
hypocotyl length (mm)
WT
pif3
pif4
pif5
prr7
prr7pif3
prr7pif4
prr7pif5

Figure 3

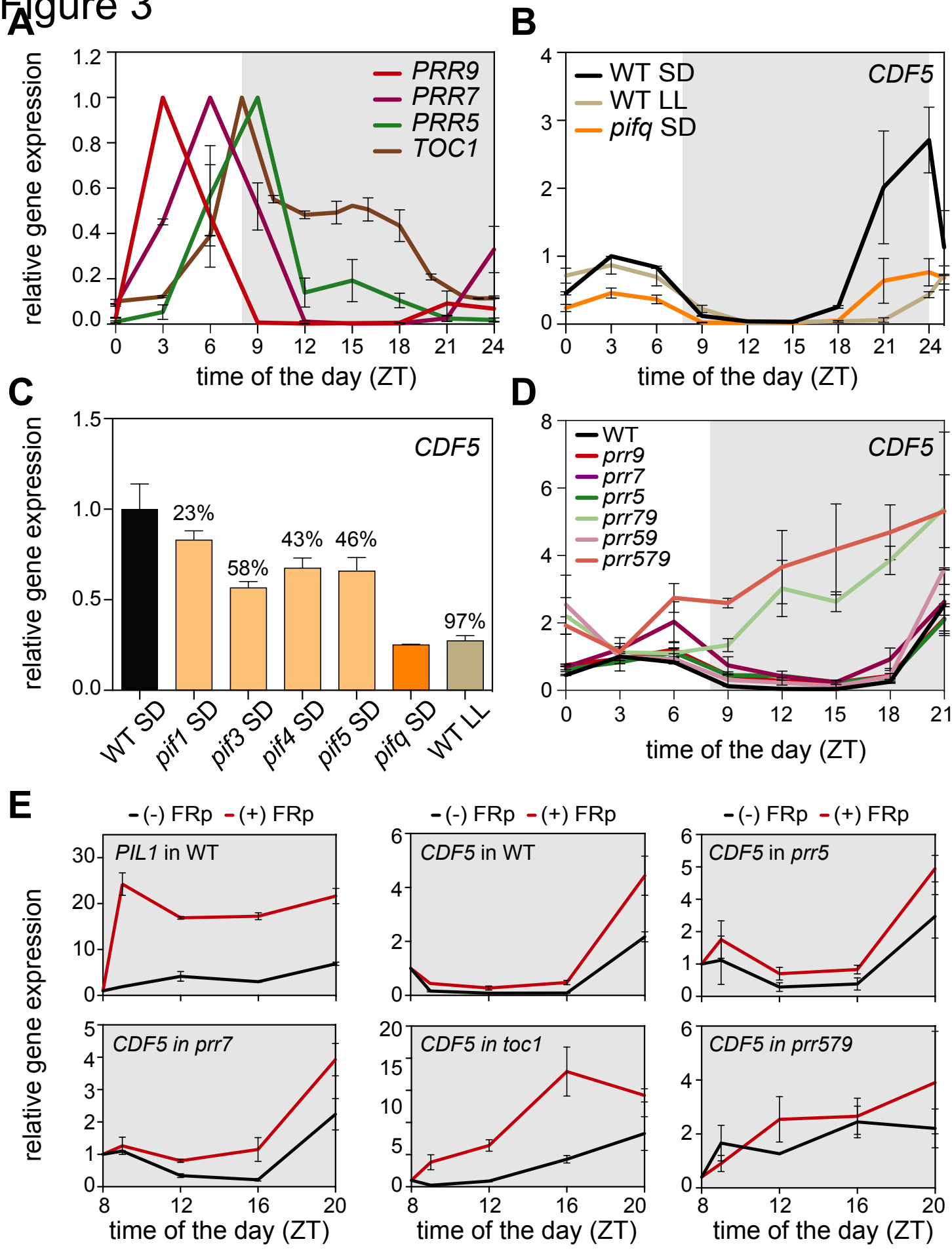
A
relative gene expression
PRR9
PRR7
PRR5
TOC1
time of the day (ZT)
B
WT SD
WT LL
pifq SD
CDF5
time of the day (ZT)
C
relative gene expression
CDF5
23%
58%
43%
46%
97%
WT SD
pif1 SD
pif3 SD
pif4 SD
pif5 SD
pifq SD
WT LL
D
WT
prr9
prr7
prr5
prr79
prr59
prr579
CDF5
time of the day (ZT)
E
(-) FRp
(+) FRp
relative gene expression
PIL1 in WT
CDF5 in WT
CDF5 in prr5
CDF5 in prr7
CDF5 in toc1
CDF5 in prr579
time of the day (ZT)

Figure 4

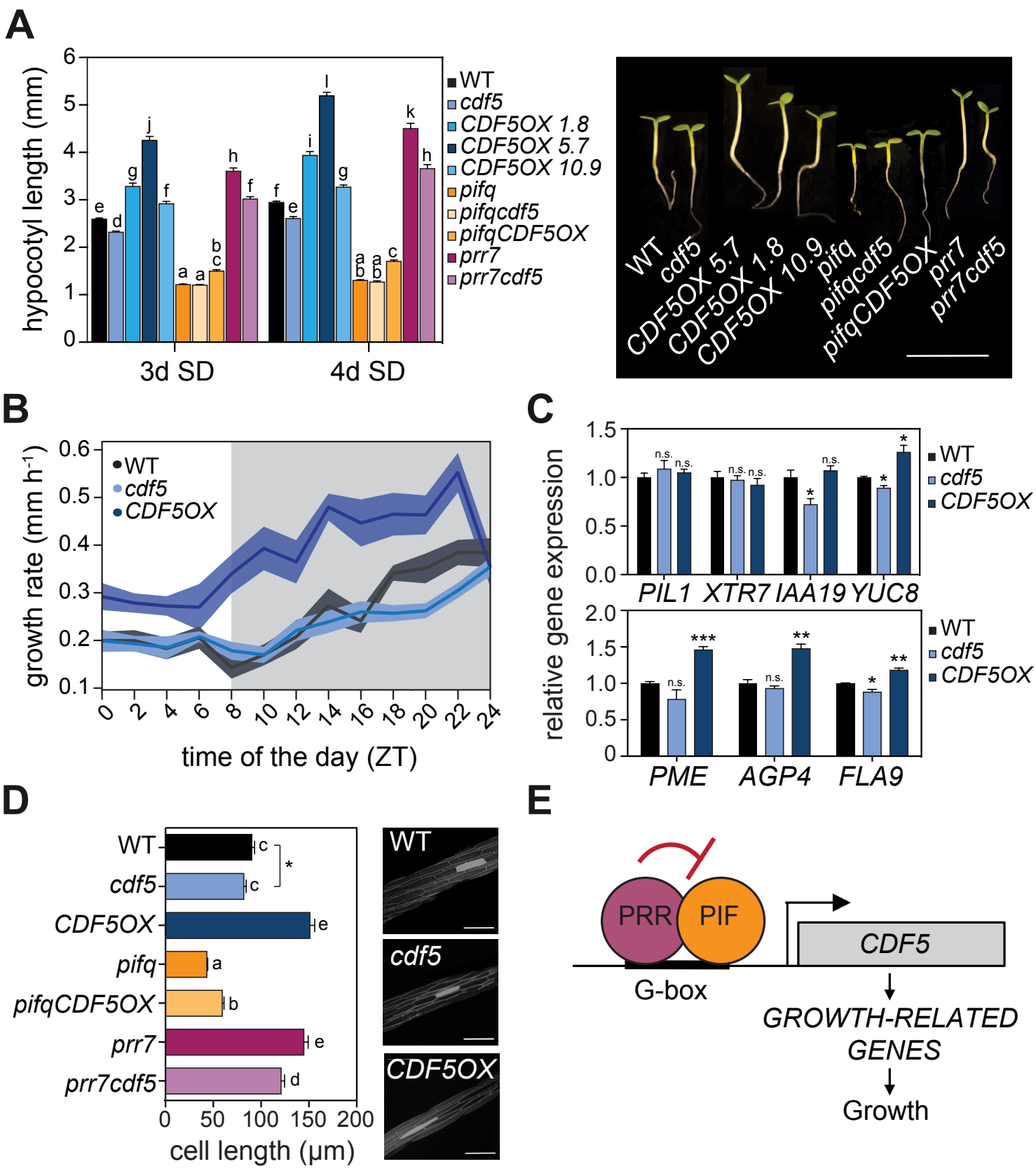
A
hypocotyl length (mm)
3d SD
4d SD
WT
cdf5
CDF5OX 1.8
CDF5OX 5.7
CDF5OX 10.9
pifq
pifqcdf5
pifqCDF5OX
prr7
prr7cdf5
WT
cdf5
CDF5OX 5.7
CDF5OX 1.8
CDF5OX 10.9
pifq
pifqcdf5
pifqCDF5OX
prr7
prr7cdf5
B
growth rate (mm h-1)
time of the day (ZT)
WT
cdf5
CDF5OX
C
relative gene expression
PIL1
XTR7
IAA19
YUC8
PME
AGP4
FLA9
n.s.
WT
cdf5
CDF5OX
D
WT
cdf5
CDF5OX
pifq
pifqCDF5OX
prr7
prr7cdf5
cell length (μm)
E
PRR
PIF
G-box
CDF5
GROWTH-RELATED GENES
Growth

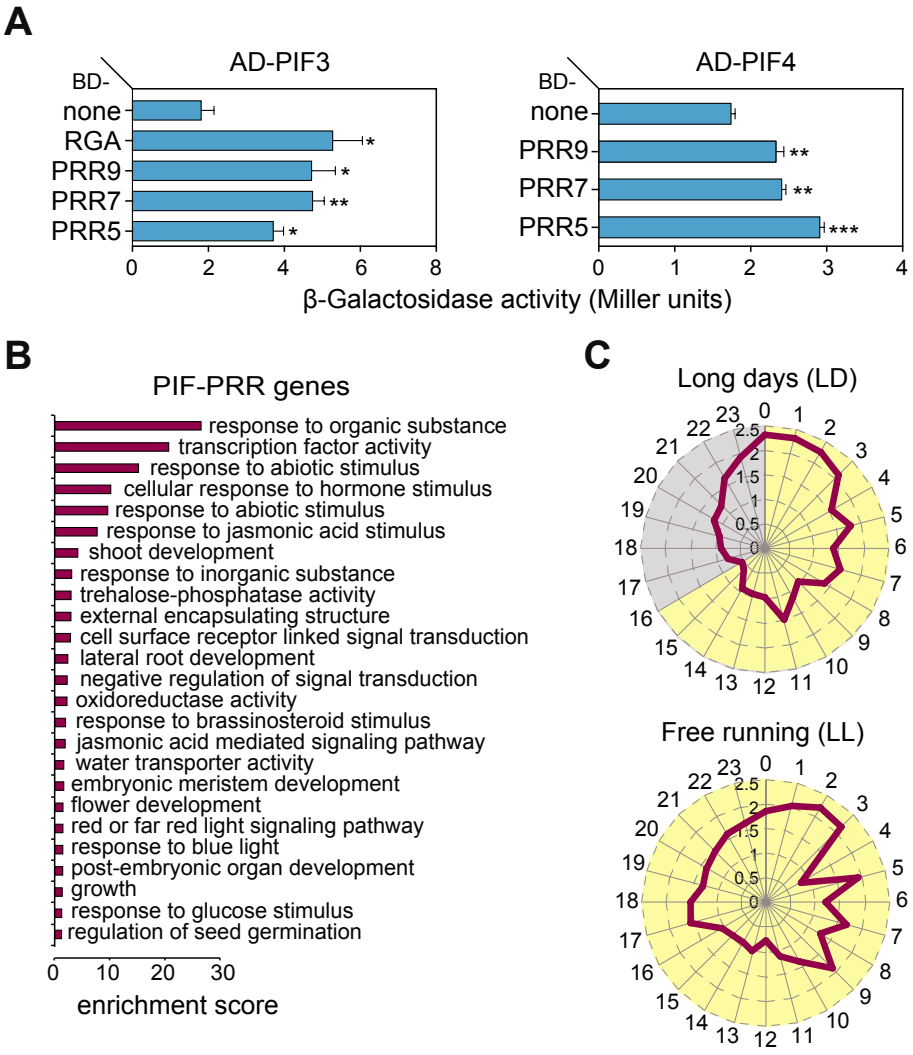

Figure S1. Related to Figure 1. Yeast-two-hybrid assays showing the interaction between PIF3, PIF4, and PRR9/7/5, and gene ontology (GO) and phaser analysis in LD and LL of PIF-PRR genes. (A) β-galactosidase activities from yeast two-hybrid assays showing interactions between PIF3 (left), PIF4 (right) and PRR5, PRR7, and PRR9. Error bars indicate SE (n = 3). Significance level is relative to the BD alone control (*P<0.05; **P<0.01 and ***P<0.001). DELLA protein RGA is included as positive control for PIF3 interactions [S1]. **(B)** Cluster analysis of the most enriched GO annotations for PIF-PRR genes. **(C)** Comparison of expression phases in long days (top) and free running (bottom) conditions of the 1,460 "PIF–PRR" gene set defined in Figure 1A and provided in Dataset 1. Phases as defined by PHASER (phaser.mocklerlab.org) are indicated on the circumference, and fold-change phase enrichment of genes (count/expected) is shown on the radius. Day is shown in yellow; night is shown in grey.

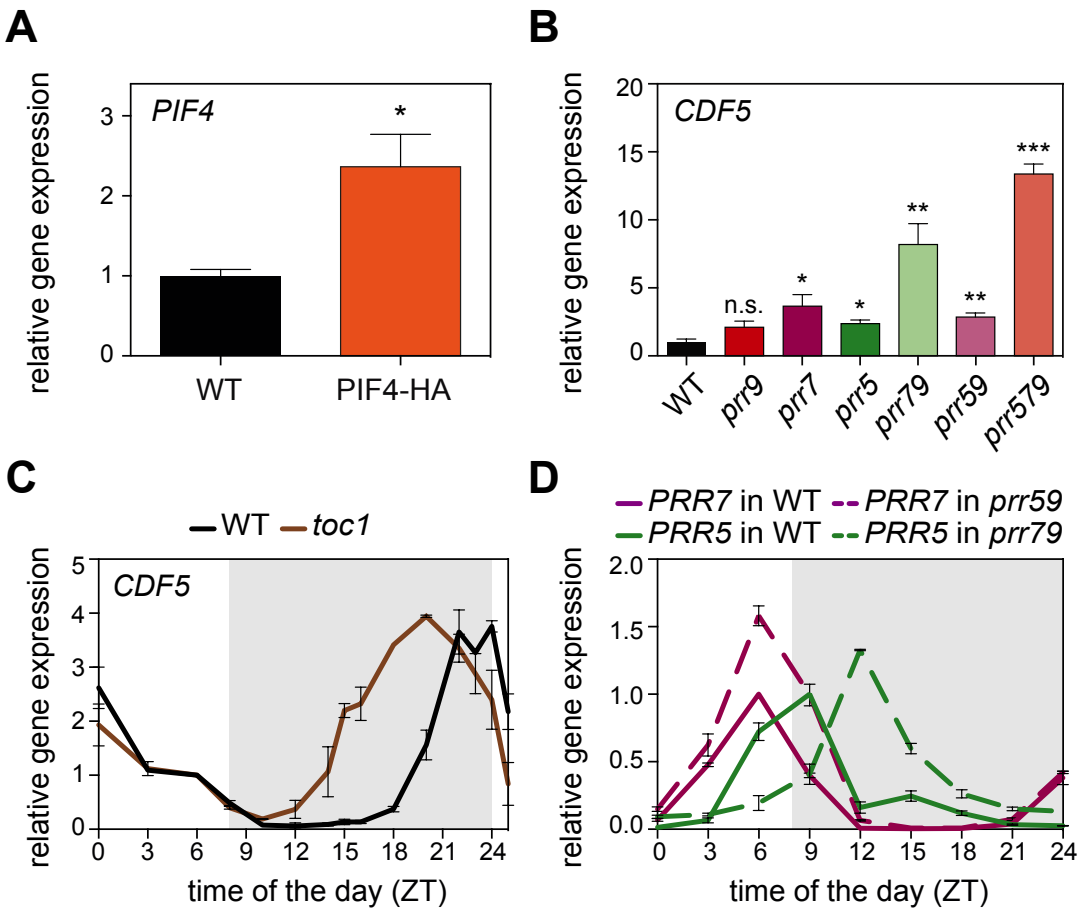

Figure S2. Related to Figures 2 and 3. *PIF4, CDF5*, *PRR5* and *PRR7* expression analyses in PIF4-HA overexpressing plants, and in *toc1, prr5, prr7, and prr9* single and higher order mutant combinations. *PIF4* expression in WT and *35S::PIF4-HA* (PIF4-HA) seedlings at ZT8 **(A)** and *CDF5* expression in WT and *prr* mutants at ZT9 **(B)** during the third day of growth in SD. Data are from three independent biological replicates relative to WT set at one. Error bars indicate SE. Statistically significant differences between mean values by Student's *t*-test relative to WT are shown (**P*<0.05; ***P*<0.01 and ****P*<0.001). n.s., not significant. **(C)** *CDF5* expression in WT and *toc1*. **(D)** *PRR5* and *PRR7* expression in WT and *prr79 and prr59*, respectively. (C, D) Seedlings were grown for 2 days in SD and harvested during the third day at the indicated times. Data plotted are mean ± SE relative to ZT6 for each genotype (C) or relative to its maximum expression value set at one for each gene (D), n = 2 independent biological experiments, each assayed in triplicate. (A-D) All samples were analyzed by qRT-PCR and normalized to *PP2A*.

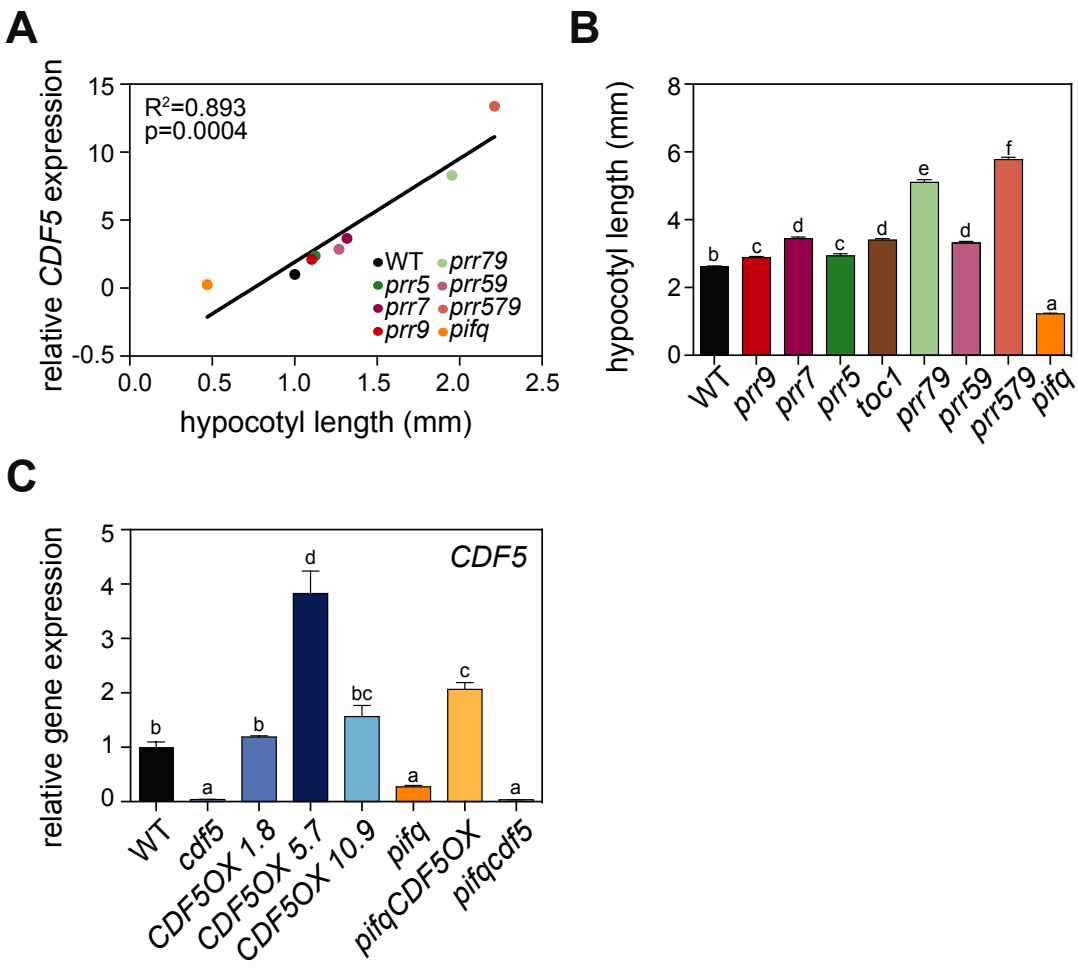

Figure S3. Related to Figures 3 and 4. *CDF5* expression in correlation with hypocotyl length and in generated *CDF5* mutant lines. (A) *CDF5* expression levels correlate with hypocotyl length. Correlation of hypocotyl length in (B) with *CDF5* expression values of WT, *prr* and *toc1* in 2-day-old SD-grown seedlings harvested at ZT9 during the third day under SD. *pifq* expression values are from Figure S2A. **(B)** Quantification of hypocotyl elongation in 3-day-old SD-grown WT, *prr*, *toc1*, and *pifq* seedlings. Data are means ± SE of at least 50 seedlings. **(C)** Characterization of *CDF5* expression levels in *CDF5OX* mutant lines. *CDF5* expression in 3-d-old SD-grown WT, *cdf5*, *CDF5OX*, *pifq*, *pifqCDF5OX*, and *pifqcdf5* seedlings at ZT24. In (A) and (C), expression was analyzed by qRT-PCR, and values were normalized to *PP2A* and are shown relative to WT levels set at one. Data are from three independent biological replicates. In (C) error bars indicate SE. Different letters shown in (B) and (C) denote statistically significant differences among means by Tukey-b test ($P<0.05$).

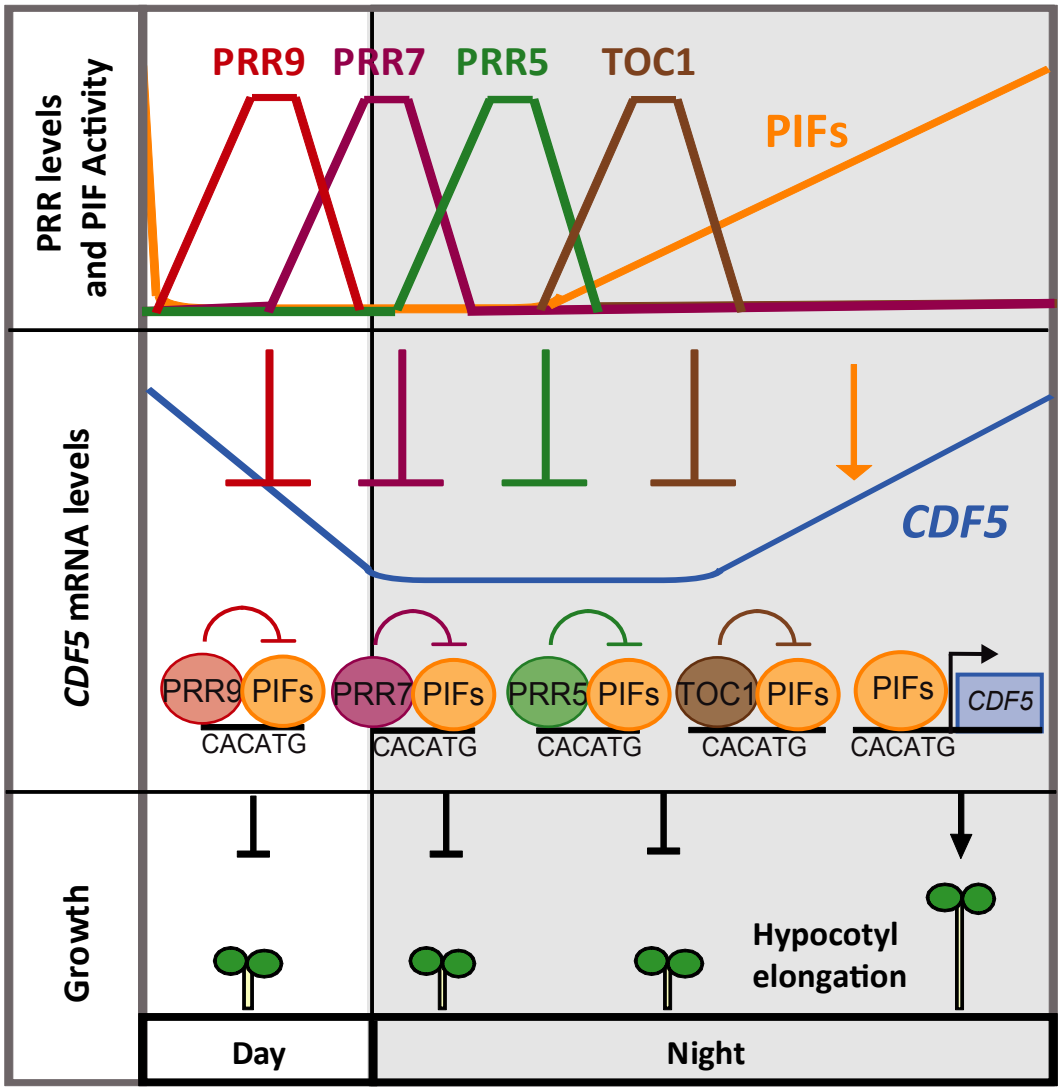

Figure S4. Related to Figure 4. Model of the proposed role of PRRs as repressors of PIF activity in gating CDF5-mediated elongation. Sequential PRR9/7/5 and PRR1/TOC1 accumulation from morning to midnight (top) represses PIF-induction of *CDF5*, a transcription factor necessary for growth-promotion (middle). PIFs are present during the day and progressively accumulate during the night concurrently to a decline in PRRs and TOC1 abundance (top). At predawn, PRRs and TOC1 are no longer present, repression on the PIFs is lifted (top), and PIFs induce *CDF5* expression (middle) to promote hypocotyl elongation (bottom). Based on current data, PRRs and PIFs could bind to the same or different nearby G-boxes, PIFs might bridge the binding of PRRs to DNA, or PRRs could compete with PIFs for binding to G-boxes.

Supplemental References

S1. Feng, S., Martinez, C., Gusmaroli, G., Wang, Y., Zhou, J., Wang, F., Chen, L., Yu, L., Iglesias-Pedraz, J.M., Kircher, S., *et al.* (2008). Coordinated regulation of Arabidopsis thaliana development by light and gibberellins. Nature *451*, 475–479.

S2. Pfeiffer, A., Shi, H., Tepperman, J.M., Zhang, Y., and Quail, P.H. (2014). Combinatorial Complexity in a Transcriptionally Centered Signaling Hub in Arabidopsis. Mol. Plant *7*, 1598–1618.

S3. Liu, T.L., Newton, L., Liu, M.-J., Shiu, S.-H., and Farré, E.M. (2016). A G-Box-Like Motif Is Necessary for Transcriptional Regulation by Circadian Pseudo-Response Regulators in Arabidopsis. Plant Physiol. *170*, 528–539.

S4. Martín, G., Soy, J., and Monte, E. (2016). Genomic Analysis Reveals Contrasting PIFq Contribution to Diurnal Rhythmic Gene Expression in PIF-Induced and - Repressed Genes. Front. Plant Sci. *7*, 962.

S5. Fornara, F., Panigrahi, K.C.S., Gissot, L., Sauerbrunn, N., Rühl, M., Jarillo, J.A., and Coupland, G. (2009). Arabidopsis DOF Transcription Factors Act Redundantly to Reduce CONSTANS Expression and Are Essential for a Photoperiodic Flowering Response. Dev. Cell *17*, 75–86.

S6. Mockler, T.C., Yu, X., Shalitin, D., Parikh, D., Michael, T.P., Liou, J., Huang, J., Smith, Z., Alonso, J.M., Ecker, J.R., *et al.* (2004). Regulation of flowering time in Arabidopsis by K homology domain proteins. Proc. Natl. Acad. Sci. U. S. A. *101*, 12759–12764.

S7. Soy, J., Leivar, P., González-Schain, N., Martín, G., Diaz, C., Sentandreu, M., Al-Sady, B., Quail, P.H., and Monte, E. (2016). Molecular convergence of clock and photosensory pathways through PIF3–TOC1 interaction and co-occupancy of target promoters. Proc. Natl. Acad. Sci. U. S. A. *113*, 4870–4875.

S8. Soy, J., Leivar, P., González-Schain, N., Sentandreu, M., Prat, S., Quail, P.H., and Monte, E. (2012). Phytochrome-imposed oscillations in PIF3 protein abundance regulate hypocotyl growth under diurnal light/dark conditions in Arabidopsis. Plant J. *71*, 390–401.

S9. http://www.tdx.cat/bitstream/handle/10803/130896/MGR_TESIS.pdf.

S10. Rawat, R., Schwartz, J., Jones, M.A., Sairanen, I., Cheng, Y., Andersson, C.R., Zhao, Y., Ljung, K., and Harmer, S.L. (2009). REVEILLE1, a Myb-like transcription factor, integrates the circadian clock and auxin pathways. Proc. Natl. Acad. Sci. U. S. A. *106*, 16883–16888.

S11. Shin, J., Park, E., and Choi, G. (2007). PIF3 regulates anthocyanin biosynthesis in an HY5-dependent manner with both factors directly binding anthocyanin biosynthetic gene promoters in Arabidopsis. Plant J. *49*, 981–994.

Circadian waves of transcriptional repression shape PIF-regulated photoperiod-responsive growth in Arabidopsis

Guiomar Martín[1], Arnau Rovira[1], Nil Veciana[1], Judit Soy[1], Gabriela Toledo-Ortiz[3,4], Charlotte M. M. Gommers[1], Marc Boix[1], Rossana Henriques[1], Eugenio G. Minguet[2], David Alabadí[2], Karen Halliday[4], Pablo Leivar[1,5], and Elena Monte[1,6,7,*]

[1]Center for Research in Agricultural Genomics (CRAG), CSIC-IRTA-UAB-UB, Campus UAB, Edifici CRAG, Bellaterra, 08193 Barcelona, Spain.

[2]Instituto de Biología Molecular y Celular de Plantas (IBMCP), CSIC-UPV, Ingeniero Fausto Elio s/n, 46022 Valencia, Spain

[3]Lancaster Environment Center, Lancaster University. Lancaster, LA1 4YQ, UK.

[4]The University of Edinburgh. CH Waddington Building, Max Born Crescent, Edinburgh, EH9 3BF, UK.

[5]Bioengineering Department, IQS School of Engineering. Via Augusta 390, 08017 Barcelona, Spain.

[6]Consejo Superior de Investigaciones Científicas (CSIC), 08028 Barcelona, Spain.

[7]Lead contact

[*]Corresponding author: elena.monte@cragenomica.es

Summary

Plants coordinate their growth and development with the environment through integration of circadian clock and photosensory pathways. In *Arabidopsis thaliana*, rhythmic hypocotyl elongation in short days (SD) is enhanced at dawn by the bHLH transcription factors PHYTOCHROME-INTERACTING FACTORS (PIFs) directly inducing expression of growth-related genes [1–6]. PIFs accumulate progressively during the night and are targeted for degradation by active phytochromes in the light, when growth is reduced. Although PIF proteins are also detected during the day hours [7–10], their growth-promoting activity is inhibited through unknown mechanisms. Recently, the core clock components and transcriptional repressors PSEUDO-RESPONSE REGULATORS PRR9/7/5 [11,12], negative regulators of hypocotyl elongation [13,14], were described to associate to G-boxes [15], the DNA motifs recognized by the PIFs [16,17], suggesting that PRR and PIF function might converge antagonistically to regulate growth. Here we report that PRR9/7/5 and PIFs physically interact and bind to the same promoter region of pre-dawn-phased, growth-related genes, and we identify the transcription factor CDF5 [18,19] as target of this interplay. In SD, *CDF5* expression is sequentially repressed from morning to dusk by PRRs and induced pre-dawn by PIFs. Consequently, *CDF5* accumulates specifically at dawn, when it induces cell elongation. Our findings provide a framework for recent TIMING OF CAB EXPRESSION 1 (TOC1/PRR1) data [5,20] and reveal that the long described circadian morning-to-midnight waves of the PRR transcriptional repressors (PRR9, PRR7, PRR5 and TOC1) [21] jointly gate PIF activity to dawn to prevent overgrowth through sequential regulation of common PIF-PRR target genes such as *CDF5*.

Results and Discussion

Genome-wide analysis of ChIP-sequencing (ChIP-seq) data for the PIF quartet (PIFq) (PIF1, 3, 4, 5)-associated [16] and PRR5-, PRR7-, and/or PRR9-associated [15] loci revealed an overlap of 1,460 genes between PIF-bound genes (57.5 % of all PIF-bound genes) and at least one of the three PRRs examined ("PIF-PRR genes") (Figure 1A left; Dataset 1). The overlap between PIF-bound and PRR5-, PRR7-, or PRR9-bound, when examined individually or in combination, is shown in Figure 1A middle (Dataset 1). Distance between PRR and PIF binding sites indicate that PRRs and PIFs associate to the same genomic regions (Figure 1A right), in accordance with results showing enrichment of G-box-containing motifs in PRR-bound regions [15,22]. We detected interaction of PIF3 and PIF4 with PRR5 (PIF4 in accordance to [20]), PRR7 and PRR9 by yeast two-hybrid assays (Figure S1A). We further confirmed PIF3-PRR interaction *in planta* by BiFc assays (Figure 1B). These data suggest that, similarly to recent findings for TOC1 and PIF3 and PIF4 [5,20], PIFs and PRRs may bind together at G-boxes to co-regulate the expression of shared PIF-PRR target genes. Based on the described activity of PRRs as transcriptional repressors [11,12,20], PIF-PRR interaction also agrees with the possibility that PRR5/7/9 might target PIFs to repress their ability to activate shared PIF-PRR target genes as shown recently for TOC1 and PIFs [5,20].

Functional classification indicated that "PIF-PRR" genes are enriched in growth-related categories (Figure S1B) and are overrepresented at the elongation phases 18-23 specifically under SD (Figure 1C, Figure S1C) (Dataset 1), suggesting that PIFs and PRRs jointly target genes involved in the induction of growth under SD conditions. We compared PRR- and PIF-bound genes with the recently defined PIF- and SD-induced (PIF/SD-induced) gene set of PIFq-regulated genes under SD containing dawn-phased and growth-related genes [4]. Strikingly, one gene (*CDF5*) was PIF/SD-induced and bound by all PRRs and PIFs (Figure 1D, Dataset 1). Previous ChIP experiments showed binding of PRR5/7/9 and possibly TOC1 to this G-box/PBE containing region [15,22,23] (Figure 1E, see legend for details). This region coincides with conserved noncoding sequences (CNS) among crucifer regulatory regions (Figure 1E) [24], suggesting that the binding sites on the *CDF5* promoter have been subjected to selective constraint, consistent with functionality relevance.

We verified binding of PRR7, TOC1, PIF3 and PIF4 to the *CDF5* promoter (*pCDF5*) region encompassing the G-boxes at different times under SD conditions by time-course analysis using ChIP-qPCR. Statistically significant and robust PRR7 binding to *pCDF5* was observed at ZT8 and ZT14, and was substantially decreased at ZT24, whereas maximum of TOC1 binding was at ZT14 (Figure 2A). For PIF3 and PIF4, tagged lines driven by the endogenous PIF3 promoter and 35S were used, respectively [25,26] (Figure S2A). Statistically significant binding of PIF3 to *pCDF5* was detected at ZT24, whereas significant PIF4 binding was detected in all three time points and incremented along the night (Figure 2A). These binding dynamics are consistent with the pattern of accumulation of each protein in SD [5,8,27]. Together, these data are consistent with binding of the PIFs, PRRs and TOC1 proteins in SD to the same region of the *CDF5* promoter located approximately 1000 bp upstream of the TSS, and with binding dictated by their protein abundance.

To examine how PIF and PRR7 interaction (Figures 1B and S1A) and binding to the *CDF5* promoter (Figure 2A) affect *CDF5* expression, we first tested *CDF5* expression in *pif* and *prr7* mutants under SD at ZT9 when PRR7 levels are maximum and PIFs start to accumulate [7,8,10,27,28]. *CDF5* levels were upregulated in *prr7* (Figure 2B), an effect strongly suppressed by the *pif* mutations in the *prr7pif* double mutants (Figure 2B), suggesting that PIFs and PRR7 regulate *CDF5* expression antagonistically as transcriptional activator and repressor, respectively. Interestingly, because PIF3 transcript and protein levels are not affected in *prr7* (Figures 2C and 2D), together these data suggest that, as described for TOC1 [5], PRR7 acts directly as transcriptional repressor of PIF3 activity in the regulation of *CDF5*. In agreement, the *prr7* long hypocotyl phenotype was also partially suppressed with genetic removal of PIF3 (Figure 2E). However, because the detected binding of PIF3 to the *CDF5* promoter at ZT9 or ZT14 was not statistically significant (Figure 2A), we cannot discard that the effect of PRRs on PIF3 might involve inhibition of PIF3 binding to *CDF5* promoter. Suppression of hypocotyl phenotype was also observed for *prr7pif4* and *prr7pif5* compared to *prr7* (Figures 2B and 2E), which suggests that PRR7 directly represses PIF4 transcriptional activity, as previously shown for TOC1 and PIF4 [20], and might also repress PIF5. This scenario might be potentially more complex given that *PIF4*/*5* transcription is regulated

by the clock under SD [2] and at least *PIF4* transcript levels are slightly higher in *prr7* (Figure 2C), in accordance with recent data showing *PIF4* de-repression in *prr* multiple mutants [29]. However, the observation that *CDF5* expression in overexpressing PIF4-HA lines at ZT8 was similar to *pif4* (Figure 2B), a time point where both PRR7 and PIF4 are co-bound to the *pCDF5* (Figure 2A), provides strong support that PRR7 directly suppresses PIF4 transcriptional activation activity towards *CDF5*.

We next examined the antagonistic PIF-PRR interaction in the direct regulation of *CDF5* across the diurnal cycle. Under SD, phytochrome imposes oscillation of PIF3 and probably PIF1 proteins to progressively accumulate during the night, and to degrade rapidly in the morning maintaining residual levels during the day [8,9]. For PIF4 and possibly PIF5, clock and light regulation result in PIF accumulation also during daytime (Figure 2C) [7,10]. In contrast, PRR accumulation is sequential (PRR9/7/5/TOC1) from morning to midnight (Figure 3A) [21,27]. We therefore expected *CDF5* to oscillate with a peak in the early morning and at the end of the night (where presence of the PIFs is maximum) and a trough from morning to midnight (when PRRs accumulate). Indeed, *CDF5* in the WT was detected during the first part of the day (ZT0-ZT3), then declined to almost undetectable levels through ZT15, and accumulated after ZT15 to peak at dawn (Figure 3B). Expression in *pifq* SD and in WT LL at dawn (a condition where PIFs do not accumulate) [28] was lower than WT SD (Figure 3B), supporting the notion that transcript induction leading to the oscillatory pattern of *CDF5* expression in SD depends on the presence of the PIFs (Figure 3B). Analysis of *CDF5* levels in single *pif* and multiple *pifq* (defective in PIF1/3/4/5) mutants at ZT24 showed that the PIF quartet (PIFq) collectively induces *CDF5* expression at dawn, with PIF1 having a lesser contribution (Figure 3C). *CDF5* transcript levels dropped in the WT after 1h of morning light (Figure 3B), concurrent with phy-induced PIF degradation. In contrast, at ZT9, when *CDF5* expression in the WT is almost non-detectable, *CDF5* expression was significantly higher in *prr5*, *prr7*, *prr79*, *prr59*, and *prr579,* with a major contribution for PRR7 (Figure S2B). Compared to WT, *CDF5* expression was higher in *prr7* from ZT3 through midnight (Figure 3D), whereas in *prr59* and *prr79* mutants *CDF5* expression was only slightly higher at dawn in *prr59* and higher from dusk to dawn in *prr79* (Figure 3D). In *toc1*, de-repression of *CDF5* was early compared to WT (Figure S2C), similar to

other PIF-TOC1 co-targets [5]. Because cross-regulation was described in the PRRs [30], with nuclear accumulation of TOC1 depending partly on PRR5, it is likely that TOC1 contributes to the phenotype of PRR5-deficient mutant backgrounds. We also characterized *PRR5* and *PRR7* expression in *prr79* and *prr59* double mutants, respectively. Levels of *PRR5* and *PRR7* were ~1.5-fold higher in *prr59* and *prr79* compared to WT, and *PRR5* phase was delayed in *prr79,* indicative of intricate cross-regulatory pathways (Figure S2D). Significantly, *CDF5* expression in the *prr579* mutant from ZT3-ZT21 was almost linear (Figure 3D), in accordance with the PRRs (with TOC1 possibly also contributing) being responsible for the repression of *CDF5* expression from morning to midnight.

To further examine the PIF-PRR antagonistic interplay, we artificially induced PIF accumulation at the beginning of the night period when PRR levels are high (Figure 3A) [27] by giving a far-red light pulse (FRp) at ZT8 [5,28]. As control we used *PIL1*, a direct PIF target and marker gene for PIF abundance and activity [8]. *PIL1* levels accumulated in the WT immediately after the FRp (Figure 3E), in agreement with the rapid accumulation of PIF proteins after a FRp [9,25,31], and to PRRs not interfering significantly with PIF activity in the regulation of *PIL1,* in accordance with *PIL1* not being a direct target of all PRRs [15]. In striking contrast, expression induction of the PIF-PRR target *CDF5* was repressed in the WT during the first part of the night (ZT8-ZT16) after a FRp, similarly to the control (-FRp) samples (Figure 3E). Interestingly, this repression was much lower in *prr5* and *prr7*, and not observed in *prr579*. In *toc1*, early *CDF5* expression compared to WT (Figures 3E and S2C) was more evident in (+FRp) samples.

Although part of the effect seen in *prr* mutants might come from elevated PIF4/5 levels due to their transcriptional derepression (Fig 2C), together these data support the conclusion that the PRR9/7/5 and TOC1 prevent the transcriptional activation of *CDF5* by PIFs. Given the sequential pattern of expression of *PRR9, 7, 5,* and *TOC1* (Figure 3A) [21], and the progressive accumulation of the PIFs along the night in SD conditions [8], our findings suggest that *CDF5* is sequentially targeted by *PRR9, 7, 5,* and *TOC1* to repress its expression from morning to midnight (when PRR and TOC1 levels are high), to gate PIF direct induction of *CDF5* to dawn when the levels of PRRs and TOC1 are low

and PIFs reach a peak in abundance. We propose that *CDF5* might be a novel target of this PRR and PIF interplay in the promotion of hypocotyl elongation.

Our findings suggest a model where the antagonistic regulation of *CDF5* gene expression by PRRs and PIFs described above might underlie rhythmic growth under SD. In agreement, we observed correlation between the magnitude of hypocotyl length under our SD conditions and *CDF5* levels in *prr* and *pifq* mutants (Figures S3A and S3B). To test this model genetically, we generated seedlings ectopically expressing *CDF5* in a *cdf5* mutant background *(CDF5OX)* (Figure S3C), and quantified the hypocotyl phenotype of WT, *CDF5OX*, and *cdf5* lines under SD. *cdf5* mutants were slightly shorter than WT SD-grown seedlings, whereas *CDF5OX* lines suppressed the *cdf5* phenotype and showed a range from subtle to robustly elongated hypocotyls compared to WT (Figures 4A). We analyzed the elongation rate of *cdf5* and *CDF5OX* lines under SD compared to WT (Figure 4B). As described, the growth rate of WT seedlings is highest during the second half of the night [2]. Elongation rate of *cdf5* seedlings was similar to WT during the day and first part of the night, but it was reduced during the last part of the night, when *CDF5* expression in the WT is maximum, consistent with their short phenotype. Interestingly, elongation rate of *CDF5OX* seedlings was constantly high during the day and most part of the night (Figure 4B). Together, our data suggest that transcriptional control of *CDF5* expression by the PIFs and PRRs is a key regulatory mechanism in growth control.

Next, to genetically test the interplay between CDF5, PIFs and PRRs, we generated *prr7cdf5*, *pifqcdf5* and *pifqCDF5OX* and mutants (Figure S3C) to study their hypocotyl phenotypes. We observed that in SD the quintuple *pifqcdf5* mutant displayed a phenotype similar to *pifq*, indicating that the *cdf5* mutation did not have an additive effect on *pifq* mutation (Figure 4A). This result agrees with PIFq and CDF5 acting in the same signaling pathway. Overexpression of *CDF5* in the *pifq* background partially restored the *pifq* phenotype (Figures 4A), providing additional evidence that CDF5 contributes to growth downstream of the PIFs. Finally, comparison of *prr7* with *prr7cdf5* mutants showed that the long phenotype of *prr7* under SD is reduced when CDF5 is removed in *prr7cdf5* (Figures 4A), suggesting that exaggerated growth in *prr7* is partially a consequence of having elevated levels of CDF5. Together, our results confirm our model

where PRRs and PIFs directly and antagonistically regulate *CDF5* expression to precisely gate CDF5 growth-promoting activity to the end of the night.

We hypothesized that CDF5 might control the expression of growth-related genes at dawn downstream of PIFq. We selected a few PIF-regulated [4], growth-related cell wall [32] and SD growth-marker genes [6,8] to test for their expression in *cdf5* and *CDF5OX* lines. As shown in Figure 4C, *PIL1* and *XTR7* were not significantly affected in *cdf5* or *CDF5OX*, and *IAA19*, *YUCCA8* and three selected cell wall related genes (*AGP4*, *PME*, and *FLA9*) show either significant down-regulation in *cdf5* (*IAA19*), up-regulation in *CDF5OX* (*PME, AGP4*), or both (*YUC8* and *FLA9*), compared to the WT. Interestingly, *AGP4* and *PME* are not PIF-bound genes. These results suggest branching downstream of PIFq, with CDF5 regulating a subset of the PIFq-regulated growth-related genes, in accordance to the partial suppression of the *pifq* phenotype by *CDF5OX* shown above (Figure 4A). Examination of the hypocotyl cell size in SD-grown WT, *cdf5* and *CDF5OX* seedlings by confocal microscopy imaging clearly showed elongated cells in *CDF5OX* hypocotyls compared to WT, whereas cells in *cdf5* appeared shorter (Figure 4D left), which was confirmed by quantification of the hypocotyl cell length (Figure 4D right). Next, we tested *prr7*, which exhibited a longer cell phenotype partially suppressed by genetic removal of *CDF5* in *prr7cdf5* (Figure 4D). In contrast, cell length in *pifq* was shorter than WT, a phenotype that was partially recovered by *CDF5OX* (Figure 4C right). Together, these results support a role for CDF5 in the promotion of cell elongation under the inductive growth condition of SDs downstream of PRRs and PIFs.

Conclusions

Here we found that members of the PRR family of transcriptional repressors (PRR5, 7, and 9), with a key role in the regulation of the central circadian oscillator and clock output processes in plants [12], target growth-related genes that are directly induced by the growth-promoting PIF transcription factors. Given the coincident DNA-binding specificity of PRRs and PIFs (Figure 1A) [15,33], the PIF-PRR physical interaction in the nucleus (Figures 1B and S1A), and their accumulation dynamics during short-day photoperiods (Figure 3A) [2,7,8,11,21], we propose a model in which successive binding of the PRR9, PRR7, and PRR5 to the G-box elements of shared PIF and PRR target genes (like the growth-promoting *CDF5*) acts to sequentially repress transcription of the

PIF-induced transcriptional network starting in the morning (Figure 4E, Figure S4). Given that PRR9/7/5 have not been shown to bind DNA directly, our results agree with the possibility that PIFs might bridge the binding of PRRs to DNA, although competition by direct binding of PRR to G-boxes, or through a PRR- and G-box- binding factor different than PIFq, cannot be completely discarded based on our results. These findings define an expanded framework for previous results showing PRR1/TOC1 repression of PIF transcriptional activity at midnight [5]. At dawn, PRRs and TOC1 are not present, PIF protein accumulation reaches a maximum, and elongation is promoted by PIF-induced expression of growth-promoting genes like *CDF5* (Figure 4E). Collectively, our data reveal that gating of growth occurs not only at the post-dusk hours of the night as previously described for TOC1 [5], but instead starts in the morning and covers all the day period until midnight through the sequential action of the PRR family of transcriptional repressors. The molecular mechanism described here could explain why growth rate under short-day photoperiods is low [2] from morning to midnight in the presence of low PIF3 and PIF1 [9,34] and considerable high amounts of PIF4 (and likely PIF5) [7,10], a regulation critical for fitness by preventing overgrowth (Figure 4A). Our results reveal that gating of growth has evolved in plants to encompass the orchestrated sequential action of members of the PRR family (PRR9/7/5/1) of transcriptional repressors that peak in waves from morning to midnight. This function highlights the dual role of the PRR family of clock oscillator components, as regulators of central clock components and cycling outputs [11,21,35], and as repressors of the physiological output of growth in combined regulation with light pathways that control accumulation of PIFs.

Acknowledgements

We thank D. Somers, S.Prat, G. Coupland, and R. McClung for sharing seed and plasmid resources. We thank G. Steele for generating double and triple *prr* mutants, and the *prrpif* mutant combinations. The work in this manuscript was supported by grants from the Spanish "Ministerio de Economía y Competitividad" (MINECO) BIO2012-31672 and BIO2015-68460-P, and from the Generalitat de Catalunya 2014-SGR-1406 to E.M.; by Marie Curie IRG PIRG06-GA-2009-256420 grant to P.L.; by the European Commission (PCIG2012-GA-2012-334052) and by MINECO (BIO2015-70812-ERC; RYC-2011-

09220) to R.H.; by Royal Society Grant RG2016R1 to G. T-O; by MINECO BIO2013-43184-P to D.A; by MINECO AGL2014-57200-JIN to E.G.M. We acknowledge financial support by the CERCA programme/Generalitat de Catalunya and from MINECO through the "Severo Ochoa Programme for Centers of Excellence in R&D" 2016-2019 (SEV-2015-0533)".

Author contributions

G.M., P.L., and E.M. conceived and designed the study, G.M., A.R., N.V., J.S., G.T-O., C.M.M.G., M.B., R.H., E.G.M., D.A., K.H., P.L., and E.M. acquired, analyzed and interpreted data. G.M., P.L., and E.M. wrote the manuscript.

Declaration of Interests

The authors declare no competing interests.

References

1. Niwa, Y., Yamashino, T., and Mizuno, T. (2009). The Circadian Clock Regulates the Photoperiodic Response of Hypocotyl Elongation through a Coincidence Mechanism in Arabidopsis thaliana. Plant Cell Physiol. *50*, 838–854.

2. Nozue, K., Covington, M.F., Duek, P.D., Lorrain, S., Fankhauser, C., Harmer, S.L., and Maloof, J.N. (2007). Rhythmic growth explained by coincidence between internal and external cues. Nature *448*, 358–361.

3. Nomoto, Y., Kubozono, S., Yamashino, T., Nakamichi, N., and Mizuno, T. (2012). Circadian Clock- and PIF4-Controlled Plant Growth: A Coincidence Mechanism Directly Integrates a Hormone Signaling Network into the Photoperiodic Control of Plant Architectures in Arabidopsis thaliana. Plant Cell Physiol. *53*, 1950–1964.

4. Martín, G., Soy, J., and Monte, E. (2016). Genomic Analysis Reveals Contrasting PIFq Contribution to Diurnal Rhythmic Gene Expression in PIF-Induced and -Repressed Genes. Front. Plant Sci. *7*, 962.

5. Soy, J., Leivar, P., González-Schain, N., Martín, G., Diaz, C., Sentandreu, M., Al-Sady, B., Quail, P.H., and Monte, E. (2016). Molecular convergence of clock and photosensory pathways through PIF3–TOC1 interaction and co-occupancy of target promoters. Proc. Natl. Acad. Sci. U. S. A. *113*, 4870–4875.

6. Nozue, K., Harmer, S.L., and Maloof, J.N. (2011). Genomic Analysis of Circadian Clock-, Light-, and Growth-Correlated Genes Reveals PHYTOCHROME-INTERACTING FACTOR5 as a Modulator of Auxin Signaling in Arabidopsis.

Plant Physiol. *156*, 357–372.

7. Bernardo-García, S., de Lucas, M., Martínez, C., Espinosa-Ruiz, A., Davière, J.-M., and Prat, S. (2014). BR-dependent phosphorylation modulates PIF4 transcriptional activity and shapes diurnal hypocotyl growth. Genes Dev. *28*, 1681–1694.

8. Soy, J., Leivar, P., González-Schain, N., Sentandreu, M., Prat, S., Quail, P.H., and Monte, E. (2012). Phytochrome-imposed oscillations in PIF3 protein abundance regulate hypocotyl growth under diurnal light/dark conditions in Arabidopsis. Plant J. *71*, 390–401.

9. Monte, E., Tepperman, J.M., Al-Sady, B., Kaczorowski, K.A., Alonso, J.M., Ecker, J.R., Li, X., Zhang, Y., and Quail, P.H. (2004). The phytochrome-interacting transcription factor, PIF3, acts early, selectively, and positively in light-induced chloroplast development. Proc. Natl. Acad. Sci. U. S. A. *101*, 16091–16098.

10. Yamashino, T., Nomoto, Y., Lorrain, S., Miyachi, M., Ito, S., Nakamichi, N., Fankhauser, C., and Mizuno, T. (2013). Verification at the protein level of the PIF4-mediated external coincidence model for the temperature-adaptive photoperiodic control of plant growth in Arabidopsis thaliana. Plant Signal. Behav. *8*, e23390.

11. Nakamichi, N., Kiba, T., Henriques, R., Mizuno, T., Chua, N.-H., and Sakakibara, H. (2010). PSEUDO-RESPONSE REGULATORS 9, 7, and 5 Are Transcriptional Repressors in the Arabidopsis Circadian Clock. Plant Cell *22*, 594–605.

12. Farré, E.M., and Liu, T. (2013). The PRR family of transcriptional regulators reflects the complexity and evolution of plant circadian clocks. Curr. Opin. Plant Biol. *16*, 621–629.

13. Nakamichi, N., Kita, M., Ito, S., Yamashino, T., and Mizuno, T. (2005). PSEUDO-RESPONSE REGULATORS, PRR9, PRR7 and PRR5, Together Play Essential Roles Close to the Circadian Clock of Arabidopsis thaliana. Plant Cell Physiol. *46*, 686–698.

14. Kaczorowski, K.A., and Quail, P.H. (2003). Arabidopsis PSEUDO-RESPONSE REGULATOR7 Is a Signaling Intermediate in Phytochrome-Regulated Seedling Deetiolation and Phasing of the Circadian Clock. Plant Cell *15*, 2654–2665.

15. Liu, T.L., Newton, L., Liu, M.-J., Shiu, S.-H., and Farré, E.M. (2016). A G-Box-Like Motif Is Necessary for Transcriptional Regulation by Circadian Pseudo-Response Regulators in Arabidopsis. Plant Physiol. *170*, 528–539.

16. Pfeiffer, A., Shi, H., Tepperman, J.M., Zhang, Y., and Quail, P.H. (2014). Combinatorial Complexity in a Transcriptionally Centered Signaling Hub in Arabidopsis . Mol. Plant *7*, 1598–1618.

17. Martínez-García, J.F., Huq, E., and Quail, P.H. (2000). Direct Targeting of Light Signals to a Promoter Element-Bound Transcription Factor. Science *288*, 859–863.

18. Fornara, F., de Montaigu, A., Sánchez- Villarreal, A., Takahashi, Y., Ver Loren van Themaat, E., Huettel, B., Davis, S.J., and Coupland, G. (2015). The GI–CDF module of Arabidopsis affects freezing tolerance and growth as well as flowering. Plant J. *81*, 695–706.

19. Fornara, F., Panigrahi, K.C.S., Gissot, L., Sauerbrunn, N., Rühl, M., Jarillo, J.A., and Coupland, G. (2009). Arabidopsis DOF Transcription Factors Act Redundantly to Reduce CONSTANS Expression and Are Essential for a Photoperiodic Flowering Response. Dev. Cell *17*, 75–86.

20. Zhu, J.-Y., Oh, E., Wang, T., and Wang, Z.-Y. (2016). TOC1–PIF4 interaction mediates the circadian gating of thermoresponsive growth in Arabidopsis. Nat. Commun. *7*, 13692.

21. Matsushika, A., Makino, S., Kojima, M., and Mizuno, T. (2000). Circadian Waves of Expression of the APRR1/TOC1 Family of Pseudo-Response Regulators in Arabidopsis thaliana: Insight into the Plant Circadian Clock. Plant Cell Physiol. *41*, 1002–1012.

22. Nakamichi, N., Kiba, T., Kamioka, M., Suzuki, T., Yamashino, T., Higashiyama, T., Sakakibara, H., and Mizuno, T. (2012). Transcriptional repressor PRR5 directly regulates clock-output pathways. Proc. Natl. Acad. Sci. U. S. A. *109*, 17123–17128.

23. Huang, W., Pérez-García, P., Pokhilko, A., Millar, A.J., Antoshechkin, I., Riechmann, J.L., and Mas, P. (2012). Mapping the Core of the Arabidopsis Circadian Clock Defines the Network Structure of the Oscillator. Science *336*, 75–79.

24. Haudry, A., Platts, A.E., Vello, E., Hoen, D.R., Leclercq, M., Williamson, R.J., Forczek, E., Joly-Lopez, Z., Steffen, J.G., Hazzouri, K.M., *et al*. (2013). An atlas of over 90,000 conserved noncoding sequences provides insight into crucifer regulatory regions. Nat Genet *45*, 891–898.

25. Lorrain, S., Allen, T., Duek, P.D., Whitelam, G.C., and Fankhauser, C. (2008). Phytochrome-mediated inhibition of shade avoidance involves degradation of growth-promoting bHLH transcription factors. Plant J. *53*, 312–323.

26. Al-Sady, B., Ni, W., Kircher, S., Schäfer, E., and Quail, P.H. (2006). Photoactivated Phytochrome Induces Rapid PIF3 Phosphorylation Prior to Proteasome-Mediated Degradation. Mol. Cell *23*, 439–446.

27. Fujiwara, S., Wang, L., Han, L., Suh, S.-S., Salomé, P.A., McClung, C.R., and Somers, D.E. (2008). Post-translational Regulation of the Arabidopsis Circadian Clock through Selective Proteolysis and Phosphorylation of Pseudo-response

366 Regulator Proteins. J. Biol. Chem. *283*, 23073–23083.

367 28. Soy, J., Leivar, P., and Monte, E. (2014). PIF1 promotes phytochrome-regulated
368 growth under photoperiodic conditions in Arabidopsis together with PIF3, PIF4,
369 and PIF5. J. Exp. Bot. *65*, 2925–2936.

370 29. Hayama, R., Sarid- Krebs, L., Richter, R., Fernández, V., Jang, S., and Coupland,
371 G. (2017). PSEUDO RESPONSE REGULATORs stabilize CONSTANS protein
372 to promote flowering in response to day length. EMBO J. *36*, 904–918.

373 30. Wang, L., Fujiwara, S., and Somers, D.E. (2010). PRR5 regulates phosphorylation,
374 nuclear import and subnuclear localization of TOC1 in the Arabidopsis circadian
375 clock. EMBO J. *29*, 1903–1915.

376 31. Shen, H., Moon, J., and Huq, E. (2005). PIF1 is regulated by light-mediated
377 degradation through the ubiquitin-26S proteasome pathway to optimize
378 photomorphogenesis of seedlings in Arabidopsis. Plant J. *44*, 1023–1035.

379 32. Pelletier, S., Van Orden, J., Wolf, S., Vissenberg, K., Delacourt, J., Ndong, Y.A.,
380 Pelloux, J., Bischoff, V., Urbain, A., Mouille, G., *et al*. (2010). A role for pectin
381 de-methylesterification in a developmentally regulated growth acceleration in
382 dark-grown Arabidopsis hypocotyls. New Phytol. *188*, 726–739.

383 33. Heyndrickx, K.S., de Velde, J. Van, Wang, C., Weigel, D., and Vandepoele, K.
384 (2014). A Functional and Evolutionary Perspective on Transcription Factor
385 Binding in Arabidopsis thaliana. Plant Cell *26*, 3894-3910.

386 34. Huq, E., Al-Sady, B., Hudson, M., Kim, C., Apel, K., and Quail, P.H. (2004).
387 PHYTOCHROME-INTERACTING FACTOR 1 Is a Critical bHLH Regulator of
388 Chlorophyll Biosynthesis. Science *305*, 1937–1941.

389 35. Kamioka, M., Takao, S., Suzuki, T., Taki, K., Higashiyama, T., Kinoshita, T., and
390 Nakamichi, N. (2016). Direct Repression of Evening Genes by CIRCADIAN
391 CLOCK-ASSOCIATED1 in the Arabidopsis Circadian Clock. Plant Cell *28*, 696–
392 711.

393 36. Kikis, E.A., Khanna, R., and Quail, P.H. (2005). ELF4 is a phytochrome-regulated
394 component of a negative-feedback loop involving the central oscillator
395 components CCA1 and LHY. Plant J. *44*, 300–313.

396 37. Leivar, P., Monte, E., Oka, Y., Liu, T., Carle, C., Castillon, A., Huq, E., and Quail,
397 P.H. (2008). Multiple Phytochrome-Interacting bHLH Transcription Factors
398 Repress Premature Seedling Photomorphogenesis in Darkness. Curr. Biol. *18*,
399 1815–1823.

400 38. Khanna, R., Shen, Y., Marion, C.M., Tsuchisaka, A., Theologis, A., Schäfer, E.,
401 and Quail, P.H. (2008). The Basic Helix-Loop-Helix Transcription Factor PIF5
402 Acts on Ethylene Biosynthesis and Phytochrome Signaling by Distinct

Mechanisms. Plant Cell *19*, 3915-3929.

39. Michael, T.P., Salomé, P.A., Yu, H.J., Spencer, T.R., Sharp, E.L., McPeek, M.A., Alonso, J.M., Ecker, J.R., and McClung, C.R. (2003). Enhanced Fitness Conferred by Naturally Occurring Variation in the Circadian Clock. Science *302*, 1049–1053.

40. Fujimori, T., Yamashino, T., Kato, T., and Mizuno, T. (2004). Circadian-Controlled Basic/Helix-Loop-Helix Factor, PIL6, Implicated in Light-Signal Transduction in Arabidopsis thaliana. Plant Cell Physiol. *45*, 1078–1086.

41. Más, P., Alabadí, D., Yanovsky, M.J., Oyama, T., and Kay, S.A. (2003). Dual Role of TOC1 in the Control of Circadian and Photomorphogenic Responses in Arabidopsis. Plant Cell *15*, 223–236.

42. Liu, T., Carlsson, J., Takeuchi, T., Newton, L., and Farré, E.M. (2013). Direct regulation of abiotic responses by the Arabidopsis circadian clock component PRR7. Plant J. *76*, 101–114.

43. Nicol, J.W., Helt, G.A., Blanchard Steven G., J., Raja, A., and Loraine, A.E. (2009). The Integrated Genome Browser: free software for distribution and exploration of genome-scale datasets. Bioinformatics *25*, 2730–2731.

44. Huang, D.W., Sherman, B.T., Tan, Q., Collins, J.R., Alvord, W.G., Roayaei, J., Stephens, R., Baseler, M.W., Lane, H.C., and Lempicki, R.A. (2007). The DAVID Gene Functional Classification Tool: a novel biological module-centric algorithm to functionally analyze large gene lists. Genome Biol. *8*, R183.

45. Toledo-Ortiz, G., Johansson, H., Lee, K.P., Bou-Torrent, J., Stewart, K., Steel, G., Rodríguez-Concepción, M., and Halliday, K.J. (2014). The HY5-PIF Regulatory Module Coordinates Light and Temperature Control of Photosynthetic Gene Transcription. PLoS Genet. *10*, e1004416.

46. Ni, M., Tepperman, J.M., and Quail, P.H. (1998). PIF3, a Phytochrome-Interacting Factor Necessary for Normal Photoinduced Signal Transduction, Is a Novel Basic Helix-Loop-Helix Protein. Cell *95*, 657–667.

47. Wang, L., Kim, J., and Somers, D.E. (2013). Transcriptional corepressor TOPLESS complexes with pseudoresponse regulator proteins and histone deacetylases to regulate circadian transcription. Proc. Natl. Acad. Sci. U. S. A. *110*, 761–766.

48. Tanaka, Y., Kimura, T., Hikino, K., Goto, S., Nishimura, M., Mano, S., and Nakagawa, T. (2012). Gateway Vectors for Plant Genetic Engineering: Overview of Plant Vectors, Application for Bimolecular Fluorescence Complementation (BiFC) and Multigene Construction. InTech.

49. Martín, G., Leivar, P., Ludevid, D., Tepperman, J.M., Quail, P.H., and Monte, E. (2016). Phytochrome and retrograde signalling pathways converge to

antagonistically regulate a light-induced transcriptional network. Nat. Commun. *7*, 11431.

Figure Legends

Figure 1. Analysis of coincident co-binding of PRRs and PIFs to dawn-phased genes under SD identifies *CDF5* as a PIF- and PRR5/7/9-bound gene. (A) (Left) Comparison of PIF-bound [16] and PRR5-, 7- and/or PRR9-bound genes [15] (gene lists provided in Dataset 1) defines three groups of genes: "PIF only" (1,384 genes), "PRR only" (3,013 genes), and "PIF-PRR" (1,460 genes). (Middle) Percentage of PIF-bound genes in genes bound by single or a combination of PRRs. (Right) Frequency of pairwise distance in base pairs (bp) between the PIF- and PRR- binding sites in each of the "PIF-PRR" co-bound genes. **(B)** BiFC assay of the PRRs and PIF3 fusions to N- and C-terminal fragments of YFP, respectively, in transfected onion cells. The combinations of PIF3-cYFP and TOC1-nYFP or pGW-nYFP were used as positive and negative control, respectively. (Left) YFP fluorescence image. (Center) Bright-field image. (Right) Merge of YFP fluorescence and bright-field image. **(C)** Expression phases in SD of gene sets defined in (A): "PIF–PRR" (purple), "PRR only" (pink), and "PIF only" (yellow). Phases are indicated on the circumference, and fold-change phase enrichment of genes (count/expected) on the radius. Day is shown in yellow; night in gray. See also Figure S1 and Dataset 1. **(D)** Comparison of PIF- [16], PRR5-, 7-, and PRR9-bound genes [15], and "PIF/SD-induced" genes [4] (see Dataset 1 for details) **(E)** Visualization of ChIP-seq and ChIP-qPCR data in the genomic region encompassing the *CDF5* locus co-bound by PIFs, PRRs and TOC1. For PIF (orange), ChIP-seq tracks show the pile-up of all the reads obtained from MACS analyses (model based for ChIP-seq) of the dataset from each experiment [16]. Each corresponding WT-ChIP/input control is overlaid in dark gray. For PRR (purple), filled rectangles indicate the PRR9, PRR7 and PRR5 peaks defined by ChIP-seq in [15]. Empty rectangles indicate peaks only described by ChIP-qPCR, in [22] for PRR9 and in Figure 2A for TOC1. Conserved non-coding sequences (CNS) (blue) are defined in [24]. G- and PBE-box: vertical lines indicate motif positions. See also Figure S1 and Dataset 1.

Figure 2. PRR7 represses PIF3 ability to induce *CDF5* expression in SD. (A) PRR7, TOC1, PIF3, and PIF4 binding to the G-box containing region of the *CDF5* promoter at ZT8, ZT14, and ZT24 under SD. For ChIP-qPCR analysis, samples of SD-grown *pPRR7::PRR7-GFP* (PRR7-GFP), *pTOC1::TOC1:YFP* (TMG), *pPIF3::YFP:PIF3*

(YFP-PIF3), and *35S::PIF4-HA* (PIF4-HA), were harvested at the indicated times during the third day and were immunoprecipitated using anti-GFP or anti-HA antibodies. Data are from three independent ChIP experiments, and error bars indicate SE. Statistically significant differences between mean values by Student's *t*-test relative to WT are shown (*P<0.05; **P<0.01 and ***P<0.001). n.s., not significant. WT controls were Col-0 for YFP-PIF3, PIF4-HA, and PRR7-GFP, and C24 for TMG seedlings. Ab: samples immunoprecipitated with antibody. No Ab: control samples immunoprecipitated without antibody. **(B)** *CDF5* expression levels in WT, *pif3*, *pif4*, *pif5*, *prr7*, *prr7pif3*, *prr7pif4*, *prr7pif5, and* PIF4-HA. Samples were harvested at ZT9 during the third day of growth (ZT8 for PIF4-HA), analyzed by qRT-PCR and normalized to *PP2A*. Data are from three independent biological replicates relative to WT set at one. Different letters denote statistically significant differences among means by Tukey-b test (P<0.05). Error bars indicate SE. **(C)** WT and *prr7* seedlings grown for 2 d in SD conditions were harvested during the third day at the indicated times. Expression levels of *PIF3* and *PIF4* were analyzed by qRT-PCR, and values were normalized to *PP2A*. Data plotted are mean ± SE relative to *PIF4* WT at ZT3 set at one, n = 2 independent biological experiments, each assayed in triplicate. **(D)** PIF3 protein levels in 3-day old SD-grown WT and *prr7* seedlings at ZT24. C-blue, coomassie blue; NS, non-specific bands. **(E)** Hypocotyl length in seedlings as in (B) (except for PIF4-HA) grown for 3 days in SD. Different letters denote statistically significant differences among means by Tukey-b test (P<0.05). Data are means ± SE of at least 50 seedlings. See also Figure S2.

Figure 3. PRRs and PIFs antagonistically regulate *CDF5* to dawn-phase its expression under diurnal SD conditions. **(A)** Transcriptional waves of *PRR9/7/5* and *TOC1* expression during the third day in SD at the indicated times. Each gene is expressed relative to its maximum expression value set at one. **(B-D)** *CDF5* expression in WT, *pif*, and *prr* analyzed by qRT-PCR **(B)** Expression in 2-day-old SD-grown seedlings harvested during the third day at the indicated times in seedlings kept under SD or moved to continuous light (LL). Data are relative to WT SD ZT3. **(C)** Expression in 3-day-old seedlings at ZT24 grown as in (B). Data are from two independent biological replicates and are relative to WT samples set at one. Percentage is the contribution of each PIF to *CDF5* expression in SD considering *pifq* and WT values as 0% and 100%,

respectively. Error bars indicate SE. **(D)** Expression in WT, *prr5*, *prr7*, *prr9*, *prr59*, *prr79*, and *prr579* seedlings grown for 2 d in SD conditions during the third day at the indicated times. Expression is relative to *CDF5* WT at ZT3. **(E)** *PIL1* and *CDF5* expression in WT, *prr* and *toc1* analyzed by qRT-PCR. Two-day-old SD-grown seedlings were treated with a 15-min far-red pulse (FRp) at ZT8 on the third day ((+) FRp samples, in red), and harvested during the night at ZT9, ZT12, ZT16 and ZT20. (-) FRp control samples (in black) did not receive a FRp. Data are relative to ZT8 set at one for each genotype. (A-E) All samples were normalized to *PP2A*. (A-B, D-E) Data plotted are mean ± SE, n=2 independent biological experiments, each assayed in triplicate. See also Figures S2 and S3.

Figure 4. PRR- and PIF-mediated regulation of cell elongation requires CDF5. (A) Hypocotyl length of WT, *cdf5*, *CDF5OX*, *pifq*, *pifqCDF5OX*, *prr7*, and *prr7cdf5* grown for 3 and 4 days in SD (left). Data are means ± SE of at least 35 seedlings. Different letters denote statistically significant differences among means by Tukey-b test ($P<0.05$). Visible phenotypes of 3-day-old seedlings are shown in the right. Scale bar = 5 mm. **(B)** Hypocotyl elongation rate for WT, *cdf5* and *CDF5OX 5.7* under SD conditions. Seedling growth was monitored every 2 hours during the third day. Average of 12 seedlings is shown, and SE is indicated by the shaded area. **(C)** Expression of PIF-regulated growth marker genes (top) and cell wall genes (bottom) in 3-day-old SD-grown WT, *cdf5* and *CDF5OX 5.7* seedlings at ZT24, analyzed by qRT-PCR and normalized to *PP2A*. Data are from three independent biological replicates normalized to WT set at one. Error bars indicate SE. Statistically significant differences between mean values by Student's *t*-test relative to WT are shown (*$P<0.05$; **$P<0.01$ and ***$P<0.001$). n.s., not significant. **(D)** (Left) Visual phenotypes of cell area in 3d-old SD-grown WT, *cdf5* and *CDF5OX 5.7* seedling hypocotyls. Scale bar = 200μm. (Right) Quantification of cell length in WT, *cdf5*, *CDF5OX 5.7*, *pifq*, *pifqCDF5OX* (*pifqOX* in the figure), *prr7*, and *prr7cdf5*. Seedlings were grown for 3 days in SD. Data are means ± SE of at least 100 cells from 3-4 independent seedlings. Different letters or an asterisk denote statistically significant differences among means by Tukey-b test ($P<0.05$) or by t-test ($P<0.05$), respectively. **(E)** Model of the proposed role of PRRs as repressors of PIF activity to regulate cell elongation through CDF5. PIFs bind to the *CDF5* promoter and induce *CDF5*

transcription in the absence of PRRs. If PRRs are present, PRRs repress PIF transcriptional activity though direct PIF-PRR interaction. Based on current data, PRRs and PIFs could bind to the same or different nearby G-boxes, or alternatively, PRRs could bind indirectly to G-boxes through DNA-bound PIFs or other G-box and PRR-binding factors. Sequential PRR9/7/5 and PRR1/TOC1 accumulation from morning to midnight gate PIF-induction of *CDF5* to dawn, when it induces hypocotyl cell elongation by upregulating growth-related genes like *YUC8*, or *FLA9*. See also Figures S3 and S4.

STAR Methods

Contact for Reagent and Resource Sharing

Further information and requests for resources and reagents should be directed to and will be fulfilled by the Lead Contact, Elena Monte (elena.monte@cragenomica.es).

Experimental Model

The *Arabidopsis thaliana* (L.) accession Columbia (Col-0), C24, and mutants used here were obtained from the mentioned references or generated in this work (See Key Resources Table).

Method Details

Seedling Growth and Hypocotyl and Cell Measurements

Arabidopsis thaliana seeds used in this manuscript include the previously described *cdf5-1* [19], *toc1-101* [36], *pPRR7::PRR7-GFP* (PRR7-GFP) [27], *pPIF3::YFP:PIF3* (YFP-PIF3) [26], *p35S::PIF4-HA* [25], *pif1-1* [34], *pif3-3* [9], *pif4-2* [37], *pif5-3* [38], *pifq* [37], *prr5-1*, *prr7-3*, and *prr9-1* [39], *pif3-1* [9], *pif4-101* [25], *pil6-1* (*pif5* mutant) [40], and the newly generated *prr7-3pif3-1* (*prr7pif3*), *prr7-3pif4-101* (*prr7pif4*), *prr7-3pil6-1* (*prr7pif5*), *prr7-3prr9-1* (*prr79*), *prr5-1prr9-1* (*prr59*), *prr5-1prr7-3prr9-1* (*prr579*), and *prr7-3cdf5-1* (*prr7cdf5*) in Col-0 ecotype, and *pTOC1::TOC1:YFP* (TMG) [41] in C24 ecotype. *CDF5OX* lines were generated by cloning the *CDF5* ORF under the regulation of the 35S promoter in the pH7FWG2 vector. The resulting 35S::CDF5-GFP construct was transformed into *cdf5* to generate *CDF5OX* lines, and into *pifq* to generate *pifqCDF5OX* lines.

565 Seeds were sterilized and plated on Murashige and Skoog medium without sucrose.
566 Seedlings were stratified for 4d at 4C in darkness, and seedling growth was done in short
567 days (8h light + 16h dark) or continuous white light (85μmol·m-2·s-1) for the time
568 indicated in each experiment. Hypocotyl measurements in Figures 2E, 4A and S3B were
569 done using Image J (National Institutes of Health). Saturating FR pulses were 30μmol·m-
570 2·s-1 for 15min. Samples at ZT0 and ZT24 were collected in the dark, whereas at ZT8
571 were in the light. For hypocotyl growth rate measurements (Figure 4B), image acquisition
572 was done using the ActiveWebCam software (www.pysoft.com) under infrared light
573 background using modified webcams (Microsoft Life Cam Studio). Twelve seedlings
574 were measured individually every 2 hours throughout the diurnal cycle, the difference in
575 hypocotyl length between the two time points was calculated, and the elongation rate was
576 expressed as mm/h. The mean and SE for the 12 seedlings are represented. Cell size was
577 visualized in seedlings stained with propidium iodine (10μg/ml) (Calbiochem) using a
578 confocal laser microscope Leica SP5 (570 nm-666 nm). Cell length was measured in
579 pictures taken with an optic microscope (AixoPhot DP70) (Figure 4D).

580 ChIP-seq Data Analysis and Visualization

581 Comparison of ChIP-seq data shown in Figure 1A was performed using PIF- [16] and
582 PRR9/7/5-associated peaks from [15], which contained novel PRR9 and re-analyzed
583 ChIP-seq data for PRR5 [22] and PRR7 [42], considering only the PRR binding sites
584 located upstream of the transcriptional start site TSS as in [16]. The same comparison
585 was performed in Figure 1D adding the PIF/SD-induced gene set from [4]. Distance
586 between PIF and PRR peaks was calculated separately for all the different pair-wise
587 combinations associated to a given gene. To jointly visualize the Chip-Seq data for PRR
588 [15] and PIFs [16],and the conserved noncoding sequences (CNS) regions [24] (Figure
589 1E), the Integrated Genome Browser (IGB) [43] was used. Data was obtained from
590 http://mustang.biol.mcgill.ca (CNS), GSE71397 (PRRs) and GSE43286 (PIFs).
591 Expression phases shown in Figures 1C and S1C were analyzed using the PHASER tool
592 (http://phaser.mocklerlab.org) for SD (Col-0_SD), LD (longday), and LL (LL23_LDHH).
593 The PHASER tool generated over-representation p-values for each phase (Dataset 1).
594 DAVID system [44] was used to identify enriched GO biological terms (Figure S1B).

595 Chromatin Immunoprecipitation (ChIP) Assays

Chromatin immunoprecipitation (ChIP) and ChIP-qPCR assays (Figure 2A) were performed as in [5,45]. For PIF3-YFP, all process was performed in the dark under green safelight. Seedlings (3g) were vacuum-infiltrated with 1% formaldehyde and cross-linking was quenched by vacuum infiltration with 0.125 M glycine for 5 min. Tissue was ground, and nuclei-containing cross-linked protein and DNA were purified by sequential extraction on Extraction Buffer 1 (0.4M Sucrose, 10 mM Tris-HCL pH8, 10mM $MgCl_2$, 5mM ß-mercaptoethanol, 0.1mM PMSF, 50 µM MG132, proteinase inhibitor cocktail), Buffer 2 (0.25M Sucrose, 10mM Tris-HCL pH8, 10mM $MgCl_2$, 1% Triton X-100, 5mM ß-mercaptoethanol, 0.1mM PMSF, 50 µM MG132, proteinase inhibitor cocktail), and Buffer 3 (1.7M Sucrose, 10 mM Tris-HCL pH8, 0.15% Triton X-100, 2mM $MgCl_2$, 5mM ß-mercaptoethanol, 0.1mM PMSF, 50 µM MG132, proteinase inhibitor cocktail). Nuclei were resuspended in nuclei lysis buffer (50 mM Tris-HCL pH8, 10 mM EDTA, 1 % SDS, 50 µM MG132, proteinase inhibitor cocktail), sonicated for 10X 30sec, and diluted 10X in Dilution Buffer (0.01% SDS, 1% Triton X-100, 1.2 mM EDTA, 16.7 mM Tris-HCL pH8, 167 mM NaCl). Overnight incubation was performed with the corresponding antibody (or with no antibody as control) at 4C overnight, and immunoprecipitation was performed using dynabeads. Washes were done sequentially in Low Salt Buffer (0.1% SDS, 1% Triton X-100, 2 mM EDTA, 20 mM Tris-HCL pH8, 150 mM NaCl), High Salt Buffer (0.1% SDS, 1% Triton X-100, 2 mM EDTA, 20 mM Tris-HCL pH8, 500 mM NaCl), LiCl Buffer (0.25M LiCl, 1% NP40, 1% deoxycholic acid sodium, 1 mM EDTA, 10 mM Tris-HCL pH8), and TE X1. Immunocomplexes were eluated in Elution Buffer (1%SDS, 0.1M $NaHCO_3$), de-crosslinked overnight at 65C in 10 mM NaCl, and then treated with proteinase K. DNA was purified using Qiagen columns, eluted in 100 uL of Qiagen elution buffer, and 2 uL were used for qPCR (ChIP-qPCR) using *CDF5* promoter-specific primers (Table S1) spanning the region containing the predicted binding sites for the PIFs [16]. Three biological replicates were performed for all the "Antibody" samples (two for WT TMG at ZT8), and one for the "No Antibody". Calculations of percent input were done following the protocol available at www.thermofisher.com.

Yeast Two-Hybrid Assays

For yeast two-hybrid assays shown in Figure S1A, we used PIF3 (pGAD424) and PIF4 (pGADT7) described previously [7,46]. PRR fragments were PCR-amplified from PRR templates [47] with primers containing restriction sites (XmaI/BamHI for PRR5 and PRR9, EcoRI/XmaI for PRR7) (Table S1), cloned into pTOPO vector (NZYTech), sequenced and cloned into pGBKT7 (Clontech). To assess interactions, constructs were co-transformed into yeast AH109 cells (Clontech). Yeast transformants were selected on synthetic dropout medium (SD) deficient in leucine and tryptophan (-LT), and interaction was assayed quantitatively by a ß-Galactosidase assay performed using ortho-nitrophenyl- ß-D-galacpyranoside as a substrate following manufacturer´s instructions.

Bimolecular Fluorescence Complementation (BiFC) Assays

For bimolecular fluorescence complementation (BiFC) shown in Figure 1B, the coding regions of PIF3 and TOC1 [5] were cloned into pGWcY and pGWnY vectors [48], respectively. PRR5-, PRR7- and PRR9-nYFP are from [47]. Preparation of samples and bombardment of onion cells were done as in [5]. Briefly, the inner layers of spring onions were cut in 2 x 2 cm squares and used for particle bombardment. Each sample was transfected with 1 μg of each plasmid coupled to tungsten particles using a Biolistic Particle Delivery System PDS-1000 (Bio-Rad). After bombardment, onions were exposed to a saturating 15 min FR pulse and incubated overnight in dark conditions. The upper epidermal layer was removed, placed in a microscope slide and visualized using a confocal laser scanning microscope Olympus FV1000 (Objective Lens UPLSAPO 20X, Laser Wavelength: 514 nm, Emission window: 525-600 nm).

Protein Extraction and Immunoblot

Total protein extracts to detect endogenous PIF3 were prepared from 3 day-old SD-grown seedlings harvested at ZT24 in the dark (Figure 2D). Total protein extracts to detect endogenous PIF3 were prepared from 3 day-old SD-grown seedlings harvested at ZT24 in the dark (Figure 2D). Extraction buffer and protein quantification were done essentially as described [49]: Samples were collected and frozen in liquid nitrogen, and manually ground under frozen conditions before resuspension in boiling extraction buffer (100 mM MOPS (pH 7.6), 2% SDS, 10% glycerol, 4mM EDTA, 50mM Sodium metabisulfite ($Na_2S_2O_5$), $2gl^{-1}$ aprotinin, $3gl^{-1}$ leupeptin, $1gl^{-1}$ pepstatin and 2 mM

PMSF). Total protein was quantified using a Protein DC kit (Bio-Rad), and ß-mercaptoethanol was added just before loading. Aliquots of 100 ug for each sample were treated for 5min at 95C and subjected to 12.5% SDS- PAGE gels. Proteins were then transferred to Immobilon-P membrane (Millipore), and immunodetection of endogenous PIF3 was performed using a anti-PIF3 antibody [26] (1:10,000 dilution) incubated with Hikari solution (Nacalai Tesque). Peroxidase-linked anti rabbit secondary antibody (1:5,000 dilution) and a SuperSignal West Femto chemiluminescence kit (Pierce) were used for detection of luminescence using LAS-4000 Image imaging system (Fujifilm). The membrane was stained with Coomassie blue as a loading control.

Gene Expression Analysis

Quantitative RT-PCR, RNA extraction, cDNA synthesis and qRT-PCR were done as described [49]. Briefly, 1 mg of total RNA extracted using the RNeasy Plant Mini Kit (Qiagen) were treated with DNase I (Ambion) according to the manufacturer's instructions. First-strand cDNA synthesis was performed using the SuperScript III reverse transcriptase (Invitrogen) and oligo dT as a primer (dT30). cDNA was then treated with RNase Out (Invitrogen) before 1:20 dilution with water, and 2 ul was used for real-time PCR (Light Cycler 480; Roche) using SYBR Premix Ex Taq (Takara) and primers at a 300 nM concentration. Gene expression in time-course analyses (Figures 2C, 3A, 3B, 3D, 3E, S2C and S2D) was measured in two independent biological replicates, with three technical replicates for each biological sample, and the mean of the biological replicates ± SE is shown. For specific time points in Figures 2B, 4C, S2A, S2B, and S3C, gene expression was measured in three independent biological replicates, and in Figure 3C, corresponds to two biological replicates, with three technical replicates for each biological sample. *PP2A* (*AT1G13320*) was used for normalization.

Quantification and Statistical Analysis

Differences between means were statistically analyzed by one-way analysis of variance using Tukey-b post hoc multiple comparison test (IBM SPSS Statistics Software) or homoscedastic Student's t-test (Excel Microsoft), as indicated in the figure legends. Statistically significant differences were defined as those with a P value < 0.05. Significance level is indicated as * $P < 0.05$, ** $P < 0.01$ and *** $P < 0.001$.

Supplemental Tables

Dataset 1: Comparison of genome-wide loci associated to PIFs and PRR9, 7 and 5. Related to Figure 1.

Table S1: List of Oligonucleotides. Related to STAR Methods.

CellPress

TABLE FOR AUTHOR TO COMPLETE

Please upload the completed table as a separate document. ***Please do not add subheadings to the Key Resources Table.*** *If you wish to make an entry that does not fall into one of the subheadings below, please contact your handling editor. (****NOTE:*** *For authors publishing in Current Biology, please note that references within the KRT should be in numbered style, rather than Harvard.)*

KEY RESOURCES TABLE

REAGENT or RESOURCE	SOURCE	IDENTIFIER
Antibodies		
Anti-GFP	Invitrogen	Cat# A11122
Peroxidase-linked anti rabbit secondary antibody	Sigma	Cat# NA934
Anti-PIF3	[26]	N/A
Anti-HA	Abcam	Cat# 9110
Bacterial and Virus Strains		
AH109	Clontech	N/A
E. coli DH5α	N/A	N/A
A. tumefaciens GV3031	N/A	N/A
Chemicals, Peptides, and Recombinant Proteins		
Formaldehyde	ThermoFisher Scientific	Cat# 28908
Glycine	GE Healthcare Life Sciences	Cat# 17-1323-01
EDTA	Thermo Scientific	Cat# 17892
Tris-HCL	Sigma	Cat# C4706-2G
Proteinase K	ThermoFisher Scientific	Cat# EO0491
Sucrose	Applichem	Cat# A1125.1000
MgCl2	Calbiochem	Cat# 442611
PMSF	Applichem	Cat# A0999,0025
MG132	Merck	Cat# 474790
Proteinase Inhibitor Cocktail	Roche	Cat# 4693116001
Triton X-100	Applichem	Cat# A1388.10000
NaCl	Scharlau	Cat# SO02271000
LiCl	Merck	Cat# 1,056,790,250
NP40	Sigma	Cat# 74385
Deoxycholic acid sodium	Sigma	Cat# D6750
$NaHCO_3$	Merck	Cat# 6329
Dropout medium (-AHLT)	Clontech	Cat# 630428
Yeast Nitrogen Base w/o aa & ammonium sulfate	Conda	Cat# 1553.00
Ammonium Sulfate	Sigma	Cat# A4418
D-Glucose	Applichem	Cat# 3O000431
European bacteriological Agar	Conda	Cat# 1800.00
His	Sigma	Cat# H8125
Trp	Sigma	Cat# T0254
Leu	Sigma	Cat# L8912
Ade	Sigma	Cat# A9126

Propidium iodine	Calbiochem	Cat# 537059-
Ortho-nitrophenyl- ß-D-galacpyranoside	ThermoFisher Scientific	Cat# 34055
DNase I	Ambion	Cat# AM2224
RNase Out	Invitrogen	Cat# 10777019
SYBR Premix Ex Taq	Roche	Cat# 04707516001
MOPS (pH 7.6)	Sigma	Cat# M1254
SDS	Amresco	Cat# 0227
Glycerol	Applichem	Cat# A2926
EDTA	Thermo Scientific	Cat# 17892
Aprotinin	Applichem	Cat# A2132
Leupeptin	Applichem	Cat# A2183
Pepsatin	Applichem	Cat# A2205
PMSF	Applichem	Cat# A0999
ß-mercaptoethanol	Fluka	Cat# 03700
GFP Agarose Beads	MBL	Cat# D153-8
rProtein A-Sepharose	Bionova	Cat# 1-888-752-2568
Hikari solution	Nacalai Tesque	Cat# 02270-81
Sodium metabisulfite	Sigma	Cat# 255556
XmaI	Roche	Cat# ER0171
BamHI	Roche	Cat# 10 220 612 001
EcoRI	Roche	Cat# 10 703 737 001
T4 DNA Ligase	NZYtech	Cat# MB00703
BP Clonase II	Gateway	Cat# 11789-020
LR Clonase II	Gateway	Cat# 11791-020
Critical Commercial Assays		
RNeasy Plant Mini	Qiagen	Cat# 74904
SuperScript III reverse transcriptase	Invitrogen	Cat# 18080044
Protein DC	Bio-Rad	Cat# 5000121
SuperSignal West Femto chemiluminescence	Thermo Scientific	Cat# 34095
QIAquick gel extraction kit	Qiagen	Cat# QIA28704
Dynabeads	Invitrogen	Cat# 10004D
Immobilon-P membrane	Millipore	Cat# IPVH00010
Experimental Models: Organisms/Strains		
Col-0	N/A	N/A
C24	N/A	N/A
cdf5-1	[19]	N/A
toc1-101	[36]	N/A
pPRR7::PRR7-GFP (PRR7-GFP)	[27]	N/A
pPIF3::YFP:PIF3 (YFP-PIF3)	[26]	N/A
p35S::PIF4-HA (PIF4-HA)	[25]	N/A
pTOC1::TOC1:YFP (TMG)	[41]	N/A
pif1-1	[34]	N/A
pif3-3	[9]	N/A
pif4-2	[37]	N/A

pif5-3	[38]	N/A
pifq	[37]	N/A
prr5-1	[39]	N/A
prr7-3	[39]	N/A
prr9-1	[39]	N/A
pif3-1	[9]	N/A
pif4-101	[25]	N/A
pil6-1 (pif5)	[40]	N/A
prr7-3pif3-1 (*prr7pif3*)	This paper	N/A
prr7-3pif4-101 (*prr7pif4*)	This paper	N/A
prr7-3pil6-1 (*prr7pif5*)	This paper	N/A
prr7-3prr9-1 (*prr79*)	This paper	N/A
prr5-1prr9-1 (*prr59*)	This paper	N/A
prr5-1prr7-3prr9-1 (*prr579*)	This paper	N/A
prr7-3cdf5-1 (*prr7cdf5*)	This paper	N/A
35S::CDF5-GFP (*CDF5OX*)	This paper	N/A
pifqCDF5OX	This paper	N/A
pifqcdf5	This paper	N/A
Oligonucleotides		
See Table S2	N/A	N/A
Recombinant DNA		
pH7FWG2	Gateway	N/A
PIF3 in pGAD424	[46]	N/A
PIF4 in pGADT7	[7]	N/A
NZY-A PCR cloning kit	NZYTech	Cat# MB05302
pGBKT7	Clontech	Cat# PT3248-5
pGWcY	[48]	N/A
pGWnY	[48]	N/A
Software and Algorithms		
ActiveWebCam software (www.pysoft.com)	N/A	N/A
Integrated Genome Browser (IGB)	[43]	N/A
PHASER (http://phaser.mocklerlab.org)	N/A	N/A
DAVID system	[44]	N/A
IBM SPSS Statistics Software	N/A	N/A
Excel	N/A	N/A

Figure 1

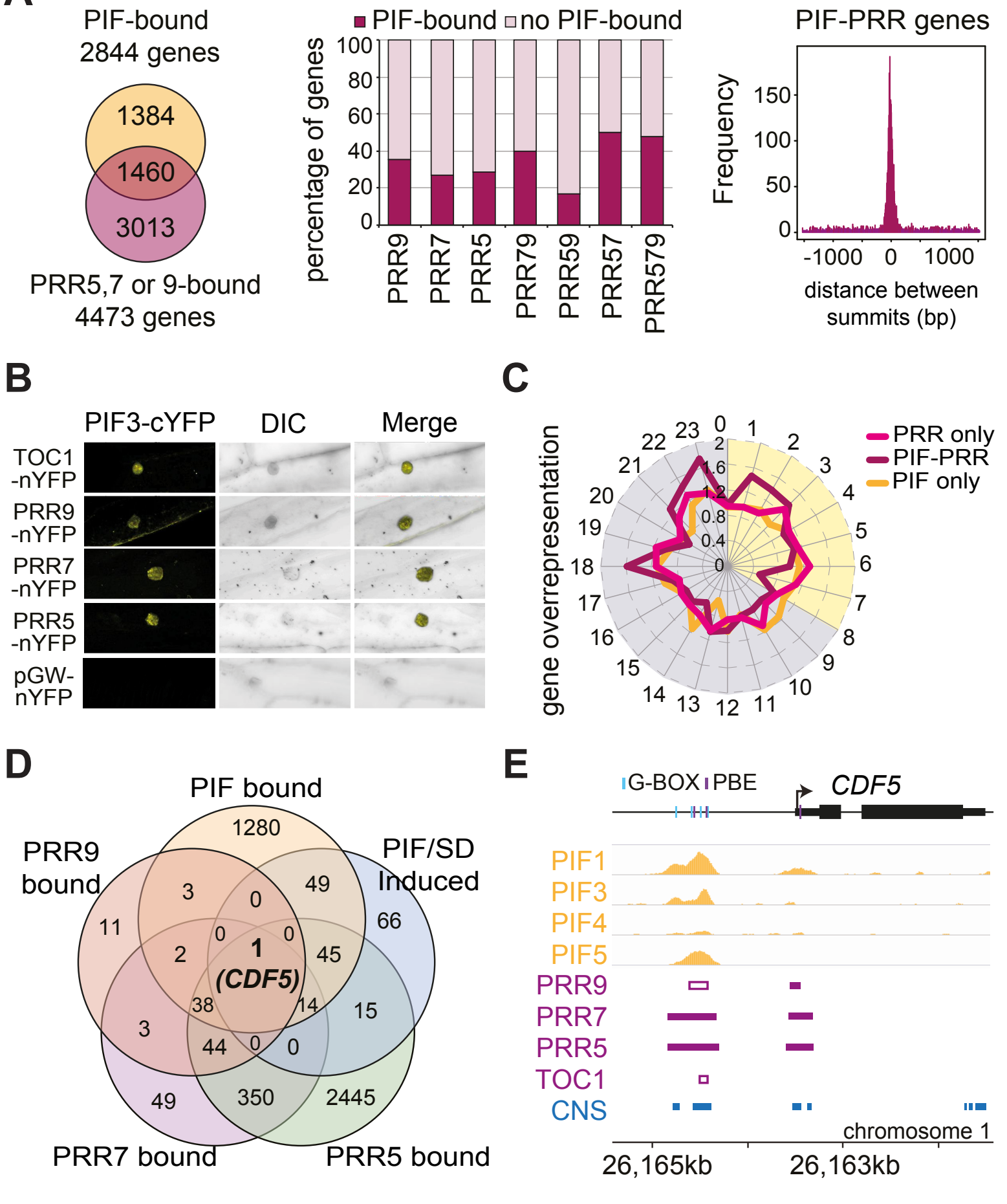
A
PIF-bound
2844 genes
1384
1460
3013
PRR5,7 or 9-bound
4473 genes
PIF-bound
no PIF-bound
percentage of genes
100
80
60
40
20
0
PRR9
PRR7
PRR5
PRR79
PRR59
PRR57
PRR579
PIF-PRR genes
Frequency
150
100
50
0
-1000
0
1000
distance between
summits (bp)
B
PIF3-cYFP
DIC
Merge
TOC1
-nYFP
PRR9
-nYFP
PRR7
-nYFP
PRR5
-nYFP
pGW-
nYFP
C
gene overrepresentation
PRR only
PIF-PRR
PIF only
D
PIF bound
PRR9
bound
PIF/SD
Induced
PRR7 bound
PRR5 bound
1280
3
0
49
11
66
0
0
2
1
(CDF5)
45
38
14
15
3
44
0
0
49
350
2445
E
G-BOX
PBE
CDF5
PIF1
PIF3
PIF4
PIF5
PRR9
PRR7
PRR5
TOC1
CNS
chromosome 1
26,165kb
26,163kb

Figure 2

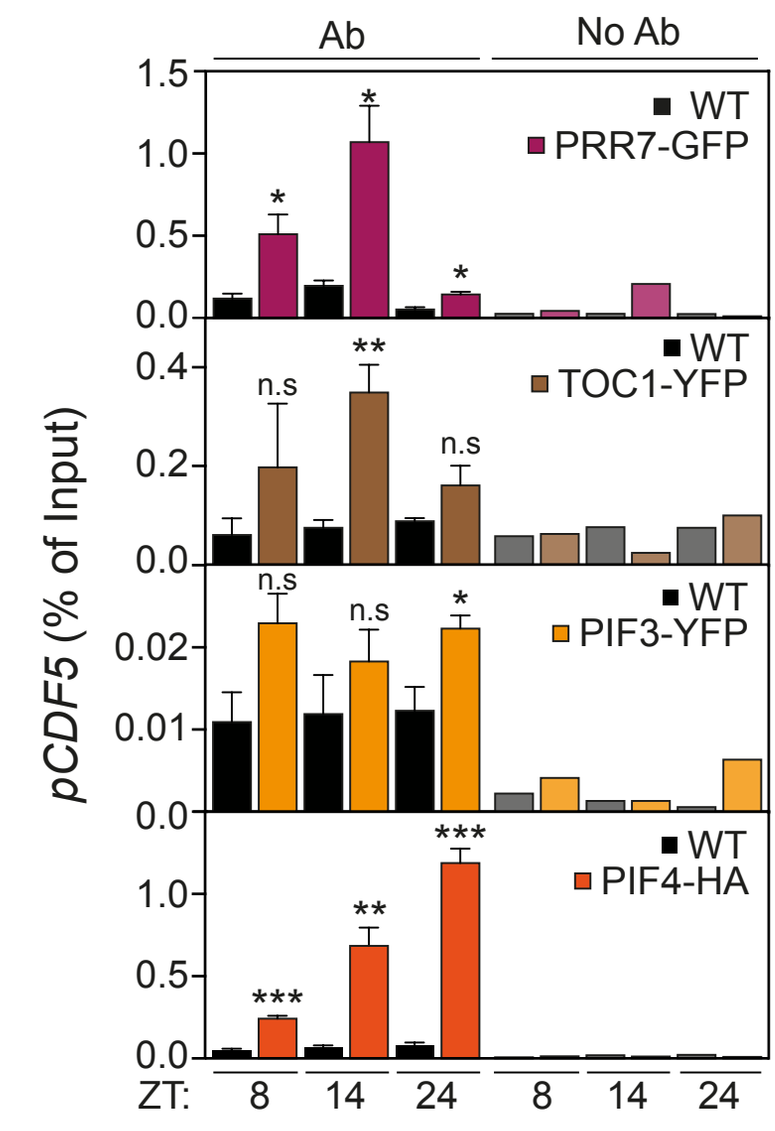
A
Ab
No Ab
WT
PRR7-GFP
TOC1-YFP
PIF3-YFP
PIF4-HA
pCDF5 (% of Input)
n.s
ZT:
8
14
24

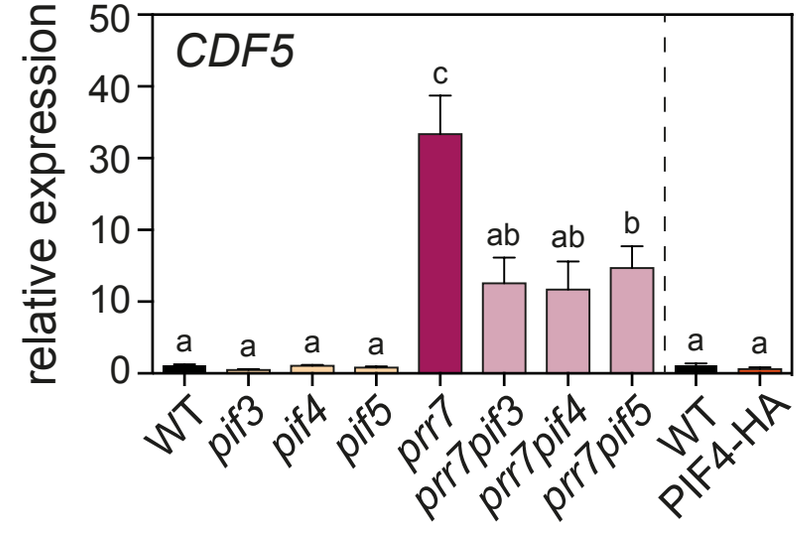
B
CDF5
relative expression
WT
pif3
pif4
pif5
prr7
prr7pif3
prr7pif4
prr7pif5
PIF4-HA

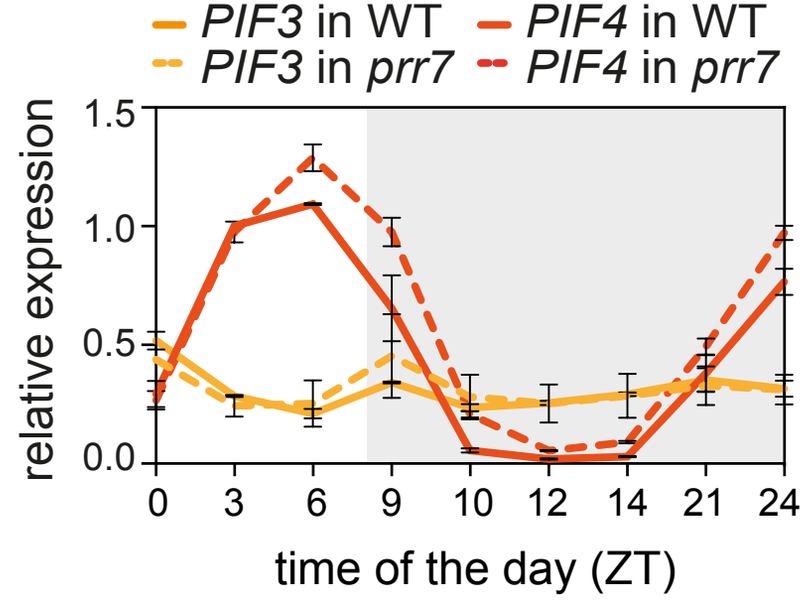
C
PIF3 in WT
PIF4 in WT
PIF3 in prr7
PIF4 in prr7
relative expression
time of the day (ZT)

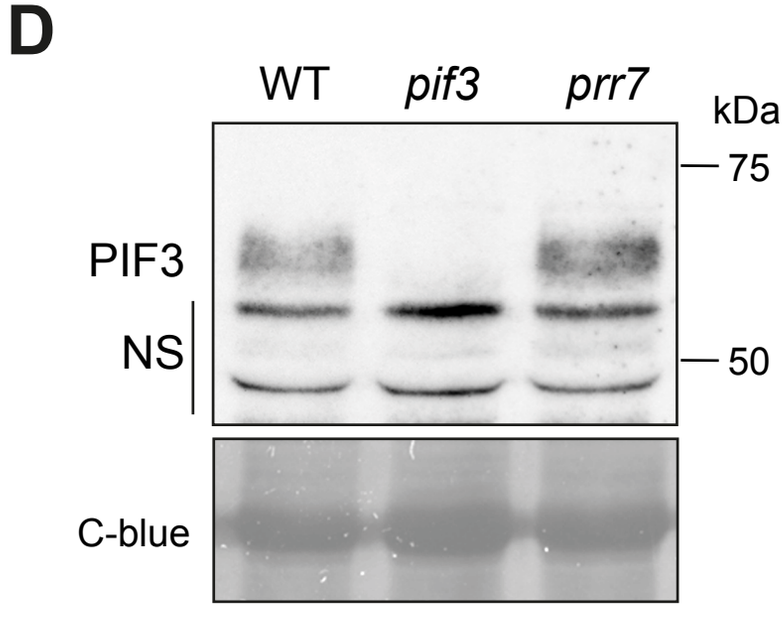
D
WT
pif3
prr7
kDa
75
50
PIF3
NS
C-blue

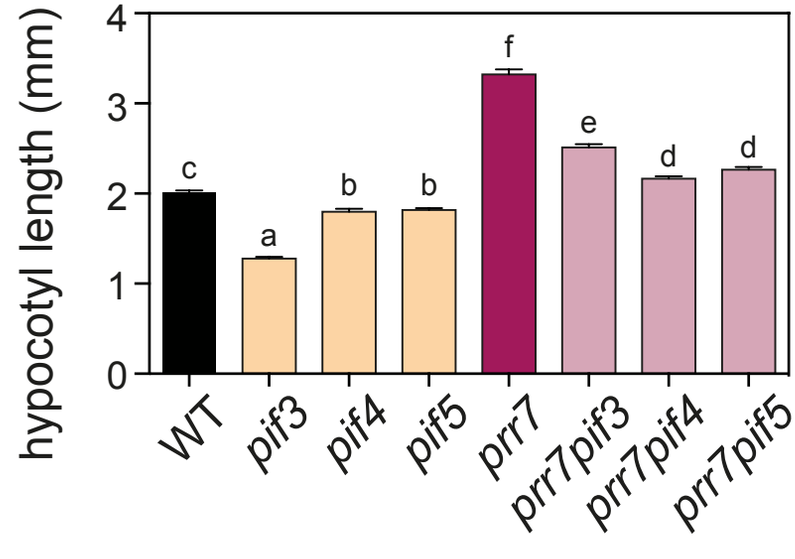
E
hypocotyl length (mm)
WT
pif3
pif4
pif5
prr7
prr7pif3
prr7pif4
prr7pif5

Figure 3

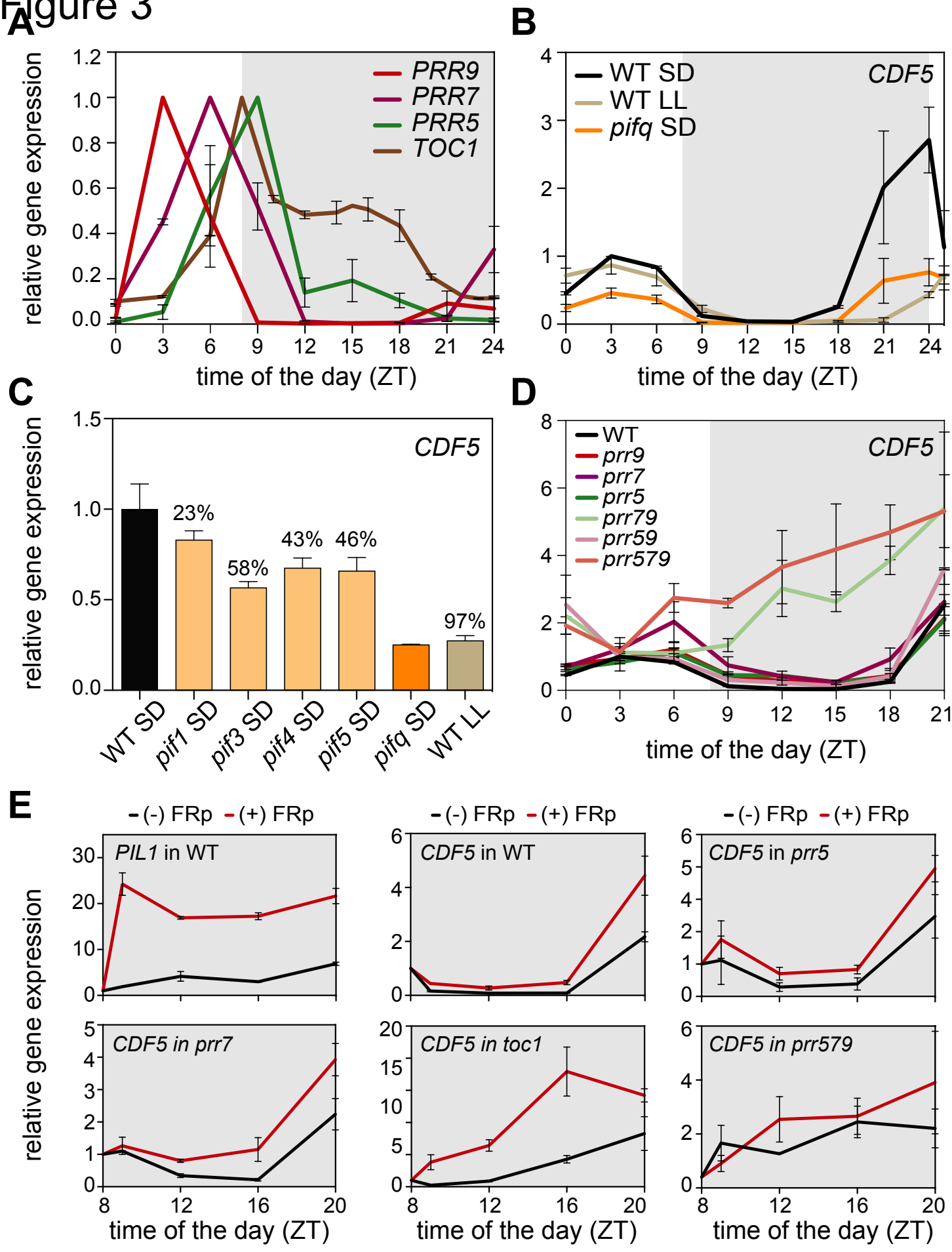
A
relative gene expression
PRR9
PRR7
PRR5
TOC1
time of the day (ZT)
B
WT SD
WT LL
pifq SD
CDF5
time of the day (ZT)
C
relative gene expression
CDF5
23%
58%
43%
46%
97%
WT SD
pif1 SD
pif3 SD
pif4 SD
pif5 SD
pifq SD
WT LL
D
WT
prr9
prr7
prr5
prr79
prr59
prr579
CDF5
time of the day (ZT)
E
(-) FRp
(+) FRp
relative gene expression
PIL1 in WT
CDF5 in WT
CDF5 in prr5
CDF5 in prr7
CDF5 in toc1
CDF5 in prr579
time of the day (ZT)

Figure 4

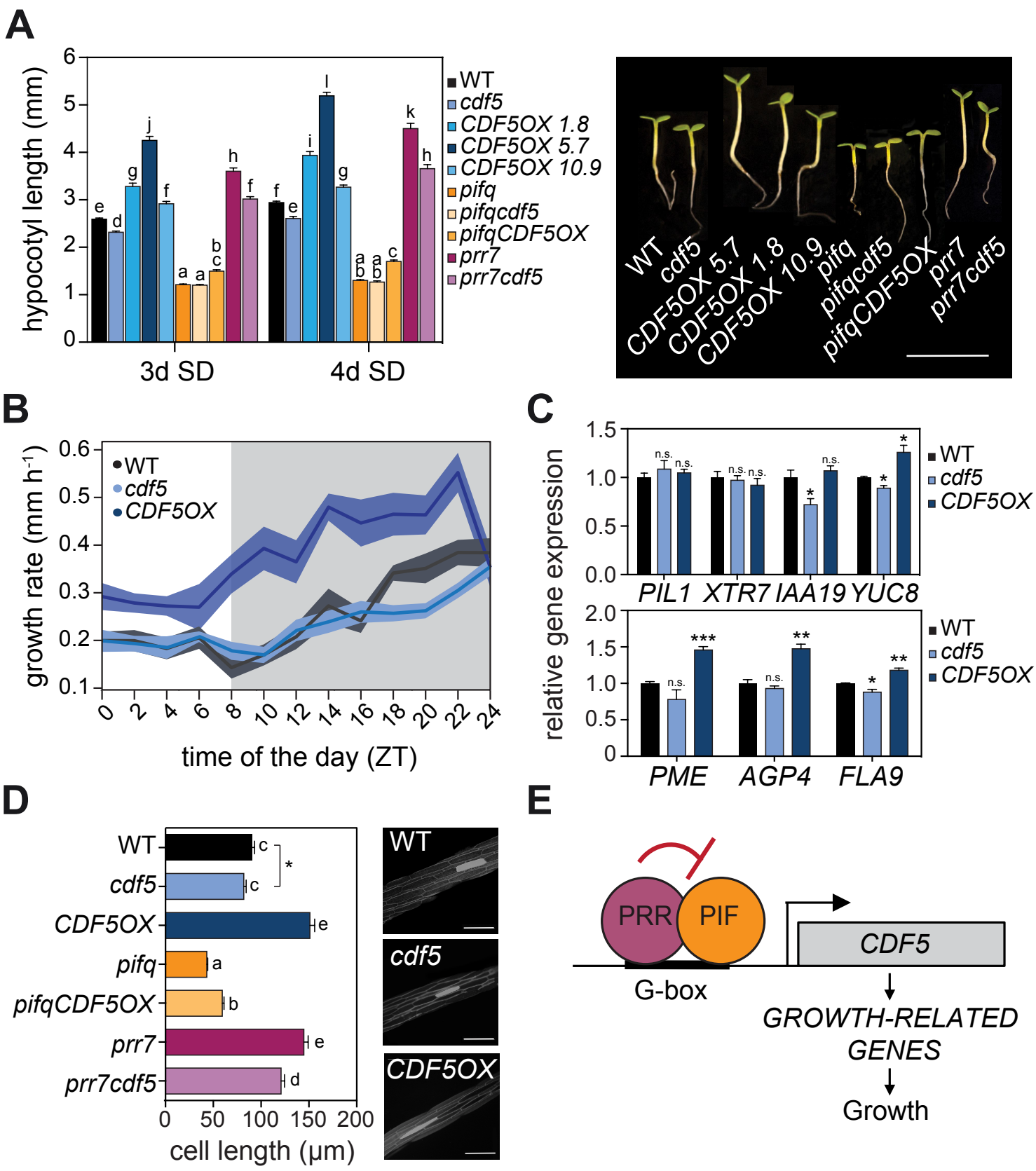
A
hypocotyl length (mm)
3d SD
4d SD
WT
cdf5
CDF5OX 1.8
CDF5OX 5.7
CDF5OX 10.9
pifq
pifqcdf5
pifqCDF5OX
prr7
prr7cdf5
WT
cdf5
CDF5OX 5.7
CDF5OX 1.8
CDF5OX 10.9
pifq
pifqcdf5
pifqCDF5OX
prr7
prr7cdf5
B
growth rate (mm h-1)
time of the day (ZT)
WT
cdf5
CDF5OX
C
relative gene expression
PIL1
XTR7
IAA19
YUC8
PME
AGP4
FLA9
n.s.
WT
cdf5
CDF5OX
D
WT
cdf5
CDF5OX
pifq
pifqCDF5OX
prr7
prr7cdf5
cell length (μm)
E
PRR
PIF
G-box
CDF5
GROWTH-RELATED GENES
Growth

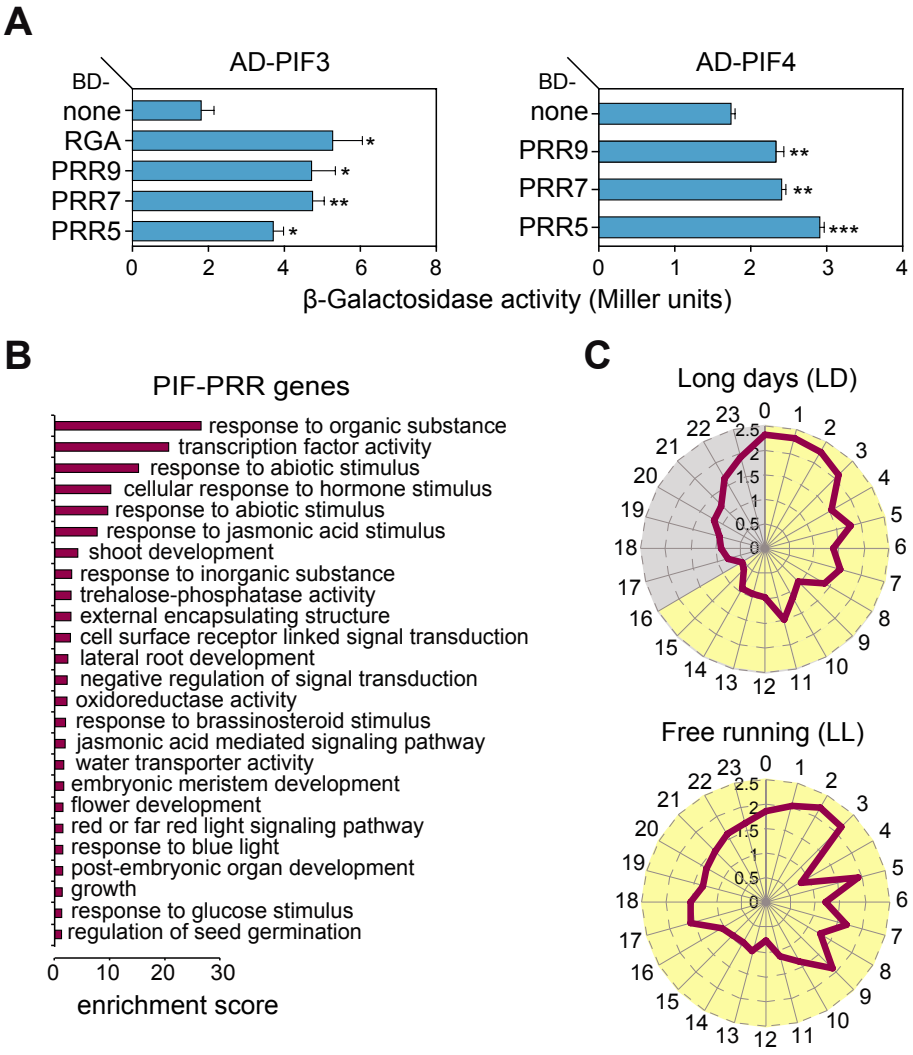

Figure S1. Related to Figure 1. Yeast-two-hybrid assays showing the interaction between PIF3, PIF4, and PRR9/7/5, and gene ontology (GO) and phaser analysis in LD and LL of PIF-PRR genes. (A) β-galactosidase activities from yeast two-hybrid assays showing interactions between PIF3 (left), PIF4 (right) and PRR5, PRR7, and PRR9. Error bars indicate SE (n = 3). Significance level is relative to the BD alone control (*P<0.05; **P<0.01 and ***P<0.001). DELLA protein RGA is included as positive control for PIF3 interactions [S1]. **(B)** Cluster analysis of the most enriched GO annotations for PIF-PRR genes. **(C)** Comparison of expression phases in long days (top) and free running (bottom) conditions of the 1,460 "PIF–PRR" gene set defined in Figure 1A and provided in Dataset 1. Phases as defined by PHASER (phaser.mocklerlab.org) are indicated on the circumference, and fold-change phase enrichment of genes (count/expected) is shown on the radius. Day is shown in yellow; night is shown in grey.

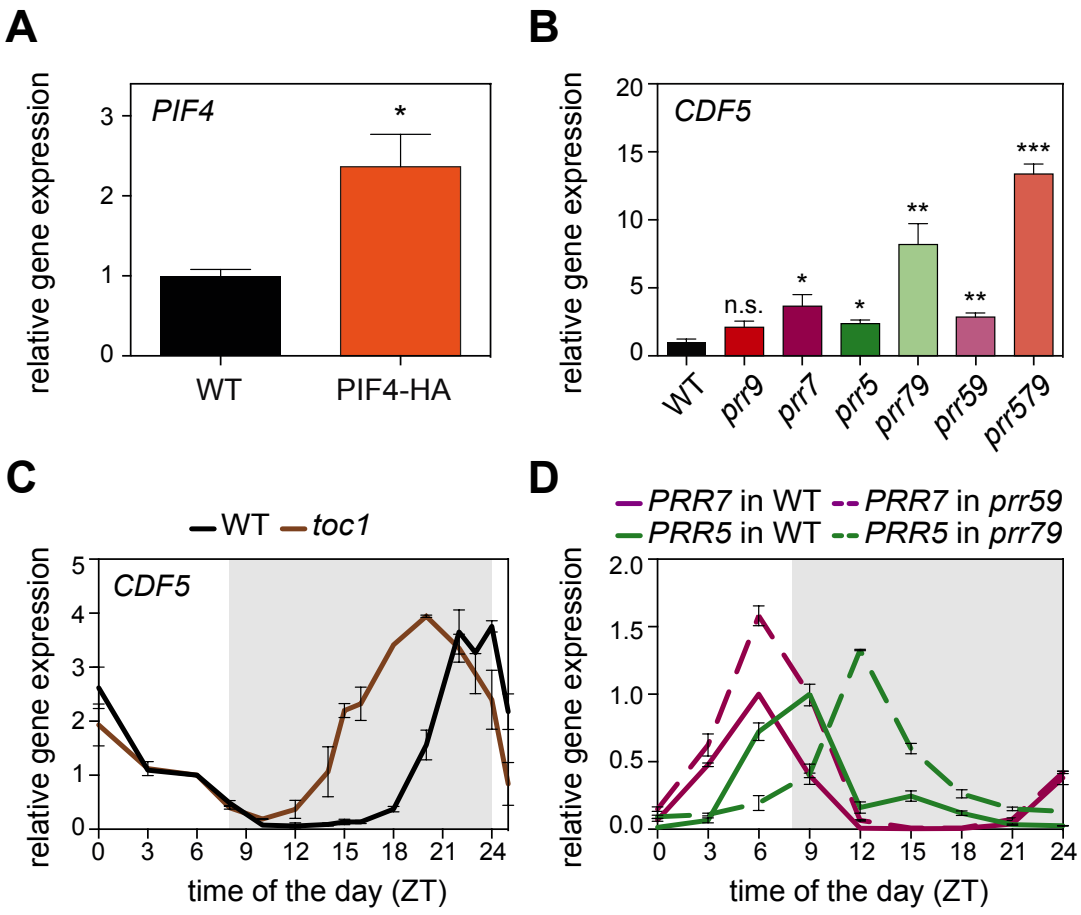

Figure S2. Related to Figures 2 and 3. *PIF4, CDF5*, *PRR5* and *PRR7* expression analyses in PIF4-HA overexpressing plants, and in *toc1, prr5, prr7, and prr9* single and higher order mutant combinations. *PIF4* expression in WT and *35S::PIF4-HA* (PIF4-HA) seedlings at ZT8 **(A)** and *CDF5* expression in WT and *prr* mutants at ZT9 **(B)** during the third day of growth in SD. Data are from three independent biological replicates relative to WT set at one. Error bars indicate SE. Statistically significant differences between mean values by Student's *t*-test relative to WT are shown (**P*<0.05; ***P*<0.01 and ****P*<0.001). n.s., not significant. **(C)** *CDF5* expression in WT and *toc1*. **(D)** *PRR5* and *PRR7* expression in WT and *prr79 and prr59*, respectively. (C, D) Seedlings were grown for 2 days in SD and harvested during the third day at the indicated times. Data plotted are mean ± SE relative to ZT6 for each genotype (C) or relative to its maximum expression value set at one for each gene (D), n = 2 independent biological experiments, each assayed in triplicate. (A-D) All samples were analyzed by qRT-PCR and normalized to *PP2A*.

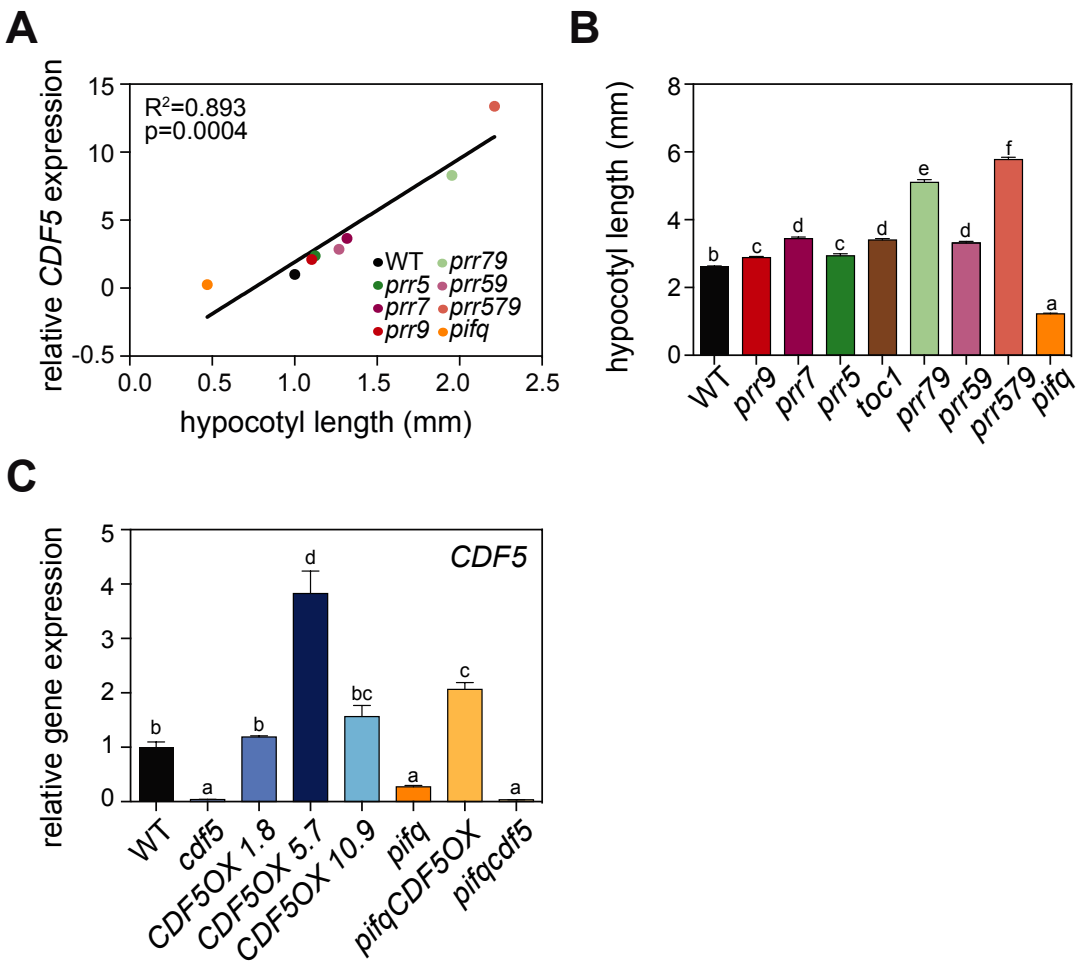

Figure S3. Related to Figures 3 and 4. *CDF5* expression in correlation with hypocotyl length and in generated *CDF5* mutant lines. (A) *CDF5* expression levels correlate with hypocotyl length. Correlation of hypocotyl length in (B) with *CDF5* expression values of WT, *prr* and *toc1* in 2-day-old SD-grown seedlings harvested at ZT9 during the third day under SD. *pifq* expression values are from Figure S2A. **(B)** Quantification of hypocotyl elongation in 3-day-old SD-grown WT, *prr*, *toc1*, and *pifq* seedlings. Data are means ± SE of at least 50 seedlings. **(C)** Characterization of *CDF5* expression levels in *CDF5OX* mutant lines. *CDF5* expression in 3-d-old SD-grown WT, *cdf5*, *CDF5OX*, *pifq*, *pifqCDF5OX*, and *pifqcdf5* seedlings at ZT24. In (A) and (C), expression was analyzed by qRT-PCR, and values were normalized to *PP2A* and are shown relative to WT levels set at one. Data are from three independent biological replicates. In (C) error bars indicate SE. Different letters shown in (B) and (C) denote statistically significant differences among means by Tukey-b test ($P<0.05$).

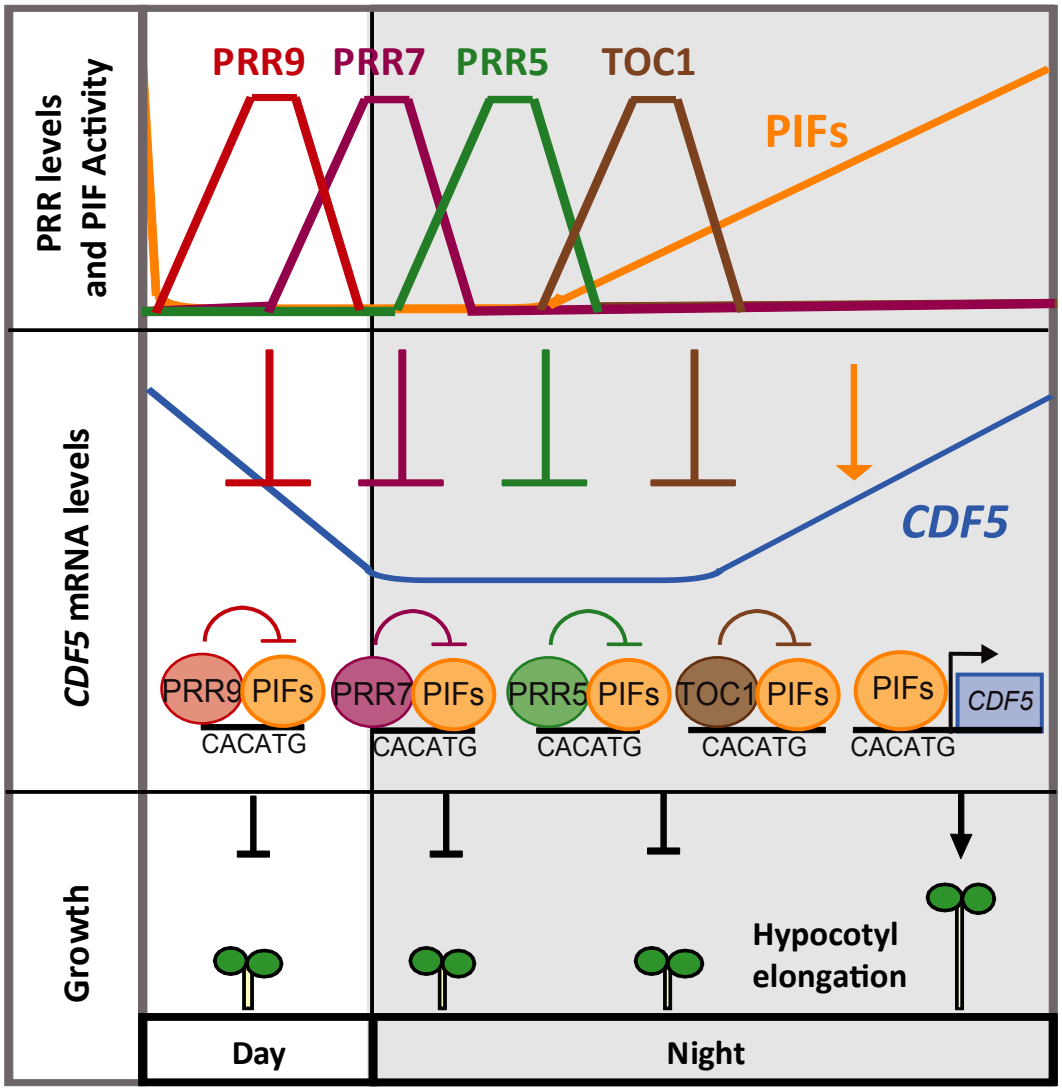

Figure S4. Related to Figure 4. Model of the proposed role of PRRs as repressors of PIF activity in gating CDF5-mediated elongation. Sequential PRR9/7/5 and PRR1/TOC1 accumulation from morning to midnight (top) represses PIF-induction of *CDF5*, a transcription factor necessary for growth-promotion (middle). PIFs are present during the day and progressively accumulate during the night concurrently to a decline in PRRs and TOC1 abundance (top). At predawn, PRRs and TOC1 are no longer present, repression on the PIFs is lifted (top), and PIFs induce *CDF5* expression (middle) to promote hypocotyl elongation (bottom). Based on current data, PRRs and PIFs could bind to the same or different nearby G-boxes, PIFs might bridge the binding of PRRs to DNA, or PRRs could compete with PIFs for binding to G-boxes.

Supplemental References

S1. Feng, S., Martinez, C., Gusmaroli, G., Wang, Y., Zhou, J., Wang, F., Chen, L., Yu, L., Iglesias-Pedraz, J.M., Kircher, S., *et al.* (2008). Coordinated regulation of Arabidopsis thaliana development by light and gibberellins. Nature *451*, 475–479.

S2. Pfeiffer, A., Shi, H., Tepperman, J.M., Zhang, Y., and Quail, P.H. (2014). Combinatorial Complexity in a Transcriptionally Centered Signaling Hub in Arabidopsis. Mol. Plant *7*, 1598–1618.

S3. Liu, T.L., Newton, L., Liu, M.-J., Shiu, S.-H., and Farré, E.M. (2016). A G-Box-Like Motif Is Necessary for Transcriptional Regulation by Circadian Pseudo-Response Regulators in Arabidopsis. Plant Physiol. *170*, 528–539.

S4. Martín, G., Soy, J., and Monte, E. (2016). Genomic Analysis Reveals Contrasting PIFq Contribution to Diurnal Rhythmic Gene Expression in PIF-Induced and - Repressed Genes. Front. Plant Sci. *7*, 962.

S5. Fornara, F., Panigrahi, K.C.S., Gissot, L., Sauerbrunn, N., Rühl, M., Jarillo, J.A., and Coupland, G. (2009). Arabidopsis DOF Transcription Factors Act Redundantly to Reduce CONSTANS Expression and Are Essential for a Photoperiodic Flowering Response. Dev. Cell *17*, 75–86.

S6. Mockler, T.C., Yu, X., Shalitin, D., Parikh, D., Michael, T.P., Liou, J., Huang, J., Smith, Z., Alonso, J.M., Ecker, J.R., *et al.* (2004). Regulation of flowering time in Arabidopsis by K homology domain proteins. Proc. Natl. Acad. Sci. U. S. A. *101*, 12759–12764.

S7. Soy, J., Leivar, P., González-Schain, N., Martín, G., Diaz, C., Sentandreu, M., Al-Sady, B., Quail, P.H., and Monte, E. (2016). Molecular convergence of clock and photosensory pathways through PIF3–TOC1 interaction and co-occupancy of target promoters. Proc. Natl. Acad. Sci. U. S. A. *113*, 4870–4875.

S8. Soy, J., Leivar, P., González-Schain, N., Sentandreu, M., Prat, S., Quail, P.H., and Monte, E. (2012). Phytochrome-imposed oscillations in PIF3 protein abundance regulate hypocotyl growth under diurnal light/dark conditions in Arabidopsis. Plant J. *71*, 390–401.

S9. http://www.tdx.cat/bitstream/handle/10803/130896/MGR_TESIS.pdf.

S10. Rawat, R., Schwartz, J., Jones, M.A., Sairanen, I., Cheng, Y., Andersson, C.R., Zhao, Y., Ljung, K., and Harmer, S.L. (2009). REVEILLE1, a Myb-like transcription factor, integrates the circadian clock and auxin pathways. Proc. Natl. Acad. Sci. U. S. A. *106*, 16883–16888.

S11. Shin, J., Park, E., and Choi, G. (2007). PIF3 regulates anthocyanin biosynthesis in an HY5-dependent manner with both factors directly binding anthocyanin biosynthetic gene promoters in Arabidopsis. Plant J. *49*, 981–994.